StruSoft

FEM-Design

FEM-Design

Geotechnical module in 3D

Theoretical background
&
Verification and validation handbook

version 4.3
2016

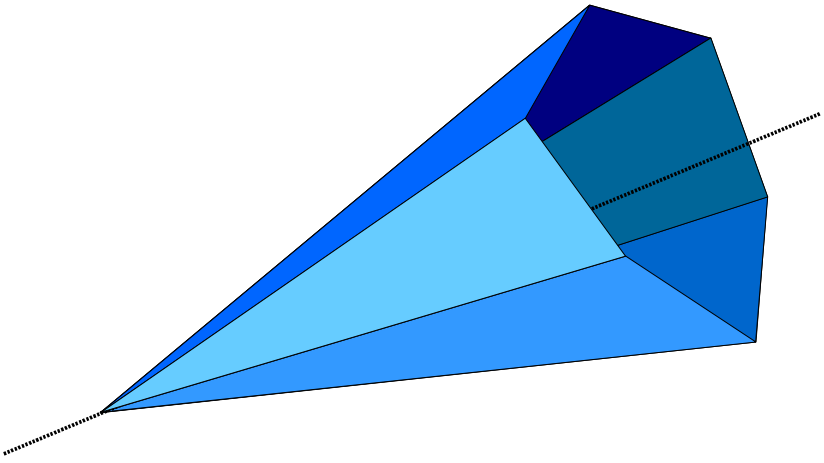

Contents

List of symbols

Scalars

c'	effective cohesion
c_u	undrained shear strength
d	increment of variables with depth
E	isotropic Young's (elastic) modulus
E_{oed}	oedometer (compression) modulus
$f(\boldsymbol{\sigma})$	Mohr-Coulomb flow rule and plastic potential
G	isotropic shear modulus
$\lvert\boldsymbol{J}\rvert$	determinant of the Jacobian matrix
K_0	coefficient of rest earth pressure
K_a	coefficient of active earth pressure
K_p	coefficient of passive earth pressure
M, M_0, M_L	compression modulus by different stress levels
M_{UR}	unloading/reloading compression modulus
M'	rate of compression modulus
p',p_0',p_L'	mean effective stress
p_C'	mean effective pre-consolidation pressure
p_w	steady state water pressure
q'	deviatoric stress
u	translation in x direction
v	translation in y direction
w	translation in z direction
x, y, z	global coordinates
γ_{dry}	dry unit weight of soil
γ_{sat}	saturated unit weight of soil
γ_{yz}, γ_{xz}, γ_{xy}	shear strains
ε_1, ε_2, ε_3	principal strains
ε_x, ε_y, ε_z	normal strains
ε_v	volumetric strain
λ	plastic multiplicator
ν	Poisson's ratio

ξ, η, ζ	parametric coordinates
$\sigma_1, \sigma_2, \sigma_3$	principal stresses
$\sigma_x, \sigma_y, \sigma_z$	normal stresses
$\tau_{yz}, \tau_{xz}, \tau_{xy}$	shear stresses
φ'	effective friction angle

Vectors

$\boldsymbol{p}$	load vector
$\boldsymbol{p}_e$	load vector of an element
$\boldsymbol{u}$	global displacement vector
$\boldsymbol{u}_e$	displacement vector of an element
$\boldsymbol{v}$	global nodal displacement vector
$\boldsymbol{v}_e$	nodal displacement vector of an element
$\boldsymbol{\sigma}$	stress vector
$\boldsymbol{\sigma}'$	effective stress vector
$\boldsymbol{\varepsilon}$	strain vector
$\boldsymbol{\varepsilon}^e$	elastic strain vector
$\boldsymbol{\varepsilon}^p$	plastic strain vector
$\boldsymbol{\varepsilon}_0$	kinematic load vector
$\Delta\boldsymbol{\sigma}$	total stress increment
$\Delta\boldsymbol{\sigma}^e$	elastic predictor stress
$\Delta\boldsymbol{\sigma}^p$	plastic corrector stress
$\Delta\boldsymbol{\varepsilon}$	total strain increment
$\Delta\boldsymbol{\varepsilon}^e$	elastic strain increment
$\Delta\boldsymbol{\varepsilon}^p$	plastic strain increment

Matrices

$\boldsymbol{B}$	strain matrix
$\boldsymbol{D}$	linear elastic material stiffness matrix
$\boldsymbol{D}^{ep}$	elasto-plastic material stiffness matrix
$\boldsymbol{J}$	Jacobian matrix
$\boldsymbol{K}$	global element stiffness matrix
$\boldsymbol{K}_e$	stiffness matrix of an element
$\boldsymbol{L}$	operator matrix

$\boldsymbol{N}$	shape function matrix

Abbreviations

CRS	constant rate of strain test
FE	finite element
FEM	finite element method
GEO	geotechnical
GWL	ground water level
IL	incremental loading test
NC	normally consolidated
NLS	non-linear soil
OC	overconsolidated
OCRp	over-consolidation ratio
PI	plasticity index

Introduction

Firstly the purpose of this documentation is to show a short summary about the elasticity in general 3D space and the theoretical background of using solid elements in a finite element calculation. Secondly the main reason of this paper is to show the different material models which are implemented in the new version of FEM-Design geotechnical module (3D Soil). Thirdly at the end of this paper the reader can find some verification and validation examples of the shown theories and problems.

1. Theory of elasticity in 3D

Before the description of the theory of the geotechnical module and the theoretical background of the different soil material models in FEM-Design a clarification about the general elasticity is required. This is necessary because in 3D it won't need any approximation respect to the geometry of the investigated element/structure such as the consideration of the ratio between the length and the width/height of a bar or the simplifications by shells according to the ratio between the width and thickness.

In general (in 3D space) the displacement field contains three different independent variables. All of these variables depend on the coordinates of the solid material (Eq. 1.1). Thus the displacement vector of a solid element comprises three different variables. As usual in the ordinary finite element technique these variables are the master variables and after the calculation of these main variables (solving the equation system) the secondary variables (slave variables) such as stresses can be determined. For more details about general elasticity see [1], [2], [3], [4] and [5].

$$\mathbf{u}=\begin{bmatrix} u(x,y,z) \\ v(x,y,z) \\ w(x,y,z) \end{bmatrix} \qquad \text{(Eq. 1.1)}$$

According to these facts the external load vector of a solid element also contains three different parts. These loads must be external forces because it is necessary to ensure the work compatibilty between the displacements and loads. Eq. 1.2 shows the external load vector which belongs to a 3D solid material.

$$\mathbf{p}=\begin{bmatrix} p_x(x,y,z) \\ p_y(x,y,z) \\ p_z(x,y,z) \end{bmatrix} \qquad \text{(Eq. 1.2)}$$

1.1 General definition of stresses

In a general 3D deformation problem the interpretation of the stresses are the following (see Figure 1.1). Figure 1.1 also shows the positive direction of the stresses on an infinitesimally small cuboid. Stress is a tensor which can be represented in Cartesian coordinate system with a matrix. In the standard deformation theory the stress tensor must be symmetric according to the Prager-Dracker postulates ([1], [2], [5] and [6]), therefore stresses are often written in vector notation based on the Voight notation system. With the vector notation there are only six independent stress components (Eq. 1.3).

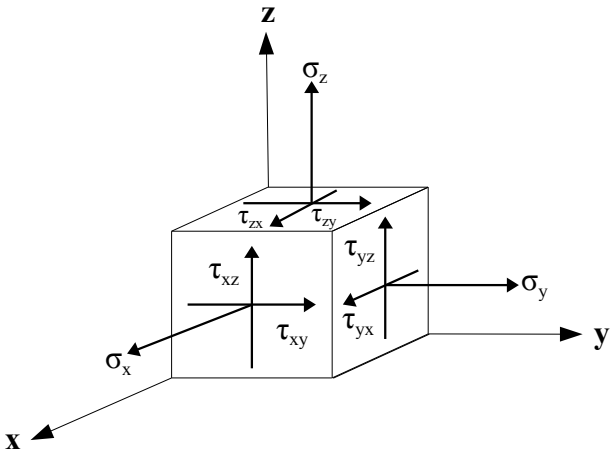

Figure 1.1 – General three-dimensional Cartesian coordinate system and sign convention for stresses

$$\boldsymbol{\sigma}=\begin{bmatrix}\sigma_x\\ \sigma_y\\ \sigma_z\\ \tau_{yz}\\ \tau_{xz}\\ \tau_{xy}\end{bmatrix} \qquad \text{(Eq. 1.3)}$$

In the three dimensional space always exist three orthogonal directions where the shear stresses are zero. The name of these directions is the directions of principal stresses and the normal stresses which belong to these directions are the principal stresses. Mathematically the principal stresses and principal directions are the solution of the well-known eigenvalue problem (see Eq. 1.4):

$$\det\left(\underline{\underline{\boldsymbol{\sigma}}}-\sigma_i\underline{\underline{\mathbf{I}}}\right)=0 \qquad \text{(Eq. 1.4)}$$

where **I** is the identity matrix. This equation gives three solutions for σ_i namely the principal stresses. The sign convention of the principal stresses in FEM-Design are as follows:

$$\sigma_1 \geqslant \sigma_2 \geqslant \sigma_3 \qquad \text{(Eq. 1.5)}$$

Compression is negative, tension is positive. It is necessary for the mathematical formulation of the material models (Chapter 3) to define the invariant of the stress tensor. For several material models the first invariant of the stresses is very common (Eq. 1.6).

$$p=\frac{\sigma_x+\sigma_y+\sigma_z}{3}=\frac{\sigma_1+\sigma_2+\sigma_3}{3} \qquad \text{(Eq. 1.6)}$$

It can be see from Eq. 1.6 that this invariant is equivalent with the mean (effective) stress. This is always the average value of the diagonal of the stress tensor (average value of the first three elements of the stress vector Eq. 1.3)

1.2 General definition of strains

In a general 3D deformation problem the interpretation of the strains are the following (see Figure 1.2). Figure 1.2 also shows the positive direction of the strains on an infinitesimally small cube. Strain is a tensor which can be represented in Cartesian coordinate system with a matrix. In the standard deformation theory the strain tensor must be symmetric according, therefore strains are often written in vector notation based on the Voight notation system. With the vector notation there are only six independent strain components (Eq. 1.7).

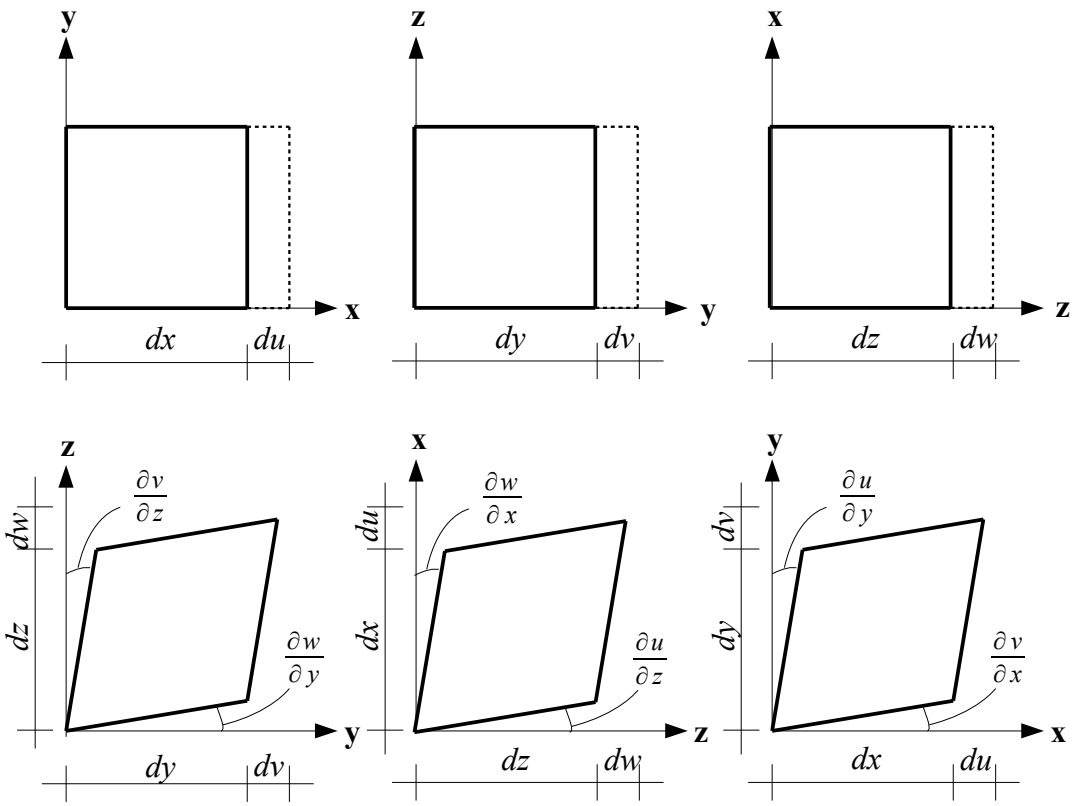

Figure 1.2 – General sign convention for strains in three-dimensional Cartesian coordinate system

$$\boldsymbol{\varepsilon}=\begin{bmatrix}\varepsilon_x\\ \varepsilon_y\\ \varepsilon_z\\ \gamma_{yz}\\ \gamma_{xz}\\ \gamma_{xy}\end{bmatrix} \qquad \text{(Eq. 1.7)}$$

In Eq. 1.7 the elements of the strain vector (according to Fig. 1.2):

$$\varepsilon_x=\frac{\partial u}{\partial x}\ ;\ \varepsilon_y=\frac{\partial v}{\partial y}\ ;\ \varepsilon_z=\frac{\partial w}{\partial z} \qquad \text{(Eq. 1.8a)}$$

$$\gamma_{yz}=\frac{\partial v}{\partial z}+\frac{\partial w}{\partial y}\ ;\ \gamma_{xz}=\frac{\partial u}{\partial z}+\frac{\partial w}{\partial x}\ ;\ \gamma_{xy}=\frac{\partial u}{\partial y}+\frac{\partial v}{\partial x} \qquad \text{(Eq. 1.8b)}$$

Thus the simplified mathematical connection between the strains and displacements (according to the small deformation theory):

$$\boldsymbol{\varepsilon}=\mathbf{L}\,\mathbf{u} \qquad \text{(Eq. 1.9)}$$

where **L** is the operator matrix:

$$\mathbf{L}=\begin{bmatrix}\frac{\partial}{\partial x} & 0 & 0\\ 0 & \frac{\partial}{\partial y} & 0\\ 0 & 0 & \frac{\partial}{\partial z}\\ 0 & \frac{\partial}{\partial z} & \frac{\partial}{\partial y}\\ \frac{\partial}{\partial z} & 0 & \frac{\partial}{\partial x}\\ \frac{\partial}{\partial y} & \frac{\partial}{\partial x} & 0\end{bmatrix} \qquad \text{(Eq. 1.10)}$$

In the three dimensional space always exist three orthogonal directions where the shear strains are zero. The name of these directions is the direction of principal strains and the strains which belong to these directions are the principal strains. Mathematically the principal strains and principal directions are the solution of the well-known eigenvalue problem (see Eq. 1.11):

$$\det\left(\underline{\underline{\boldsymbol{\varepsilon}}}-\varepsilon_i\,\underline{\underline{\mathbf{I}}}\right)=0 \qquad \text{(Eq. 1.11)}$$

where **I** is the identity matrix. This equation gives three solutions for ε_i namely the principal strains. The sign convention of the principal strains in FEM-Design are as follows:

$$\varepsilon_1\geqslant\varepsilon_2\geqslant\varepsilon_3 \qquad \text{(Eq. 1.12)}$$

Based on the co-axiality rule by isotropic elasticity the directions of principal stresses and the

directions of principal strains coincide each other.

As we mentioned at stresses the invariants of the tensors are very common variables when creating and using material models. By strains the often used is the first invariant of the strain matrix which shows the volume changing of the element thus the name of this invariant is the volumetric strain(see Eq. 1.13).

$$\varepsilon_v = \varepsilon_x + \varepsilon_y + \varepsilon_z = \varepsilon_1 + \varepsilon_2 + \varepsilon_3 \qquad \text{(Eq. 1.13)}$$

1.3 The effect of water pressure and effective stresses

The material models are the mathematical description (connection) between the stresses and strains. By soil material models this mathematical description always gives us the connection between the so called effective stress tensor and strain tensor. Therefore according to Terzaghi's principle the stress vector in the soil divided into effective stresses and water pressure (Eq. 1.14 and see [7]).

$$\boldsymbol{\sigma} = \boldsymbol{\sigma}' + \boldsymbol{\sigma}_w \qquad \text{(Eq. 1.14)}$$

Water pressure are provided by water in the pores. Positive normal stress components represent tension and **negative normal stress components represents compression**. The water pressure is fully isotropic thus the stress vector which represent the effect of water (see Fig. 1.3):

$$\boldsymbol{\sigma}_w = \begin{bmatrix} p_w \\ p_w \\ p_w \\ 0 \\ 0 \\ 0 \end{bmatrix} \qquad \text{(Eq. 1.15)}$$

All of the mentioned material models in this documentation is expressed as a relationship between the effective stresses and strains. Therefore we denote the effective stresses with a prime (') in our equations:

$$\boldsymbol{\sigma}' = \boldsymbol{\sigma} - \boldsymbol{\sigma}_w \qquad \text{(Eq. 1.16)}$$

With the effective stresses the former mentioned principal stresses and invariants can be expressed. Based on this consideration the mean effective stress:

$$p' = \frac{\sigma_x' + \sigma_y' + \sigma_z'}{3} = \frac{\sigma_1' + \sigma_2' + \sigma_3'}{3} \qquad \text{(Eq. 1.17)}$$

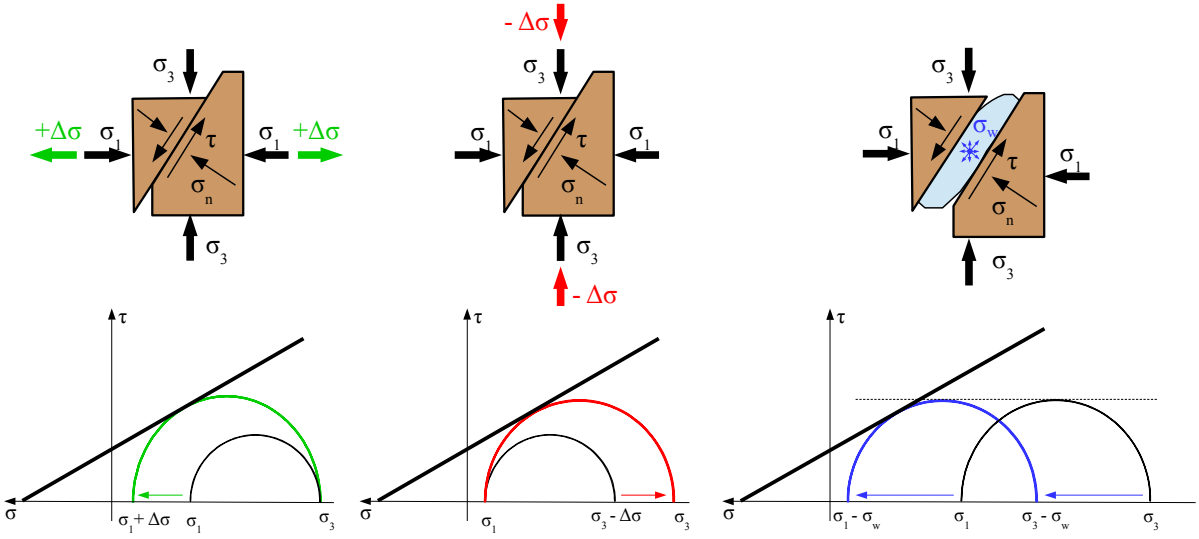

Figure 1.3 – The visualization of the effect of water pressure on effective stresses

2. Solid elements

By modelling the soil skeleton in three-dimensional space the discretization of the soil also need to be three-dimensional below the structre. By this geometrical finitization solid elements are inescapeable. In the next chapter the reader can find the different solid element types concerning the different element shapes (nodes) in FEM-Design.

2.1 Element types

Basically in FEM-Design during the geometrical finitization the general mesh generator provides four basic solid elements. All of these basic elements exist in linear form (standard - linear shape functions) and in quadratic form (fine - quadratic shape functions). According to Eq. 1.10 the shape functions of the solid elements must have C^0 continuity [8], [9].

The next figures (Fig. 2.1-2.4) show the different element types in standard and fine cases. The ξ, η, ζ coordinates are the parametric coordinates of the elements which are necessary to express the element stiffness matrices and load vectors of the solid elements. The global (x, y, z) coordinates of the nodes and the transformation matrices between ξ, η, ζ coordinates and x, y, z coordinates give us the unequivocal relationship between the two systems if the finite element mesh is correct.

Table 1 also shows the number of the nodes by the different available elements. In Fig. 2.1-2.4 the origins of the parametric coordinate system are also obvious. The midnodes are always lying on the half (midpoint) of the edges and in the middle of the sides.

Number of nodes	Standard (linear shape functions)	Fine (quadratic shape functions)
Tetrahedron	4	10
Pyramid	5	14
Wedge/Prism	6	18
Hexahedron	8	27

Table 1 – The number of nodes by standard and fine solid elements

The origin of the tetrahedron element is at a corner node. Thus the parametric coordinates of the ξ, η, ζ system are between 0 and +1. The linear and the quadratic tetrahedron elements have 4 and 10 nodes respectively (see Fig. 2.1).

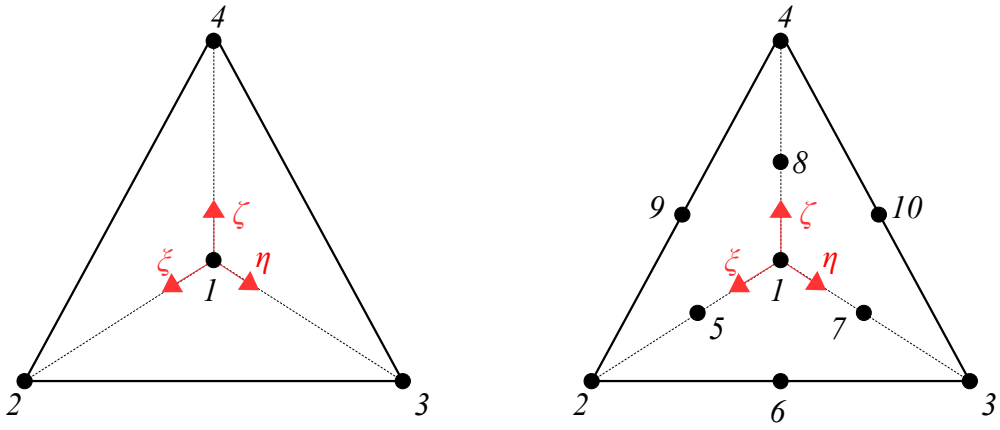

Figure 2.1 – The 4-node and the 10-node tetrahedron finite element in parametric coordinate system

The parametric coordinate system origins from the middle of the pyramid elements. Therefore the ξ, η, ζ coordinates are between –1 and +1. The linear and the quadratic pyramid elements have 5 and 14 nodes respectively (see Fig. 2.2).

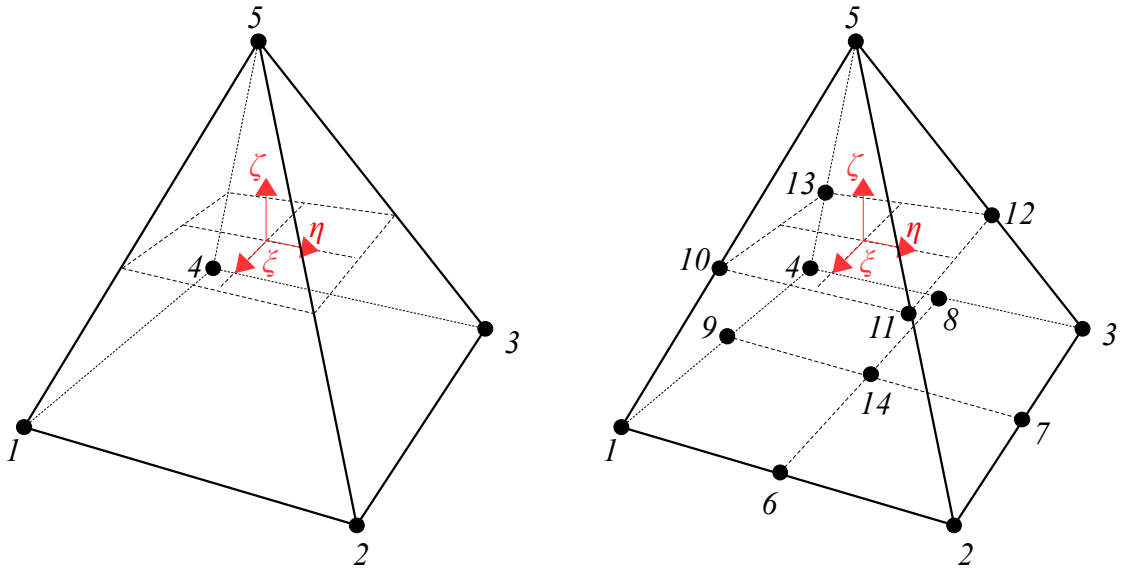

Figure 2.2 – The 5-node and the 14-node pyramid finite element in parametric coordinate system

The parametric coordinate system origins from the middle of the wedge/prism elements. Therefore the ξ, η coordinates are between 0 and +1 and the ζ coordinates are between –1 and +1. The linear and the quadratic wedge/prism elements have 6 and 18 nodes respectively (see Fig. 2.3).

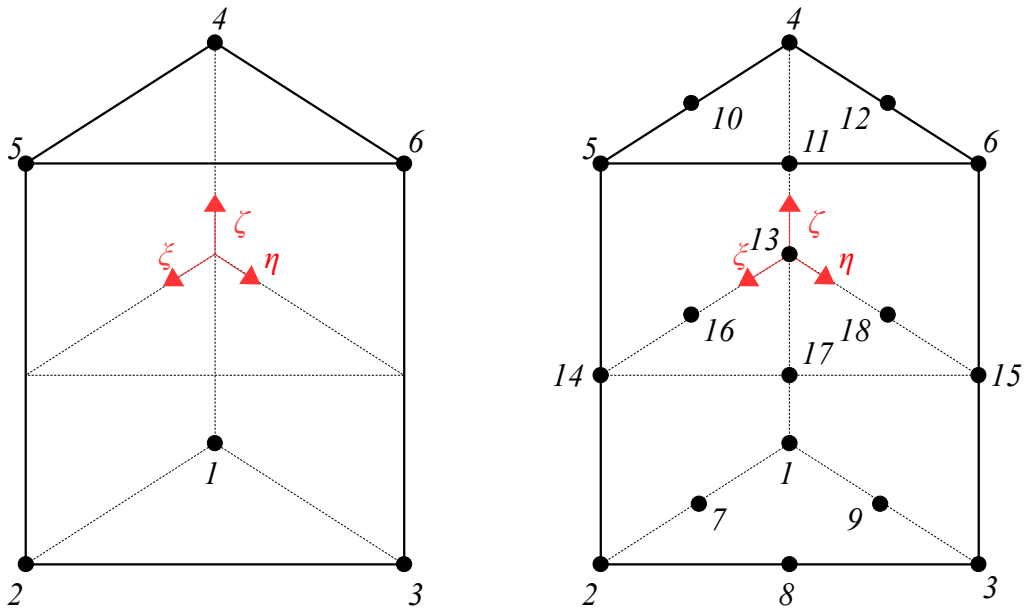

Figure 2.3 – The 6-node and the 18-node wedge/prism finite element in parametric coordinate system

The parametric coordinate system origins from the middle of the hexahedron elements. Therefore the ξ, η, ζ coordinates are between –1 and +1. The linear and the quadratic hexahedron elements have 8 and 27 nodes respectively (see Fig. 2.4).

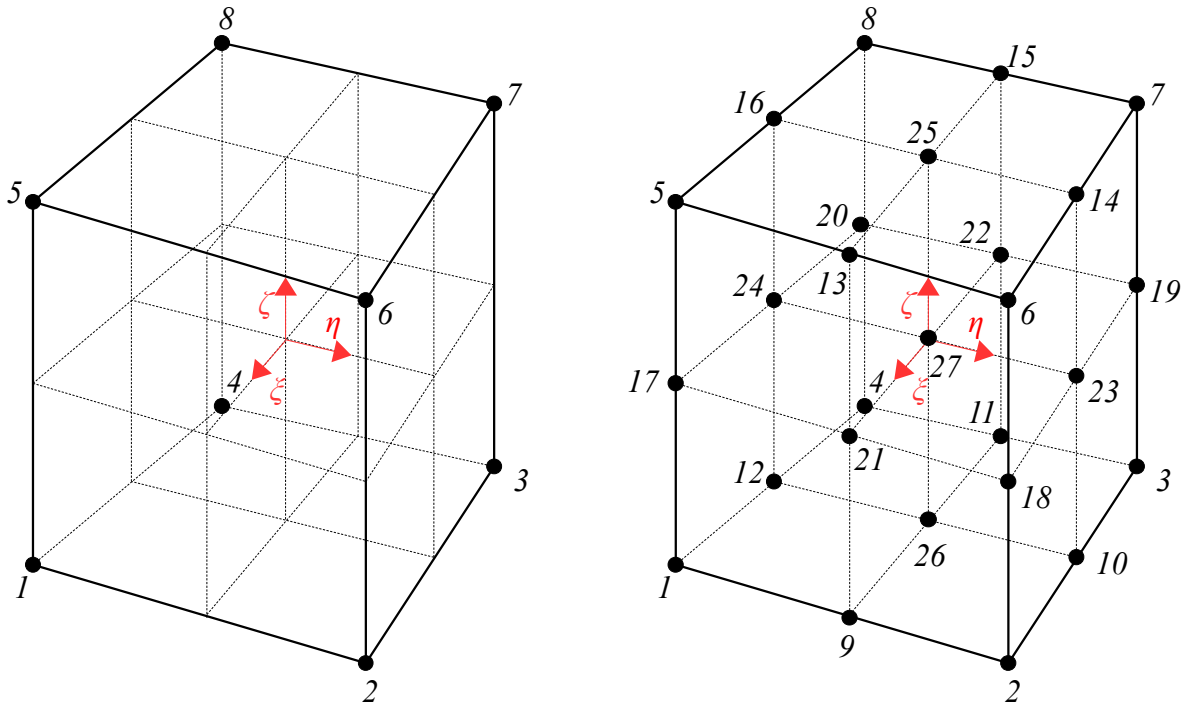

Figure 2.4 – The 8-node and the 27-node hexahedron finite element in parametric coordinate system

2.2 Integration points

The number of integration points also important besides the node number. According to the fact that the material nonlinearity and the calculation of the element stiffness matrices depend on the stress state of the integration points with a quadratic (fine) element group more accurate result can be reached [10]. By the non-linear calculation in every load-increments the stiffness matrices are calculated with numerical integration based on the stress results coming from the former load-step.

Table 2 shows the number of integration points respect to the node number of the element. Theoretically the quadratic element group gives us more accurate results but it is important that with the same element number, the computation takes more time because the size of the coefficient matrix is larger than with linear elements [8], [9].

The position and the number of integration points are also important when the effect of different locking (shear and volumetric, [11], [12] and [13]) and hourglassing come into view. Therefore in this documentation we give the number of intergation points and the position of intergation points to avoid any misunderstanding. Fig. 2.5-2.8 shows these numbers and positions by the different element types.

	Number of integration points
4-node tetrahedron	1
5-node pyramid	5
6-node wedge/prism	9
8-node hexahedron	8
10-node tetrahedron	15
14-node pyramid	13
18-node wedge/prism	18
27-node hexahedron	27

Table 2 – The number of integration points by different element types

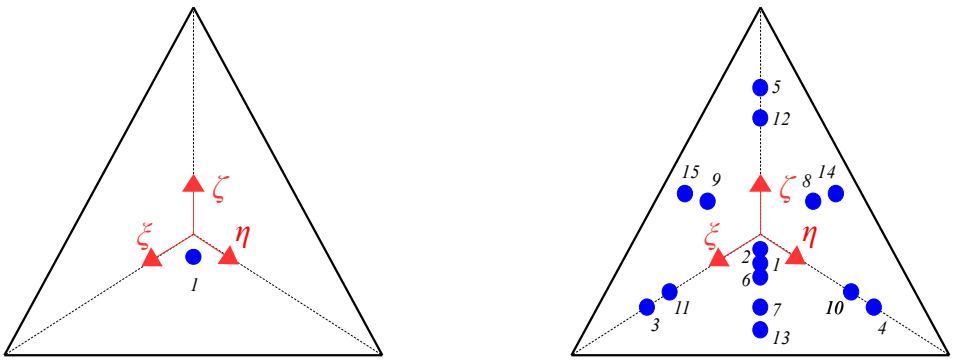

Figure 2.5 – The integration points of 4-node and 10-node tetrahedron finite element

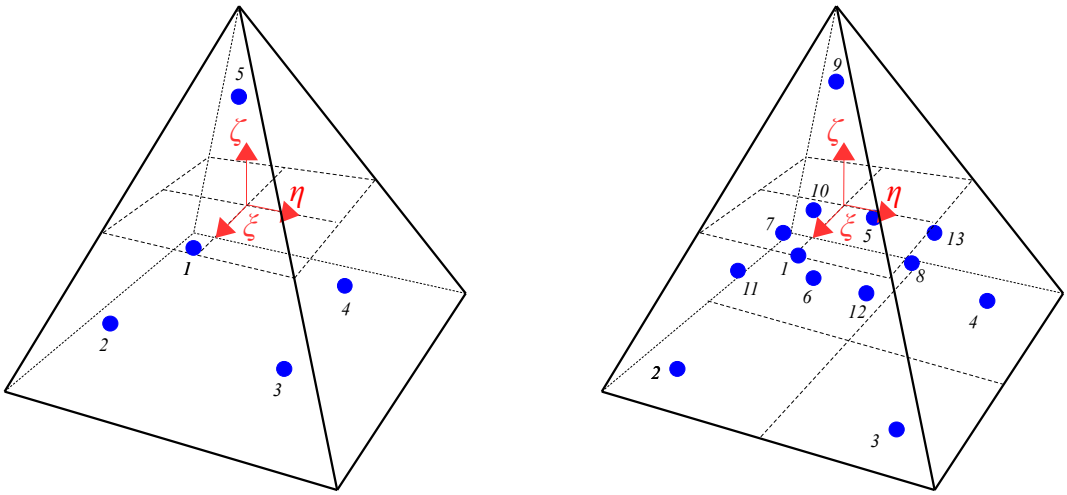

Figure 2.6 – The integration points of 5-node and 14-node pyramid finite element

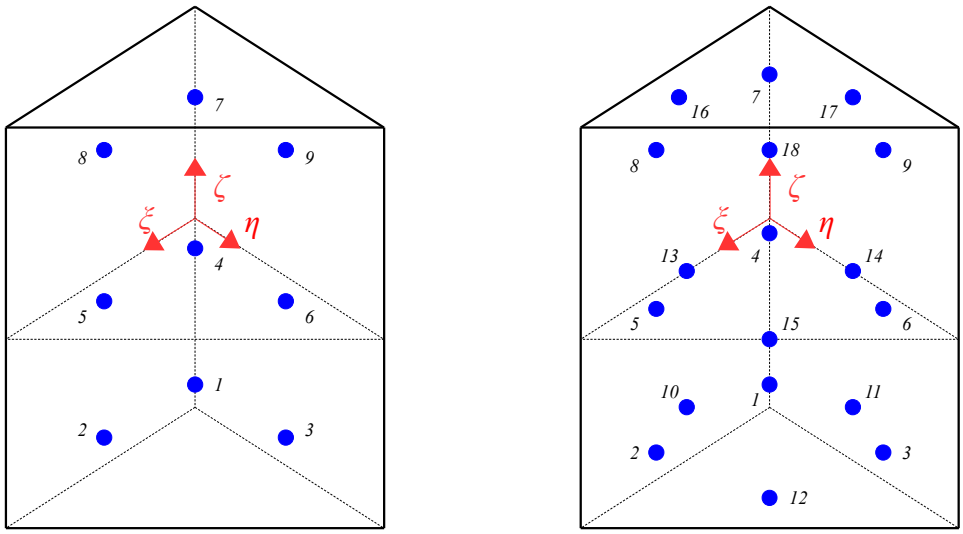

Figure 2.7 – The integration points of 6-node and 18-node wedge/prism finite element

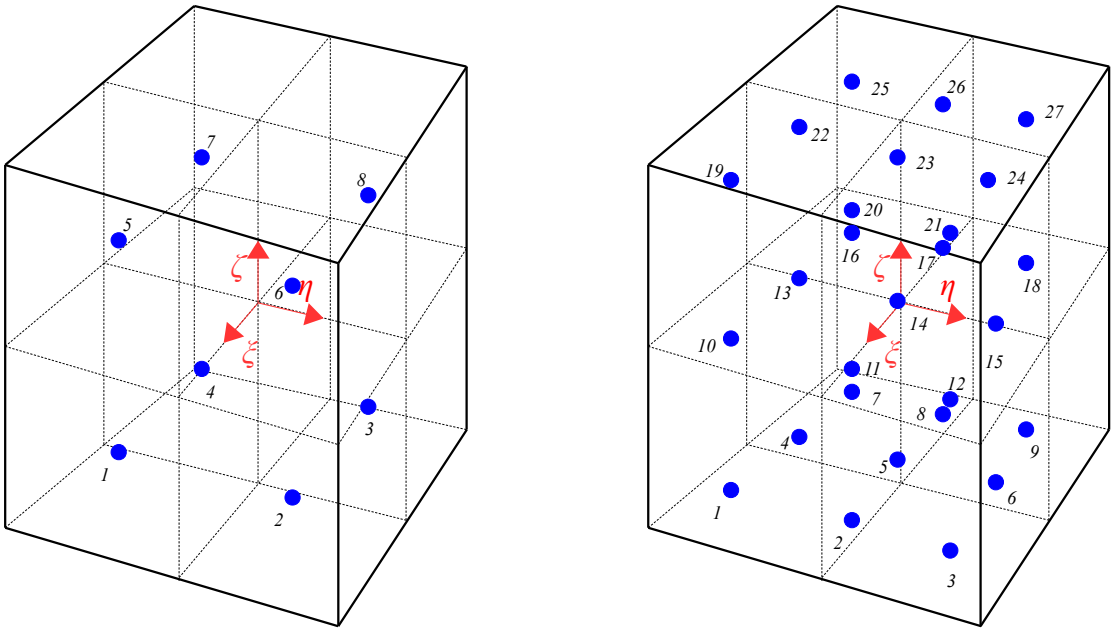

Figure 2.8 – The integration points of 8-node and 27-node hexahedron finite element

2.3 General 3D mesh generator

If "Calculate soil as solid element" is active FEM-Design automatically generates 3D finite elements for the SOIL object and compatible 2D and 1D mesh for the surface and line elements. FEM-Design 15 prefers to create hexahedron elements if possible but there are some geometrical cases where it uses tetrahedron, pyramid and wedge/prism elements in order to build an optimal spatial mesh. The 3D mesh can handle general shape of solids with geometrical situations considering boundary and inner geometry (see Fig. 2.9).

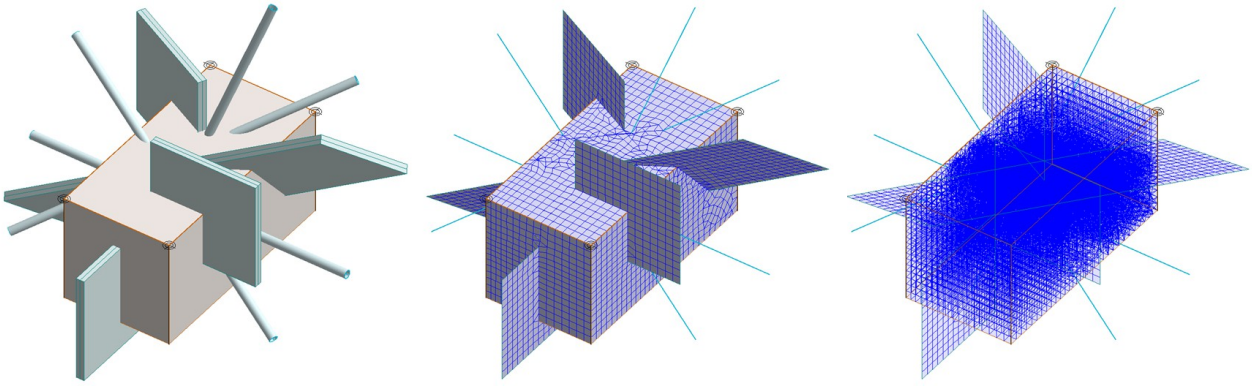

Figure 2.9 – The continuous automatic 3D mesh with inner 2D and 1D elements

3. Material models

In geomechanics the finite element method (FEM) is widely used for analyzing both ultimate limit states and servicebility limit states. FEM modelling of a geotechnical problem can offer insight into how stresses and strains distribute within the soil. This requires constitutive soil models (material models) that can predict stiffness and strength. With other words the deformation and the resistance of the soils. When the test data from the laboratory are reliable the results of the model should compare to them. For further information about soil material models and its connection with finite element calculation see: [14], [15], [16], [17], [18], [19], [20], [21], [22], [23], [24], [25], [26], [27], [28], [29], [30], [31], [32], [33] and [34].

The behaviour of soils may be modelled at different accuracy levels. In the mechanical computations the material model is the mathematical representation of the stress-strain relationship. In FEM-Design there are three different material models for soils. FEM-Design and its soil material models have been developed to perform mechanical computations of certain geotechnical problems. Keep in mind that the finite element simulation always only an approximation of the reality. This fact involves unavoidable modelling and numerical errors. It requires a different way of seeing to use the geotechnical model of FEM-Design because the accuracy of the model highly depends on the proficiency of the user. The users must have experience to modelling a problem, understanding the different soil models (and their purposes, limitations) and ability to evaluate the reliability of the mechanical results. (Similarly like other FE modelling but with more attention.)

3.1 Linear elastic material model

The linear elastic, isotropic material model is based on the general Hooke's law. This one is the most simple stress-strain relationship. In this case only two material parameters are independent [1], [5]. If the E (Young's modulus) and the ν (Poisson's ratio) are given the third paramater is not independent. Namely the G (shear modulus) can be expressed with Eq. 3.1. Although the linear elastic model only descripe the real behaviour of soils very poorly. It can be use to model very stiff subsoils, such as rocks, bedrocks. In this model the stress states are not limited at all, thus infinite stresses can arise according to the limitless strength.

$$G=\frac{E}{2(1+\nu)} \qquad \text{(Eq. 3.1)}$$

The linear elastic, isotropic material model gives us the relationship between the effective stress vector and strain vector. In matrix equation form Eq. 3.2 shows the relationship between them:

$$\boldsymbol{\sigma}'=\mathbf{D}\boldsymbol{\varepsilon} \qquad \text{(Eq. 3.2)}$$

where **D** is the material stiffness matrix (Eq. 3.3).

$$\mathbf{D}=\frac{E}{(1+\nu)(1-2\nu)}\begin{bmatrix} 1-\nu & \nu & \nu & 0 & 0 & 0 \\ \nu & 1-\nu & \nu & 0 & 0 & 0 \\ \nu & \nu & 1-\nu & 0 & 0 & 0 \\ 0 & 0 & 0 & \frac{1-2\nu}{2} & 0 & 0 \\ 0 & 0 & 0 & 0 & \frac{1-2\nu}{2} & 0 \\ 0 & 0 & 0 & 0 & 0 & \frac{1-2\nu}{2} \end{bmatrix} \qquad \text{(Eq. 3.3)}$$

Based on Eq. 3.1 the 4/4, 5/5 and 6/6 elements of **D** matrix are equal to the shear modulus. The 1/1, 2/2 and 3/3 elements of **D** matrix are the so-called oedometer modulus (E_{oed}) or with another name the compression modulus (M). Thus the relationship between Young's modulus and compression modulus:

$$E_{oed}=M=\frac{E(1-\nu)}{(1+\nu)(1-2\nu)} \quad ; \quad E=\frac{E_{oed}(1+\nu)(1-2\nu)}{(1-\nu)}=\frac{M(1+\nu)(1-2\nu)}{(1-\nu)} \qquad \text{(Eq. 3.4)}$$

3.2 Mohr-Coulomb material model

The associated linear elastic perfectly-plastic Mohr-Coulomb model imply four independent material parameters (see [35], [36] and [37]). The E (Young's modulus) and the ν (Poisson's ratio) have similar importance as in linear elasticity but by this material model two other parameters, namely the φ friction angle and the c cohesion are needed. These to parameters represent the strength properties of the soils. For each soil layers constant average material properties concidered but respect to a reference level settings the elastic parameters can be linearly various with depth. In this form the Mohr-Coulomb model does not include the stress dependency of the compression modulus. Effective stress states at failure are well described in drained situation using this criterion with effective strength parameters (φ' and c'). For undrained material the Mohr-Coulomb model may be used with zero friction angle and with the undrained shear strength (c_u) for cohesion. In that case note that the model does not contain the increasing of shear strength with consolidation (see Fig. 3.1).

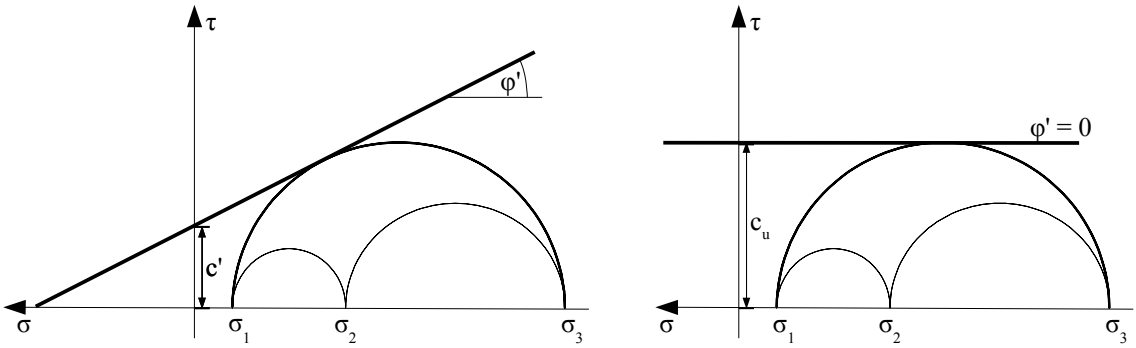

Figure 3.1 – Mohr's circles at yield, drained behaviour using effective strength parameters (left) and undrained behaviour using undrained strength parameters

3.2.1 The associated elasto-plastic material model

In FEM-Design the Mohr-Coulomb model is a so-called associated elasto-plastic model. In this case the $f(\boldsymbol{\sigma})$ flow rule (flow surface) which depends on the stress is equivalent to the plastic potential function which show us the direction of plastic strain increment. With this approximation the material stiffness matrices and the global structural stiffness matrices are symmetric. This is an advantage because the calculaton is time-saving.

The fundamental relation in a small strain plasticity is that a small strain increment is composed of an elastic and a plastic part (see [36], [38], [39] and [40]):

$$d\,\boldsymbol{\varepsilon} = d\,\boldsymbol{\varepsilon}^{e} + d\,\boldsymbol{\varepsilon}^{p} \qquad \text{(Eq. 3.5)}$$

In general perfect plasticity the plastic strains occur during yielding when

$$f(\boldsymbol{\sigma}) = 0 \qquad \text{(Eq. 3.6)}$$

and

$$\left(\frac{\partial f}{\partial \boldsymbol{\sigma}}\right)^{\mathrm{T}} d\,\boldsymbol{\sigma} = 0 \qquad \text{(Eq. 3.7)}$$

where $f(\boldsymbol{\sigma})$ is the mentioned flow rule (yield function) and $\boldsymbol{\sigma}$ is the stress vector ([36], [38], [41] and [42]). If the yield function $f(\boldsymbol{\sigma}) < 0$, it means that after a small increment the stress state is still linear elastic. With geometrical representation the stress state is located inside the flow surface (see Chapter 3.2.2). If the yield function $f(\boldsymbol{\sigma}) \geq 0$ (Eq. 3.6), it means that the stress state reached the end of the linear elastic behaviour. In this case there will be a plastic strain increment also. According to the normality rule (Eq. 3.7) the direction of the plastic strain is given if the direction of the stress increment is known. In this stress state as an elastic stress increment is related to an elastic strain increment by Hooke's law, using Eq. 3.5 gets:

$$d\,\boldsymbol{\sigma} = \mathbf{D}\,d\,\boldsymbol{\varepsilon}^{e} = \mathbf{D}\left(d\,\boldsymbol{\varepsilon} - d\,\boldsymbol{\varepsilon}^{p}\right) = \mathbf{D}\,d\,\boldsymbol{\varepsilon} - \mathbf{D}\,d\,\boldsymbol{\varepsilon}^{p} \qquad \text{(Eq. 3.8)}$$

where **D** is the linear elastic material stiffness matrix (see Eq. 3.3).

By finite element method a finite strain and finite stress increment are given in one load-step. Therefore it looks reasonable to rearrange Eq. 3.8 to:

$$d\,\boldsymbol{\sigma} = \mathbf{D}^{ep}\,d\,\boldsymbol{\varepsilon} \qquad \text{(Eq. 3.9)}$$

where $\mathbf{D}^{ep}$ is the so-called elasto-plastic material stiffness matrix. The following equations show the compilation of this matrix. In general plasticity the plastic strain increments are derived from a plastic potential $f(\boldsymbol{\sigma})$ which is equivalent with the yield function if the material model is associated.

$$d\,\boldsymbol{\varepsilon}^{p} = d\,\lambda\,\frac{\partial f}{\partial \boldsymbol{\sigma}} \qquad \text{(Eq. 3.10)}$$

where λ is the plastic multiplicator (a positive multiplier). To derive Eq. 3.9 firstly combine Eq. 3.8 and Eq. 3.10 into:

$$d\,\boldsymbol{\sigma} = \mathbf{D}\,\mathrm{d}\,\boldsymbol{\varepsilon} - d\,\lambda\,\mathbf{D}\,\frac{\partial f}{\partial \boldsymbol{\sigma}} \qquad \text{(Eq. 3.11)}$$

By subtitution Eq. 3.11 into Eq. 3.7 the λ plastic multiplicator is found to be:

$$0 = \left(\frac{\partial f}{\partial \boldsymbol{\sigma}}\right)^{\mathrm{T}} d\,\boldsymbol{\sigma} = \left(\frac{\partial f}{\partial \boldsymbol{\sigma}}\right)^{\mathrm{T}} \left(\mathbf{D}\,\mathrm{d}\,\boldsymbol{\varepsilon} - d\,\lambda\,\mathbf{D}\,\frac{\partial f}{\partial \boldsymbol{\sigma}}\right) \qquad \text{(Eq. 3.12)}$$

$$d\,\lambda = \frac{\left(\frac{\partial f}{\partial \boldsymbol{\sigma}}\right)^{\mathrm{T}} \mathbf{D}\,d\,\boldsymbol{\varepsilon}}{\left(\frac{\partial f}{\partial \boldsymbol{\sigma}}\right)^{\mathrm{T}} \mathbf{D}\,\frac{\partial f}{\partial \boldsymbol{\sigma}}} \qquad \text{(Eq. 3.13)}$$

Thus λ expressed by the known $f(\boldsymbol{\sigma})$ and **D**. With Eq. 3.13 the elasto-plastic material stiffness matrix is given:

$$\mathbf{D}^{ep} = \mathbf{D} - \frac{\mathbf{D}\,\frac{\partial f}{\partial \boldsymbol{\sigma}}\left(\frac{\partial f}{\partial \boldsymbol{\sigma}}\right)^{\mathrm{T}} \mathbf{D}}{\left(\frac{\partial f}{\partial \boldsymbol{\sigma}}\right)^{\mathrm{T}} \mathbf{D}\,\frac{\partial f}{\partial \boldsymbol{\sigma}}} \qquad \text{(Eq. 3.14)}$$

Based on Eq. 3.14 it is obvious that the elasto-plastic material stiffness matrix is symmetric if

the linear elastic perfectly plastic material model is associated (the yield function equivalent to the plastic potential).

3.2.2 The Mohr-Coulomb failure criteria

By the Mohr-Coulomb linear elastic perfectly-plastic material model the $f(\boldsymbol{\sigma})$ yield function is:

$$f(\boldsymbol{\sigma}') = \sigma'_1 - \sigma'_3 + (\sigma'_1 + \sigma'_3)\sin\varphi' - 2c'\cos\varphi' \qquad \text{(Eq. 3.15)}$$

where φ' is the effective friction angle and the c' is the effective cohesion [43]. Furthermore upon the strength parameters according to Chapter 1.3 this yield function depends on the effective principal stresses. Keep in mind that **negative normal stress components represent compression**.

This criteria (function) comes from the Mohr-Coulomb's theory. With the representation of Mohr's circle this function also can be defined as follows. In Fig. 3.2 or 3.4 there is a blue triangle. Lets write the sine funcion on this right-angled triangle with the notation of the figures:

$$\left[c'\cot\varphi' - \left(\frac{\sigma_3' + \sigma_1'}{2}\right)\right]\sin\varphi' = -\left(\frac{\sigma_3' - \sigma_1'}{2}\right) \qquad \text{(Eq. 3.16)}$$

Rearrange this equation:

$$2c'\cos\varphi' - (\sigma_3' + \sigma_1')\sin\varphi' = -(\sigma_3' - \sigma_1') \qquad \text{(Eq. 3.17)}$$

With the consideration that negative normal stresses represent compression, Eq. 3.18 can be formed.

$$0 = (\sigma_1' - \sigma_3') + (\sigma_1' + \sigma_3')\sin\varphi' - 2c'\cos\varphi' \qquad \text{(Eq. 3.18)}$$

Eq. 3.18 is equivalent with Eq. 3.15.

The active and passive stress state of earth pressure also represented with Eq. 3.17.

Fig. 3.2 shows a stress state which represents an active state of earth pressure [44]. The third effective principal stress is the minimum principal stress (compression is negative, see Eq. 1.5) and the first effective principal stress is the maximum principal stress.

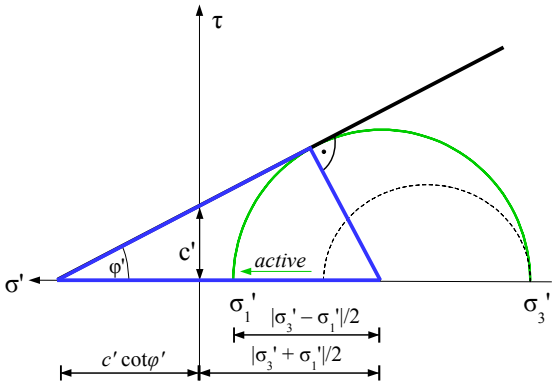

Figure 3.2 – Mohr's circle at active state

Based on this relationship and rearranging Eq. 3.17:

$$2c'\cos\varphi'+\sigma_3'(1-\sin\varphi')=\sigma_1'(1+\sin\varphi') \qquad \text{(Eq. 3.19)}$$

In active stress state regroup Eq. 3.19 the first (maximum) effective principal stress is the following:

$$2c'\frac{\cos\varphi'}{(1+\sin\varphi')}+\sigma_3'\frac{(1-\sin\varphi')}{(1+\sin\varphi')}=\sigma_1' \qquad \text{(Eq. 3.20)}$$

Using trigonometric relationships this formula is equivalent with Eq. 3.21.

$$2c'\tan\left(45^o-\frac{\varphi'}{2}\right)+\sigma_3'\tan^2\left(45^o-\frac{\varphi'}{2}\right)=\sigma_1' \qquad \text{(Eq. 3.21)}$$

Rewrite the contexts in the pharenthesis with the well-known notations[1]:

$$2c'\sqrt{K_a}+\sigma_3'K_a=\sigma_1' \qquad \text{(Eq. 3.22)}$$

1 Remember that the earth pressure at rest comes from the well-known Jáky's formula [44]. This formula shows the proportionality between the effective vertical and horizontal earth pressure at rest. Based on Jáky this earth pressure coefficient at rest: $K_0=1-\sin\varphi'=\frac{\nu}{1-\nu}$. Thus there is an unequivocal connection between the frictional angle and Poisson's ratio: $\nu=\frac{1-\sin\varphi'}{2-\sin\varphi'}$ or $\varphi'=\arcsin\left(\frac{1-2\nu}{1-\nu}\right)$.

The failure surface and the direction of the mobilized shear resistance (shear strength) in active stress state can be see in Fig. 3.3.

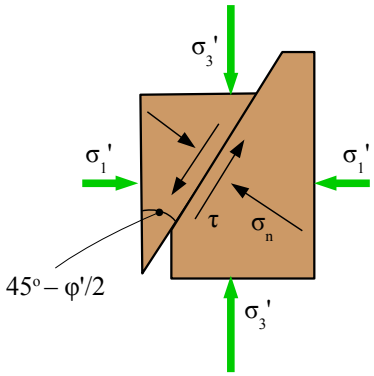

Figure 3.3 – Failure at active state

Fig. 3.4 shows a stress state which represents a passive state of earth pressure [44].

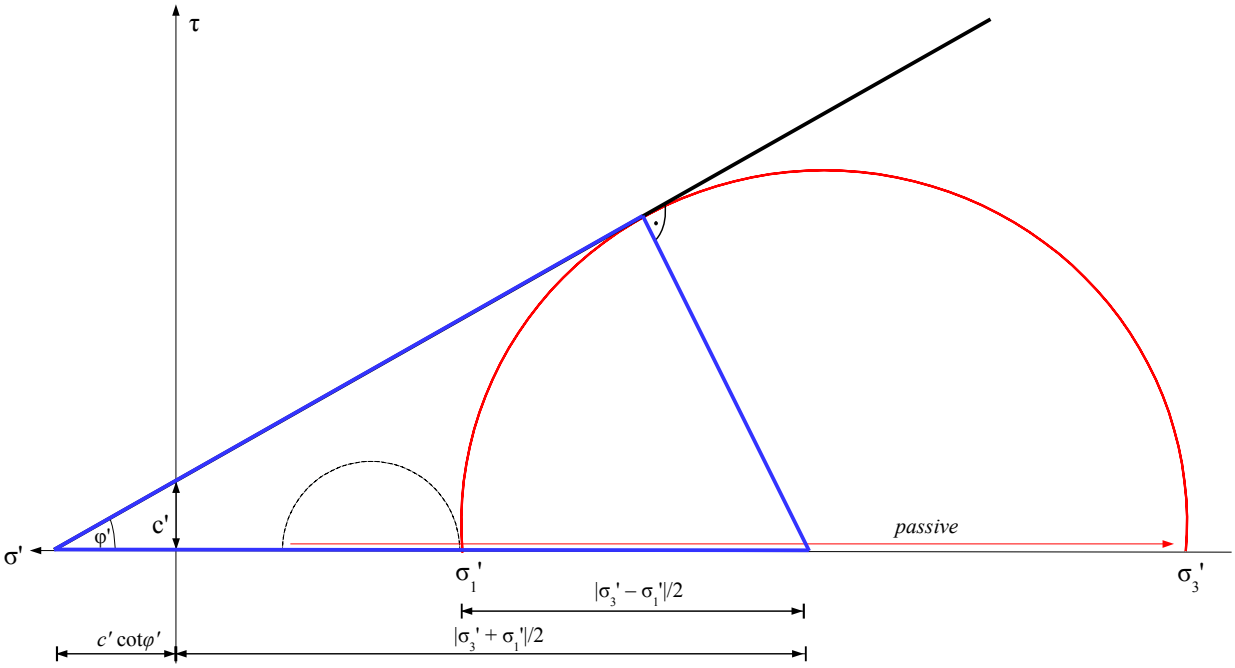

Figure 3.4 – Mohr's circle at passive state

Based on Eq 1.5 and rearranging Eq. 3.17:

$$-2c'\cos\varphi'+\sigma_1'(1+\sin\varphi')=\sigma_3'(1-\sin\varphi') \qquad \text{(Eq. 3.23)}$$

In passive stress state regroup Eq. 3.19 the third (minimum) effective principal stress is the following:

$$-2c'\frac{\cos\varphi'}{(1-\sin\varphi')}+\sigma_1'\frac{(1+\sin\varphi')}{(1-\sin\varphi')}=\sigma_3' \qquad \text{(Eq. 3.24)}$$

Using trigonometric relationships this formula is equivalent with Eq. 3.25.

$$-2c'\tan\left(45^o+\frac{\varphi'}{2}\right)+\sigma_1'\tan^2\left(45^o+\frac{\varphi'}{2}\right)=\sigma_3' \qquad \text{(Eq. 3.25)}$$

Rewrite the contexts in the pharenthesis with the well-known notations:

$$-2c'\sqrt{K_p}+\sigma_1'K_p=\sigma_3' \qquad \text{(Eq. 3.26)}$$

The failure surface and the direction of the mobilized shear resistance (shear strength) in passive stress state can be see at Fig. 3.5.

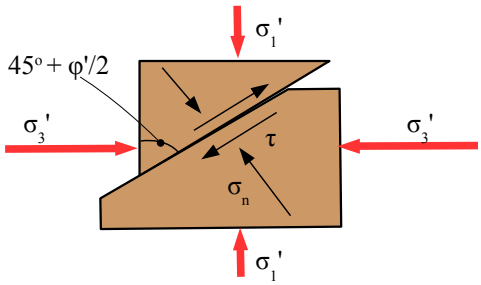

Figure 3.5 – Failure at passive state

Fig. 3.6 shows the 3D visualization of the Mohr-Coulomb failure surface in the principal stress space. One can see that it is a closed hypersurface in stress space and at the tensioned octant there is an apex [36]. Another popular view of the Mohr-Coulomb's surface can be see in Fig. 3.7 in front of the axis of hydrostatic pressure. In this view the section of the yield surface is an irregular hexagon. These visualizations are equivalent to the mathematical formula (Eq. 3.15) of Mohr-Coulomb criteria in a general 3D stress state.

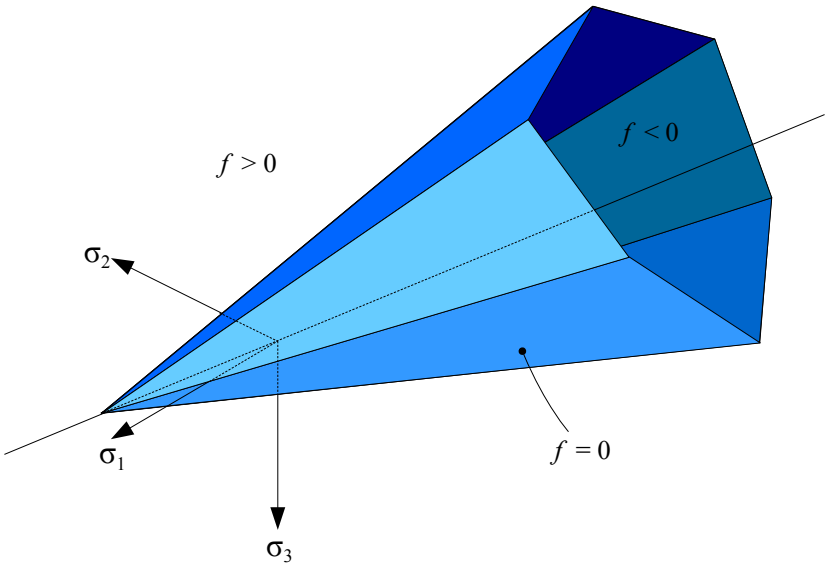

Figure 3.6 – The Mohr-Coulomb failure surface in principal stress space

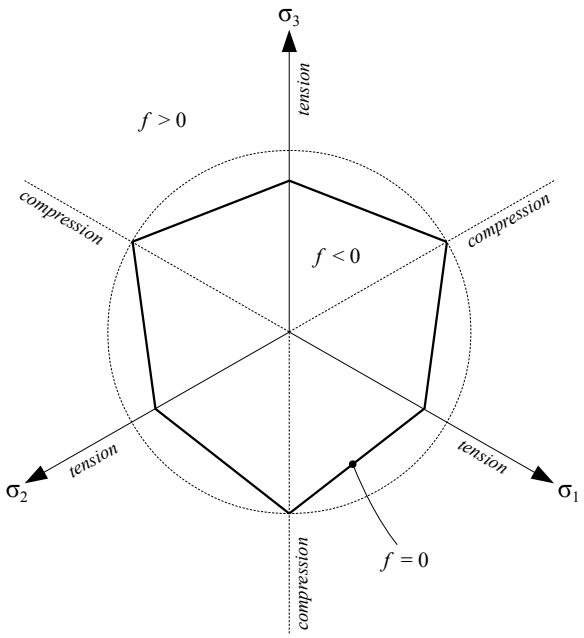

Figure 3.7 – The geometrical representation of the Mohr-Coulomb failure surface in π section

3.2.3. Returning map

For a finite strain increment the integration on Eq. 3.8 yields a finite stress increment.

$$\Delta\boldsymbol{\sigma}=\mathbf{D}\Delta\boldsymbol{\varepsilon}^{e}=\mathbf{D}\left(\Delta\boldsymbol{\varepsilon}-\Delta\boldsymbol{\varepsilon}^{p}\right)=\mathbf{D}\Delta\boldsymbol{\varepsilon}-\mathbf{D}\Delta\boldsymbol{\varepsilon}^{p}=\Delta\boldsymbol{\sigma}^{e}-\Delta\boldsymbol{\sigma}^{p} \quad \text{(Eq. 3.27)}$$

In this context the $\Delta\boldsymbol{\sigma}^{e}$ is usually referred to as the elastic predictor and the $\Delta\boldsymbol{\sigma}^{p}$ as the plastic corrector. In FE calculation finite load-increments are applied during the non-linear solution therefore after a load-step the stresses are assumed with an elastic predictor, see Eq. 3.28.

$$\boldsymbol{\sigma}_{B}=\boldsymbol{\sigma}_{A}+\Delta\boldsymbol{\sigma}^{e} \quad \text{(Eq. 3.28)}$$

But if this stress state is not valid based on the yield function (Eq. 3.15) an updated stress state is needed. The updated stresses are as follows (see also Fig. 3.8):

$$\boldsymbol{\sigma}_{C}=\boldsymbol{\sigma}_{A}+\Delta\boldsymbol{\sigma} \quad \text{(Eq. 3.29)}$$

$$\boldsymbol{\sigma}_{C}=\boldsymbol{\sigma}_{B}-\Delta\boldsymbol{\sigma}^{p} \quad \text{(Eq. 3.30)}$$

According to the normality rule (see Eq. 3.7 and Eq. 3.10) if the plasticity model is associated, the plastic corrector perpendicular to the yield surface. Basically this is the returning map algorithm which is applied if during the non-linear calculation the stress state with the predictor elastic stress increment (Eq. 3.28) is outside the flow surface (see Fig. 3.8).

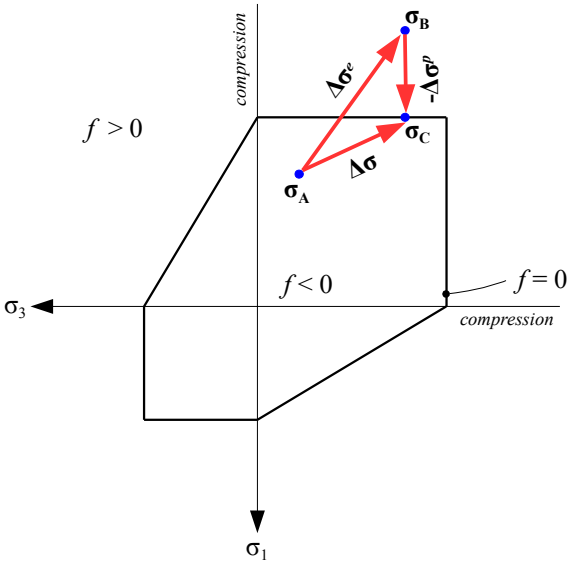

Figure 3.8 – The theory of returning map algorithm

3.3 Effective stress soil model for soft clays

When stress (load) is removed from a consolidated soil the soil will rebound, regaining some of the volume it had lost in the consolidation process (see [45], [46] and [47]). If the stress (load) is reapplied, the soil will consolidate again. The soil which had its load removed is considered to be overconsolidated. This is the case for soils which have previously had glaciers on them. The highest stress that it has been subjected to is termed the preconsolidation stress. A soil which is currently experiencing its highest stress is said to be normally consolidated. A soil could be considered underconsolidated immediately after a new load is applied but before the excess pore water pressure has had time to dissipate. **In FEM-Design always supposed that the excess water pressure has had time to dissipate thus the analysis always consider final state respect to time (time is not a variable).**

3.3.1 The over-consolidation ratio

The over consolidation ratio or OCRp is defined as the highest stress experienced (p_C' mean effective pre-consolidation pressure) divided by the current stress (p_0' mean effective stress) see Eq. 3.31. A soil which is currently experiencing its highest stress is said to be normally consolidated and to have an OCRp of one.

$$\mathrm{OCRp}=\frac{p_C'}{p_0'} \qquad \text{(Eq. 3.31)}$$

A soil is said to be normally consolidated (NC) if the current overburden pressure (column of soil overlying the plane of consideration) is the largest to which the mass has ever been subjected. It has been found by experience that prior stresses on a soil element produce an imprint or stress history that is retained by the soil structure until a new stress state exceeds the maximum previous one. The soil is said to be overconsolidated or preconsolidated (OC) if the stress history involves a stress state larger than the present overburden pressure [48]. Overconsolidated cohesive soils have received considerable attention. The behavior of overconsolidated soils under new loads is different from that of normally consolidated soils, so it is important to be able to recognize the occurrence. As mentioned earlier a normally consolidated soil has OCRp = 1 and an overconsolidated soil has OCRp > 1. OCRp values of 1-3 are obtained for lightly overconsolidated soils. Heavily overconsolidated soils might have OCRp-s > 6 to 8. An underconsolidated soil will have OCRp < 1. In this case the soil is still consolidating. Over- or preconsolidation may be caused by a geologically deposited depth of overburden hat has since partially eroded away [49]. Of at least equally common occurrence are preconsolidation effects that result from shrinkage stresses produced by alternating wet and dry cycles. These readily occur in arid and semiarid regions but can occur in more moderate climates as well. Chemical actions from naturally occurring compounds may aid in producing an overconsolidated soil deposit. Where overconsolidation occurs from shrinkage, it is common for only the top 1 to 3 meters to be overconsolidated and the underlying material to be normally consolidated. The OCRp grades from a high value at or near the ground surface to 1 at the normally consolidated interface.

The current mean effective pressure p_0' can be computed reasonably well, but the value of the mean effective preconsolidation pressure p_C' is at best an estimate, making a reliable computation for OCRp difficult. The only method at present that is reasonably reliable is to use the consolidation test to obtain p_C'. Preconsolidation pressure is the maximum effective stress that a particular soil sample has sustained in the past. This quantity is important in geotechnical engineering, particularly for finding the expected settlement of foundations and embankments [48].

Preconsolidation pressure cannot be measured directly, but can be estimated using a number of different strategies. Samples taken from the field are subjected to a variety of tests, like the constant rate of strain test (CRS) or the incremental loading test (IL). These tests can be costly due to expensive equipment and the long period of time they require. It is important to execute these tests precisely to ensure an accurate resulting plot. There are various methods for determining the preconsolidation pressure from lab data. The data is usually arranged on a semilog plot of the mean effective stress (p') or effective vertical stress versus the compression modulus (M). The constant rate of strain test approach for soil testing was developed initially as a means of measuring the properties of a soil. Because it is easy to automate, the CRS test method offers the advantage of continuous data collection during the loading process. Also from the test results we can get the stress-strain relationship of the soil specimen during the loading period. One can see these CRS results in Fig. 3.9 and 3.10 (see also [50], [51] and [52]).

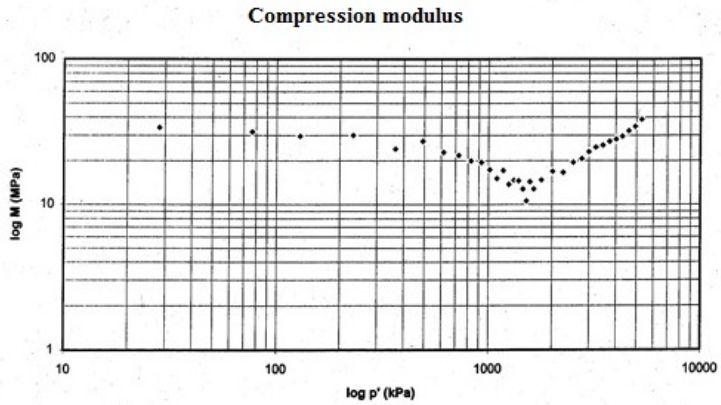

Figure 3.9 – Typical CRS test result [50]

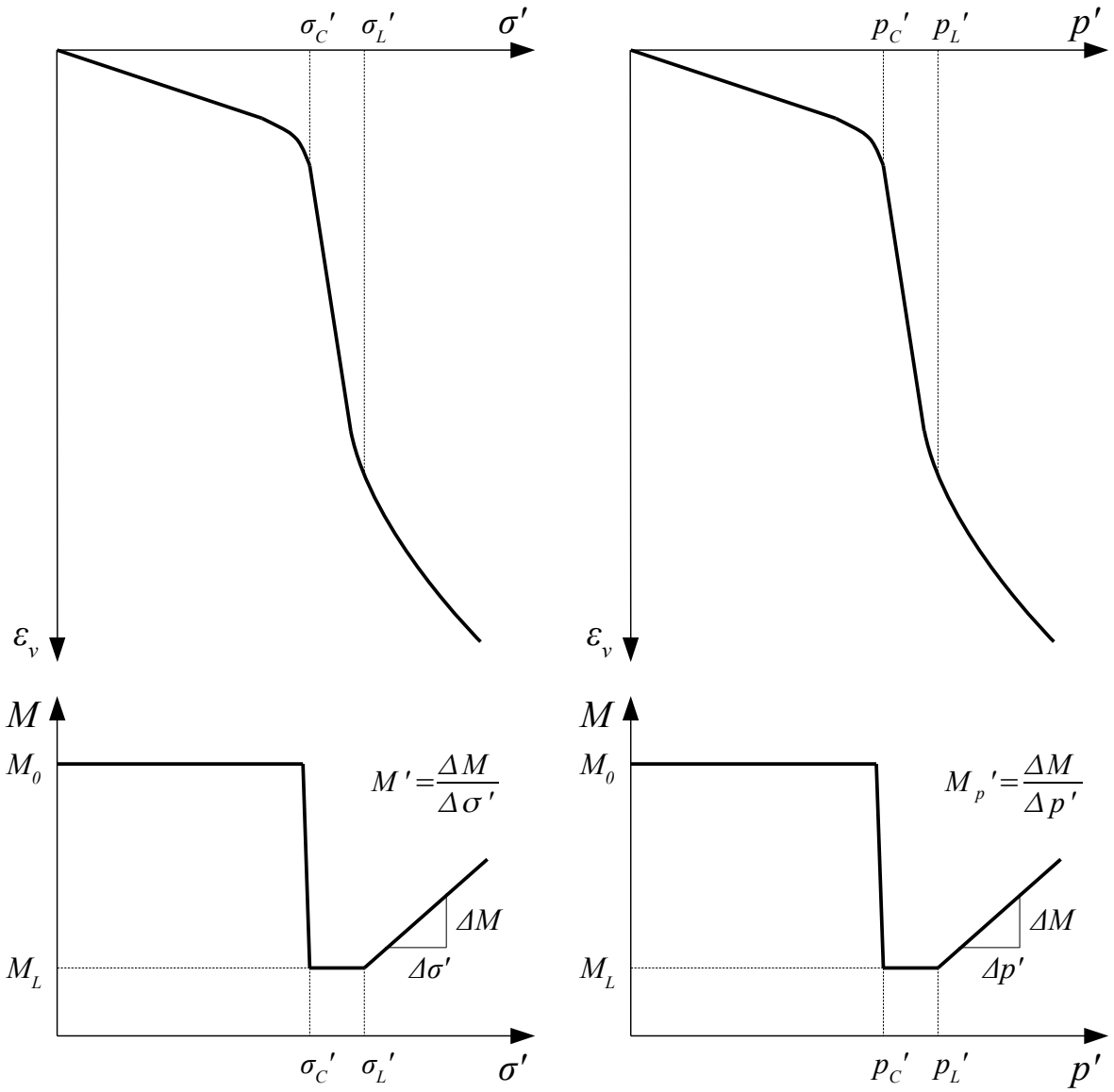

Figure 3.10 – Idealized CRS test result

3.3.2 Typical characterization of soft clays

Fig. 3.9 and 3.10 show that the compression modulus (Eq. 3.4) is stress dependant by some soft clays [53], [54] and [55]. If we would like to consider this effect during the settlement calculation an updated compression modulus (and because there is uneqiuvocal relationship with Young's modulus Eq. 3.4 and shear modulus Eq. 3.1), an updated material stiffness matrix is needed in every load-steps. In FEM-Design to follow this behaviour (Fig. 3.9 and 3.10) over-consolidated material model is available with two different input dialogs to describe the characterization of the stress-dependency.

3.3.3 The consideration of the stress dependency of compression modulus in soft clays

Based on Chapter 3.3.1, Eq. 3.31 and Fig. 3.10 the compression modulus is stress-dependent in some clays, such as Scandinavian clays [50], [51], [53], [55]. Based on Fig. 3.10 and Eq. 1.6 and 1.17 the considered compression modulus in FEM-Design after one load step depends on the first invariant of stresses in the former load-step.

The characteristics of the vertical effective stress (mean effective stress) and compression modulus diagrams are inputs in FEM-Design (see Fig. 3.11). There are two different options to give the stress-dependency in FEM-Design (over consolidated and generic model, see Fig. 3.11). Left side of Fig. 3.11 shows the known Swedish (Norwegian, Danish) characteristic of „vertical effective stress" („mean effective stress") - „compression modulus" diagram (over consolidated). But in FEM-Design it is calculated by mean effective stress because we are dealing with three dimensional problem. In the right side, after the preconsolidation vertical effective stress (preconsolidation mean effective stress) the user can implement an arbitrary dependency of compression modulus in the function of vertical effective stress (mean effective stresses) (generic).

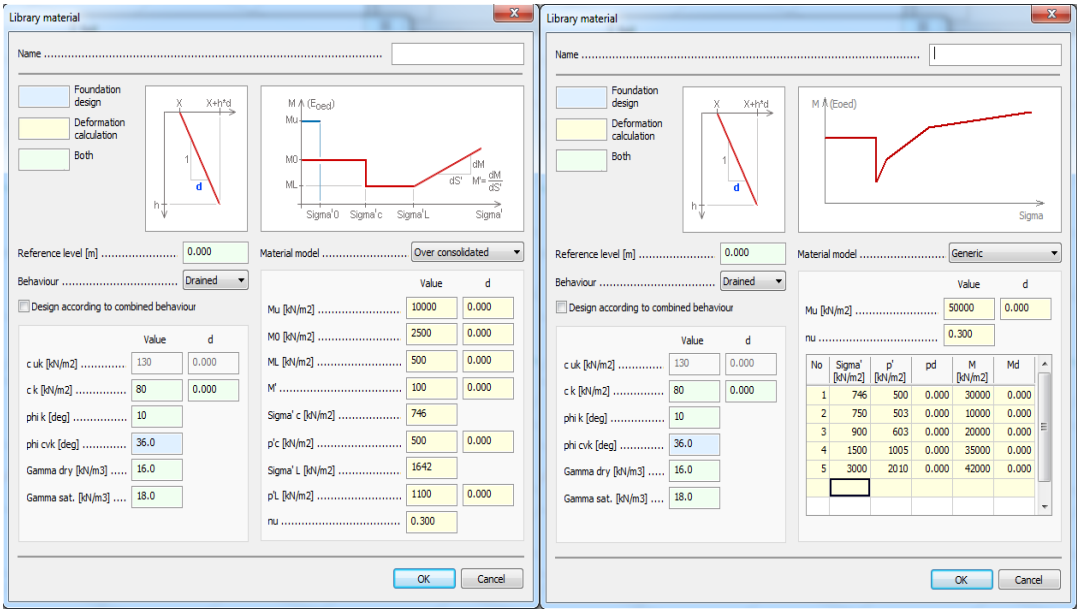

Figure 3.11 – The typified and the general stress-dependency for over-consolidated soils, only in this dialogs the σ' and p' values (compressions) have positive signs instead of negative

In the laboratory an idealized effective vertical stress – compression modulus curve will be measured (see Fig. 3.10 left side) but during the FEM-Design calculation the stress-dependency of the soil is up on the changing of the mean effective stresses (see Fig. 3.10 right side, Eq. 1.6 and the general informations about the material models in Chapter 3). **The exact connection between the effective vertical stress and mean effective stress is not known (because it is depend on the stress tensor, see Eq. 1.6) therefore during the adjustment of the curve the user can set the vertical effective stresses at the different stages (see Fig. 3.11) and FEM-Design automatically shows the relevant mean effective stresses with the**

assumption that the effective horizontal stresses are half of the effective vertical stresses thus the mean effective stresses are 2/3 of the effective vertical stresses (see also Eq. 4.18 with $K_0 = 0.5$ substitution). But because the connection between the effective vertical stress and mean effective stress is not exact the user can modify these default calculated mean effective stress values (see Fig. 3.11, e.g. $\sigma_c' \Longrightarrow p_c'$). It is available by over consolidated and generic model also.

After every load steps the material stiffness matrix will be updated with the relevant values of elastic constants based on the diagrams (see Eq. 3.3 and Eq. 4.16). For further information please check Chapter 4.5 and 5.3 also.

4. Finite element formulation

In this chapter the described equations and vectors in some case only belong to the solid element (soil) type thus not general for every finite element types, for further information on other element types please check the general „theory book" of FEM-Design or [8] and [9].

4.1 Solid element matrices and vectors

The approximation of the displacement field (Eq. 1.1) above an element can expressed with the following equation:

$$\mathbf{u}_e = \mathbf{N}\,\mathbf{v}_e \qquad \text{(Eq. 4.1)}$$

where **N** is a matrix containing the shape functions of the element and $\mathbf{v}_e$ is the nodal displacements respect to the element. According to Eq. 1.9 the connection between the diplacements and strains are as follows for an element:

$$\boldsymbol{\varepsilon}_e = \mathbf{L}\,\mathbf{u}_e \qquad \text{(Eq. 4.2)}$$

With the substitution of Eq. 4.1 into 4.2 this equation occurs:

$$\boldsymbol{\varepsilon}_e = \mathbf{L}\,\mathbf{N}\,\mathbf{v}_e \qquad \text{(Eq. 4.3)}$$

The product of the first two part of the right side of Eq. 4.3 is the strain matrix. From this point we use the following notation:

$$\mathbf{B} = \mathbf{L}\,\mathbf{N} \qquad \text{(Eq. 4.4)}$$

During the FE calculation after the mathematical (Chapter 2.1) and geometrical (Chapter 2.3) finitization the calculation of the stiffness matrices of the elements is coming. In general Eq. 4.5 shows the method of the calculation of the stiffness matrix for an element.

$$\mathbf{K}_e = \int_{V_e} \mathbf{B}^{\mathrm{T}}\,\mathbf{D}\,\mathbf{B}\,dV = \int_{V_e} \left(\mathbf{L}\,\mathbf{N}(\xi,\eta,\zeta)\right)^{\mathrm{T}}\,\mathbf{D}\left(\mathbf{L}\,\mathbf{N}(\xi,\eta,\zeta)\right)|\mathbf{J}(\xi,\eta,\zeta)|\,dV_{loc} \qquad \text{(Eq. 4.5)}$$

where addition to the presented values and variables **D** is the material model matrix (see Eq. 3.3 or Eq. 3.14) and **|J|** is the determinant of the Jacobian matrix which gives us the geometrical connection between the global and local (parametric) coordinate systems. The Jacobian matrix can expressed as follows:

$$\mathbf{J}=\begin{bmatrix} \frac{\partial x}{\partial \xi} & \frac{\partial y}{\partial \xi} & \frac{\partial z}{\partial \xi} \\ \frac{\partial x}{\partial \eta} & \frac{\partial y}{\partial \eta} & \frac{\partial z}{\partial \eta} \\ \frac{\partial x}{\partial \zeta} & \frac{\partial y}{\partial \zeta} & \frac{\partial z}{\partial \zeta} \end{bmatrix} = \begin{bmatrix} \frac{\partial}{\partial \xi} \\ \frac{\partial}{\partial \eta} \\ \frac{\partial}{\partial \zeta} \end{bmatrix} \mathbf{n}^{\mathrm{T}} \begin{bmatrix} x_1 & y_1 & z_1 \\ x_2 & y_2 & z_2 \\ x_3 & y_3 & z_3 \\ \dots & \dots & \dots \end{bmatrix}_{glob} \qquad \text{(Eq. 4.6)}$$

$$\mathbf{n}^{\mathrm{T}}=[N_1 \quad N_2 \quad N_3 \quad \dots] \qquad \text{(Eq. 4.7)}$$

where N_i is the shape function of a node and the right side of Eq. 4.6 is the matrix of the coordinates of the element nodes in global coordinate system.

The finite element calculations are unimaginable with analytical integration (see Eq. 4.5) thus during the calculation of the stiffness matrices numerical integration is necessary. Rewriting Eq. 4.5 gives us the following formula:

$$\mathbf{\Phi}(\xi,\eta,\zeta)=\mathbf{B}^{\mathrm{T}}\mathbf{D}\,\mathbf{B} \qquad \text{(Eq. 4.8)}$$

$$\mathbf{K}_{\mathbf{e}}=\sum_{i=1}^{n} w_i \mathbf{\Phi}(\xi_i,\eta_i,\zeta_i) \qquad \text{(Eq. 4.9)}$$

where Eq. 4.9 is the numerical integration with the well-known Gauss-Legendre formula (see Table 2) and w_i is the weigths of the different integration points.

After the calculation of the element stiffness matrices the calculation of the element load vectors is necessary. In addition to external forces and self-weights, kinematic loads are also an important load type. The calculation method of the kinematic loads are as follows:

$$\mathbf{p}_{\mathbf{e}}=\int_{V_e} \mathbf{B}^{\mathrm{T}}\mathbf{D}\,\boldsymbol{\varepsilon}_{\mathbf{0}}\,dV \qquad \text{(Eq. 4.10)}$$

where $\boldsymbol{\varepsilon}_{\mathbf{0}}$ is the vector of the kinematic loads on one element (such as thermal load or self-stress state (stress load)). For the rest of the load types (such as line load, surface load, point load), Eq. 4.11 shows the calculation method of the element load vectors.

$$\mathbf{p}_{\mathbf{e}}=\int_{V_e} \mathbf{N}^{\mathrm{T}}\mathbf{p}_{\mathbf{V}}\,dV+\int_{A} \mathbf{N}_A{}^{\mathrm{T}}\mathbf{p}_{\mathbf{A}}\,dA+\sum_{i=1}^{n} \mathbf{N}_{\mathbf{i}}{}^{\mathrm{T}}\mathbf{p}_{\mathbf{i}} \qquad \text{(Eq. 4.11)}$$

The first part of the right side of Eq. 4.11 represent the calculation of the load vector for volumetric loads, the second one for the surface loads and the third one for point loads.

4.2 Global equation system

In the former chapter the focus was on the stiffness matrices and load vectors of an element. In real life during the gemetrical finitization the modelled structure is splitted into several finite elements thus to calculate the displacements which are the main (master) variables (see Chapter 1) the compilation of the stiffness matrices and load vectors is necessary. After this step the global equation system of the structure can write as in Eq. 4.12.

$$\mathbf{K}\,\mathbf{v}=\mathbf{p} \qquad \text{(Eq. 4.12)}$$

where **K** is the global stiffness matrix, **p** is the global load vector and **v** is the global displacement vector which contains the displacements of the nodes.

4.3 Calculation of stresses

The final step of the finite element calculation is to express the stresses (internal forces). According to the finite element calculation the stresses are the slave (secondary) variables (see Chapter 1), thus during the finite element calculation only the essential boundary conditions (such as translation or rotation) are insured and the natural boundary conditions (such as strains, curvatures, bending moments or stresses) are not insured. In means that the convergence is very fast when the displacements are analyzed but the convergence can be very poor if stresses (internal forces) analyzed. **Therefore it is very important to use an accurate finite element mesh and element type group for the examined structure if we would like adequate results for stresses.** The displacements of an arbitrary „*P*" point can be expressed with Eq. 4.13.

$$\mathbf{u}_P=\mathbf{N}_P\,\mathbf{v}_\mathbf{e} \qquad \text{(Eq. 4.13)}$$

where $\mathbf{N}_P$ is the matrix of the shape functions – which belongs to the corresponding element which contains the selected „*P*" point – evaluated in the selected „*P*" point and $\mathbf{v}_\mathbf{e}$ is the nodal displacements of the corresponding element. With the displacements of the selected point the calculation of the stresses comes from Eq. 4.14 (see Eq. 4.3).

$$\boldsymbol{\varepsilon}_P=(\mathbf{L}\,\mathbf{N})_P\,\mathbf{v}_\mathbf{e} \qquad \text{(Eq. 4.14)}$$

With the strains the stresses can be expressed with the following equation:

$$\boldsymbol{\sigma}_P=\mathbf{D}(\boldsymbol{\varepsilon}_P-\boldsymbol{\varepsilon}_{0\,P}) \qquad \text{(Eq. 4.15)}$$

where ε_{0P} is the kinematic load in the selected „*P*" point.

4.4 The basics of non-linear calculation method in FEM-Design

When the non-linear soil calculation is active in FEM-Design, during the calculation the small displacement theory (small strains, geometrical linearity) is considered. It means that the nonlinearity comes from the consideration of nonlinear material models (Mohr-Coulomb plasticity, consideration of the stress dependency of compression modulus, etc.). It is an adequate assumption because in general when the settlements are out of small displacement theory the foundation is failed already due to plasticity.

During the nonlinear calculation Eq. 4.12 will be solved several times in respect to the relevant load steps (see Fig. 4.1). It is important that according to Eq. 3.3 and 3.14 the coefficient global stiffness matrix (Eq. 4.12) is always symmetric.

By the non-linear calculation in every load steps the element stiffness matrices will be calculated with Eq. 4.16 and 4.17.

$$\mathbf{K}_e = \int_{V_e} \mathbf{B}^T \mathbf{D}\, \mathbf{B}\, dV = \int_{V_e} (\mathbf{L}\,\mathbf{N}(\xi,\eta,\zeta))^T \mathbf{D}(\xi,\eta,\zeta)(\mathbf{L}\,\mathbf{N}(\xi,\eta,\zeta))|\mathbf{J}(\xi,\eta,\zeta)|dV_{loc} \quad \text{(Eq. 4.16)}$$

$$\mathbf{K}_e = \int_{V_e} \mathbf{B}^T \mathbf{D}^{ep}\, \mathbf{B}\, dV \quad \text{(Eq. 4.17)}$$

The difference between Eq. 4.16 and Eq. 4.5 is that the material stiffness matrices depends on the former stress state of the element (because the compression modulus could be stress-dependent, see Chapter 3.3), therefore it could be different in every integration points. When the Mohr-Coulomb plasticity is considered the material stiffness matrices (Eq. 4.17, $\mathbf{D}^{ep}$) based on Eq. 3.14.

4.4.1 The explicit solver method

FEM-Design uses explicit solver type to calculate the displacements of the structure if non-linear soil calculation is active. Based on the theory of the explicit method in the current load step calculation the stresses of the former step will be used. It means that during the calculation the material stiffness matrices (Eq. 4.16 and 4.17) in one load step will be calculated based on the calculated stresses at the integration points (see Chapter 2.1) in the end of the former load step. The whole calculation starting with an initial load step (see Fig. 4.1). After this step the increment of the displacements and stresses will be calculated and based on these data the next load step will be calculated until the total load reaches the 100 % of the applied load. It means that due to the explicit method at the end always get a solution, but for example **if the soil reaches its load-bearing capacity the quantity of the displacements or volumetric strains will be very large. In this case after the calculation „large nodal displacement" and/or „large volumetric strain" messages will be appear.**

By a general non-linear problem the exact solution is not known (such as the exact deflection for a simple slab with an arbitrary geometry). In this case if the solver uses smaller and smaller load-steps the calculated solution approaches the not known exact solution (see Fig. 4.1). It means that the solution converges to the exact solution (such as the stresses/internal forces when using smaller and smaller finite element mesh size for a linear calculation). Thus a non-linear calculation is very difficult because a sufficient finite element mesh is necessary for the analyzed problem and also a sufficient load-step control.

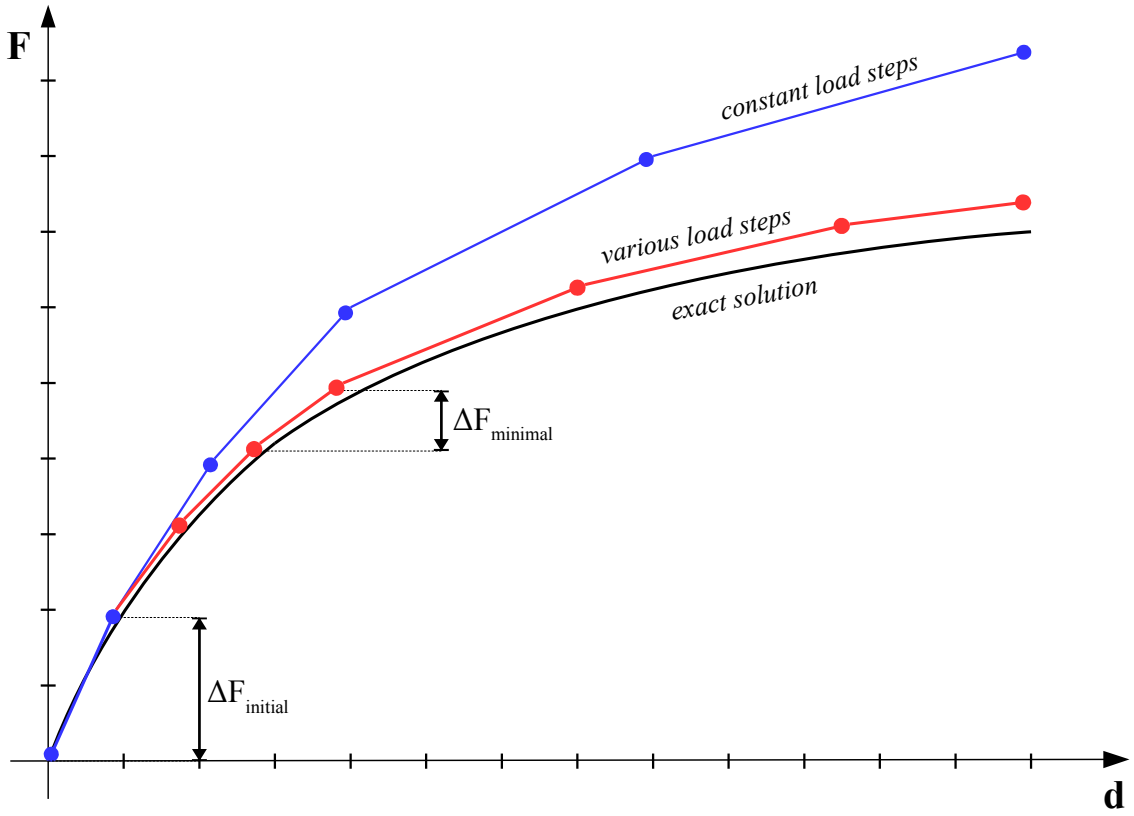

Figure 4.1 – Basic idea of the explicit solver method and the different types of load step controlling

4.4.2 Parameters to control the load-increments

The non-linear soil calculation (NLS) option contains four control parameters to reach the accurate final solution. These four parameters are as follows: initial load step [%], minimal load step [‰], volume ratio of nonlinearly active elements in one step [%] and volume ratio of plastic elements in one step [%]. By the calculation options it is optional to choose and consider the Mohr-Coulomb plasticity or only the stress-dependency for the soil (see Chapter 3.2 and 3.3).

The meaning of the first two control parameters is obvious from Fig. 4.1. The „initial

load step" is the amount of the first load step and must be given in percent [%] of the total load (see. Fig. 4.1). The „minimal load step" is the smallest load step which is possible during the calculation. It must be given in thousandths [‰] of the total load (see Fig. 4.2). It means that during the finite element calculation the smallest load step will be this minimal load step value. The third and the fourth mentioned control parameters are responsible for the automatic various load stepping to reach more precise solution than the constant load-step calculation (see Fig 4.1). The „volume ratio of nonlinearly active elements in one step" parameter is responsible to control the stress-dependant compression modulus. It means that during the calculation at most these value of soil volume can change its compression modulus. The „volume ratio of plastic elements in one step" parameter is responsible to control the Mohr-Coulomb plasticity. It means that during the calculation at most these value of soil volume can change from elastic to plastic condition. These two parameters must be given in percent [%]. To avoid infinitely small load-steps the „minimal load step" overwrite these last two parameters if in one step the load step is smaller than the minimal load step based on the third and fourth parameters. Thus in every case the minimal value of the load step is at least equal to the minimal load step parameter (see Fig 4.1).

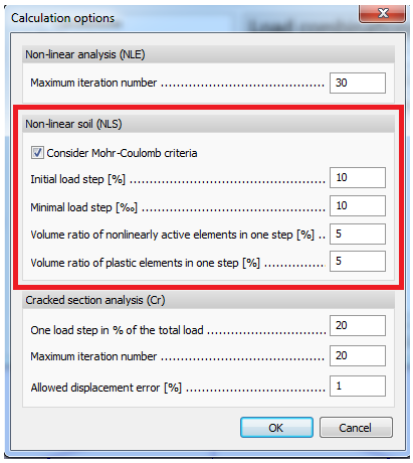

Figure 4.2 – The calculation options for non-linear soil analysis

4.5 Consideration of different load phases

In FEM-Design the non-linear soil calculation (NLS) is implemented with consideration of different phases. In this chapter the reader can find an introdution how these phases work and in which phase what will be calculated in the different load-combinations and material models. In FEM-Design there are three different automatic phases which will be explained here. The non-linear soil calculation only valid by load-combination calculations. Fig. 4.3 shows the explained example.

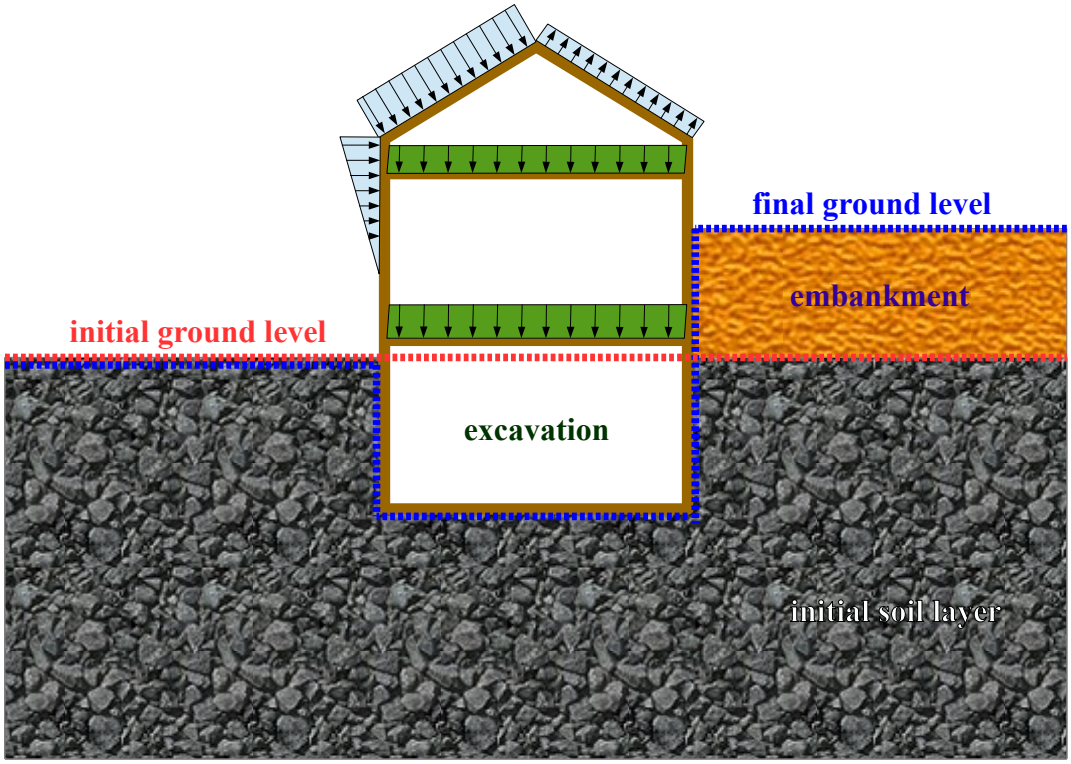

Figure 4.3 – The consideration of earth pressures and external loads in different phases

4.5.1 Phase 0

In Phase 0, FEM-Design calculates the stresses based on an analytical approximation according to the earth pressure coefficient at rest (in FEM-Design the K_0 value depends on the Poisson's ratio (see the first footnote in Chapter 3.2.2)) for the given initial (intact) ground level. This is important for the OCRp calculations, because we need these pressure values for the initial ground level. See the repeated equation below from Chapter 3.3.1. Fig. 4.4 and 4.5 shows the mean effective stress (p_0') which comes from the mentioned Phase 0 calculation. Based on these thoughts and Eq. 1.17 this p_0' equal to:

$$p_0' = \frac{\sigma_{x0}' + \sigma_{y0}' + \sigma_{z0}'}{3} = \frac{K_0\sigma_z' + K_0\sigma_z' + \sigma_z'}{3} = \frac{2K_0\sigma_z' + \sigma_z'}{3} = \sigma_z'\left(\frac{2K_0+1}{3}\right) \quad \text{(Eq. 4.18)}$$

When only the Mohr-Coulomb material model is in use these values do not have any effect on the calculation because the compression modulus is independent from stresses in the Mohr-Coulomb model during the linear elastic behaviour (before plasticity).

By the soft soil model see the meaning of the p_0' value in Fig 4.4 and 4.5. In FEM-Design in the result window the user can check the OCRp values in the integration points after the calculation, thus the user can check that the adjusted p_C' values in the material models are correct or not (see Fig. 4.6). This is the first reason why this calculation in Phase 0 is important. The second reason is that by the soil definition the user can adjust two different ground levels.

One of these ground level is the initial (intact) ground level (see Fig. 4.3 and 4.5). Based on this ground level the calculations of Eq. 4.18 are settled. The other ground level is the final ground level (see Fig. 4.3) which affect the final finite element calculation. The details of this final ground level is given in the next chapters (Chapter 4.5.2 and 4.5.3).

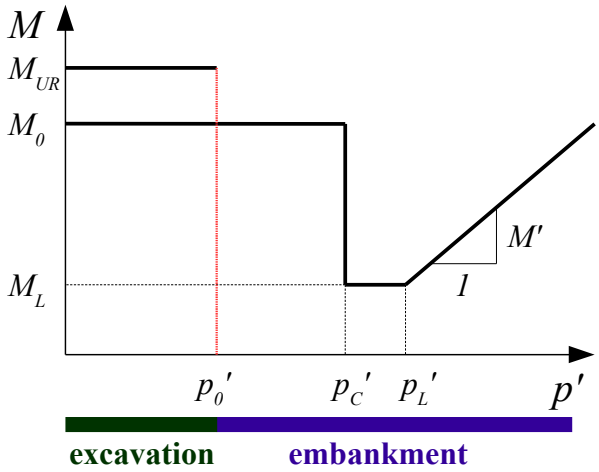

Figure 4.4 – The consideration of stress dependent compression modulus, only in this diagram the p' values (compressions) have positive signs instead of negative

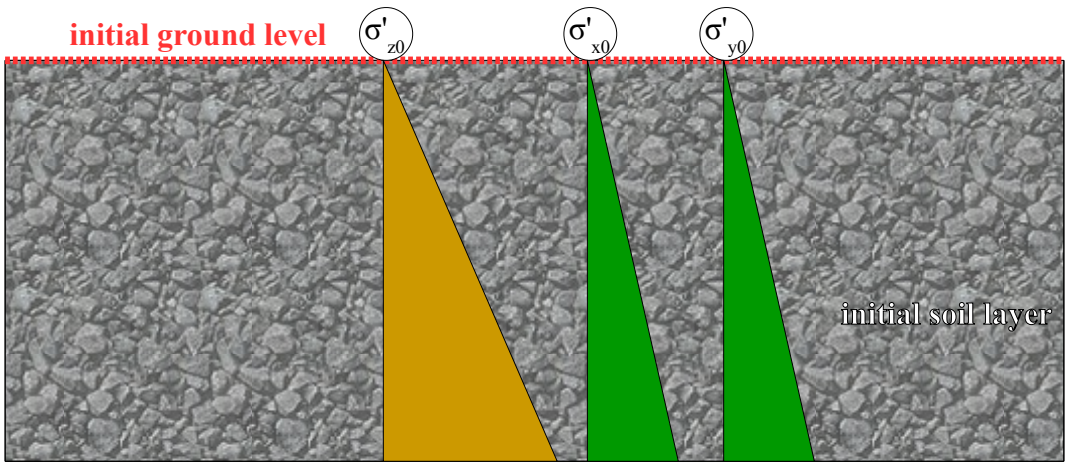

Figure 4.5 – The consideration of stresses in the soil in Phase 0

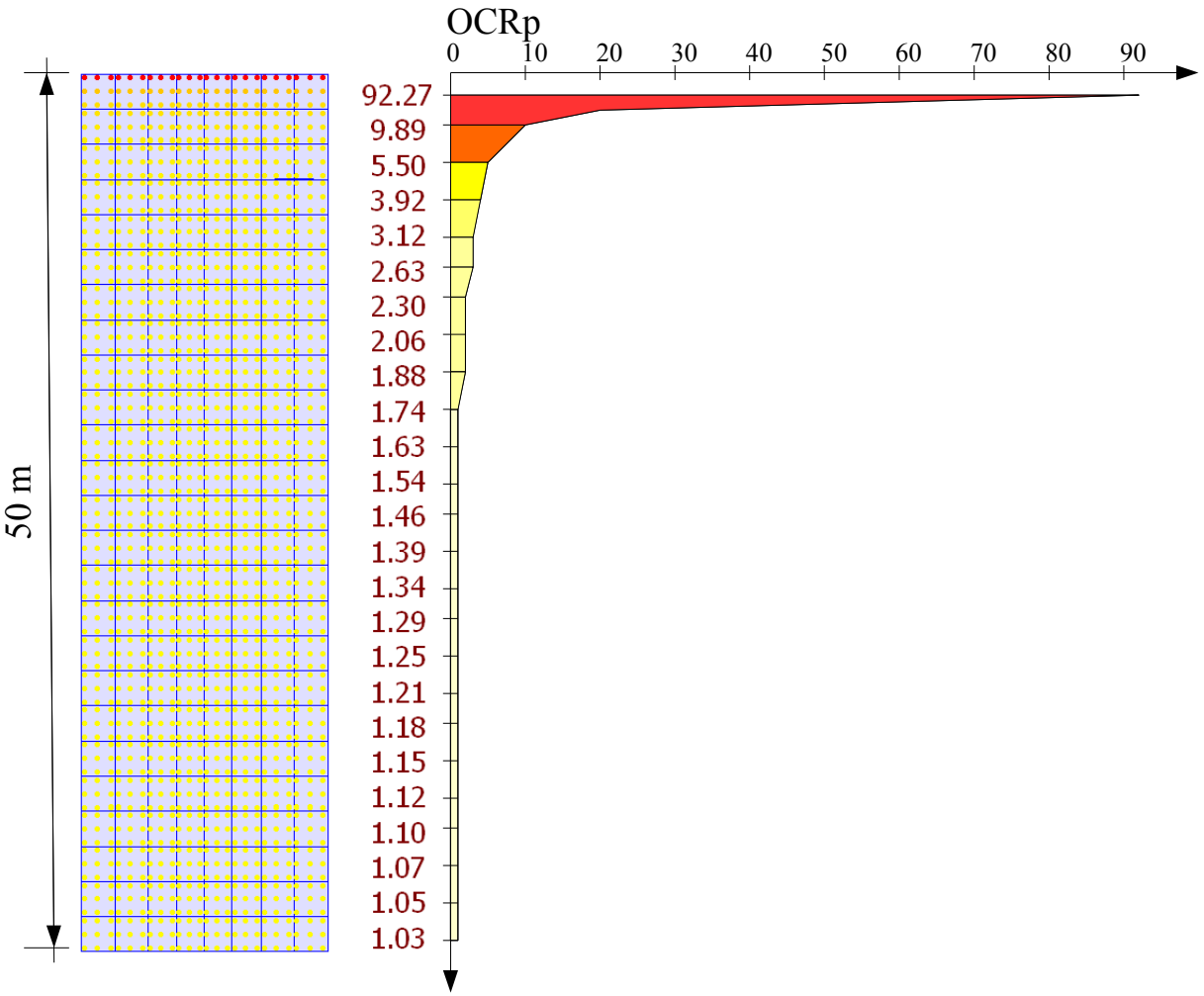

Figure 4.6 – An example for the different calculated OCRp values with depth based on Phase 0 and p_C'

4.5.2 Phase 1

In this phase the first part of the real finite element calculation is happening. In Phase 1 the self-stress state of the soil will be calculated based on the final ground level (see Fig. 4.7). In this phase only the self-weight of the soil is considered. It means that if none of the applied load cases in the active load-combination contains the self-weight of the soil then this phase will be skipped.

This phase is important by the Mohr-Coulomb material model and by the soft clay material models also, because due to the self-weight of the soil the intergation points can be in plastic state, it depends on the material parameters and the geometry also.

For the soft clay material models this phase also important because based on Fig. 4.4 and 4.7 the relevant compression modulus which need to be applied by the rest of the loads (every other load case in the load-combination above the self-weight of the soil) are defined according to this calculation.

If the user defined an excavation (Fig. 4.7), it means that based on Phase 0 the soil stress states under the excavation are below p_0' values. Until the stress states of these points based on the rest of the external loads (Fig. 4.3) do not reach p_0' values the compression modulus equal to M_{UR}. Practically it means that in the end of Phase 2 at the excavation the settlements will be very small as long as the stress states are below the calculated p_0' in Phase 0. After p_0' values the settlements depends on the characteristics of the applied soft soil model.

If the user defined an embankment (Fig. 4.7), it means that based on Phase 0 the soil stress states under the embankment are above p_0' values. The compression modulus of the soil under the embankment depends on the rest of the external loads, because the stress states are above p_0' values (Fig. 4.4). Practically it means that under the embankment the settlements depends on the characteristics of the applied soft soil model.

By the results if only the self-weight of the soil is applied in the NLS combination (no external loads), the displacements will be shown due to the self-weight of the soil and in this case Phase 2 will be skipped.

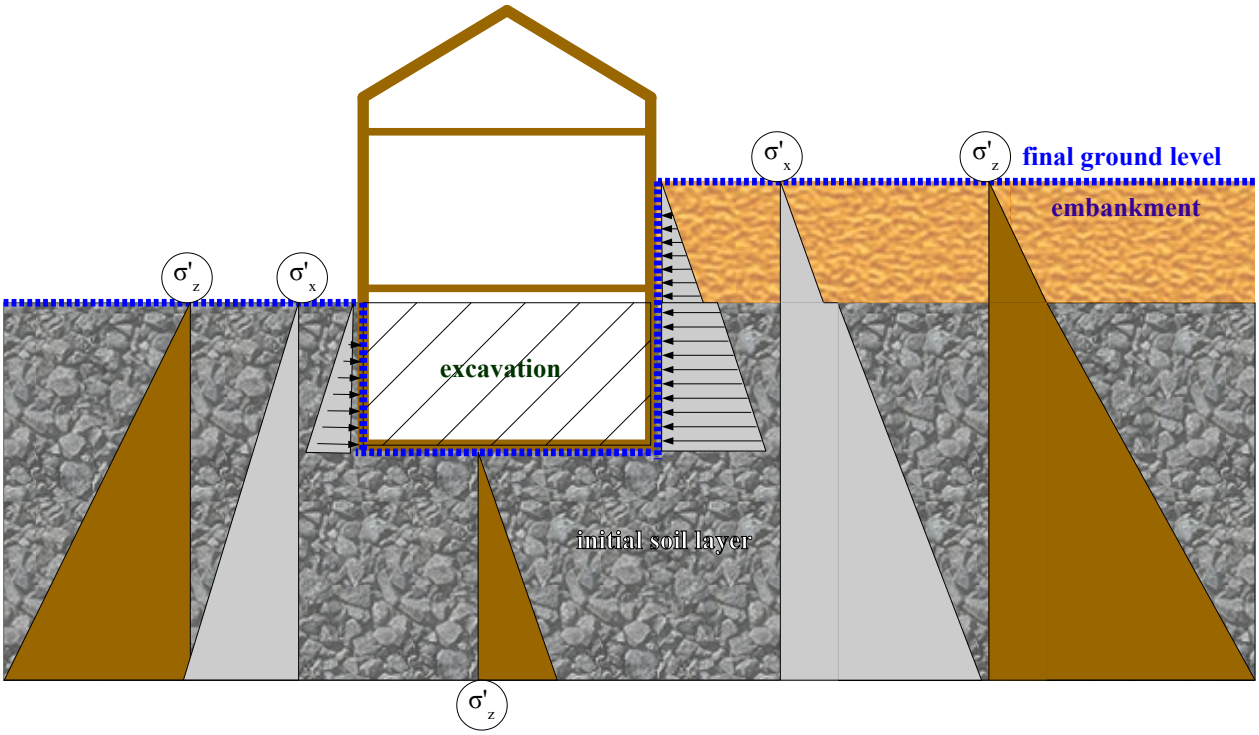

Figure 4.7 – The consideration of stresses in the soil in Phase 1

4.5.3 Phase 2

In this phase the rest of the loads in the combination will be considered (external loads, Fig. 4.8). The considered elastic modulus in one load step depend on the stress states of the soil what were calculated in Phase 1, considering Phase 0 (see Chapter 4.5.2). Phase 2 only active if in the NLS combination contains not only the self-weight of the soil but also contain other external loads. **If Phase 2 exists then the settlements (displacements) at the end of the**

calculation do not contain the displacements that comes from the self-weight of the soil (what was calculated in Phase 1). Practically, it means that if Phase 1 and Phase 2 are also active, at the end of the calculation FEM-Design subsracts the displacements of Phase 1 from the total displacements (Phase 1 displacements + Phase 2 displacements). It is reasonable because the calculations in Phase 1 only set the correct stress states of the soil for the adequate consideration of the Mohr-Coulomb material model and soft clay models for the applied external loads on the structure in the NLS load-combinations.

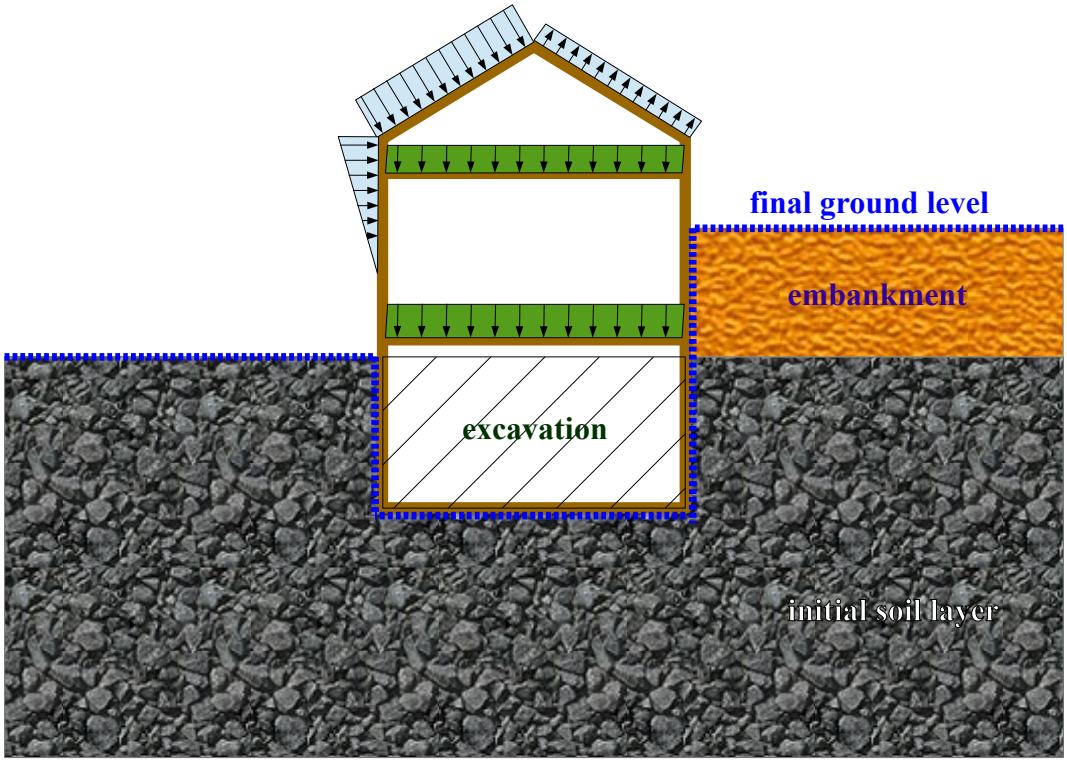

Figure 4.8 – The consideration of external loads in Phase 2

5. Soil problems with exact theoretical solutions in 3D

5.1 Verification and validation of linear elastic material model

Several elasticity problems is available with known exact solutions. As a benchmark some problems and results will be demonstrated. In this chapter several 3D linear elastic problems are described. The appropriate analytical solution may be found in the literature such as [56], [57], [58], [59], [60], [61], [62] and [63].

5.1.1 Linear elastic deformation of a cuboid

In this chapter the main purpose is to certify the linear elastic deformation based on general Hooke's law on a 2x2x2 m cuboid element with different supports and load cases (see Fig. 5.1). Four different pure stress states were analyzed and after the FEM-Design calculations the analytical solutions are also represented based on linear elasticity. The Young's modulus and the Poisson's ratio were $E = 1000$ kN/m^2 and $\nu = 0.3$ respectively in all analyzed case. Based on these two values the shear modulus $G = 384.6$ kN/m^2 . The relevant coordinate system which is valid for all figure in this subchapter can be seen in Fig. 5.2.

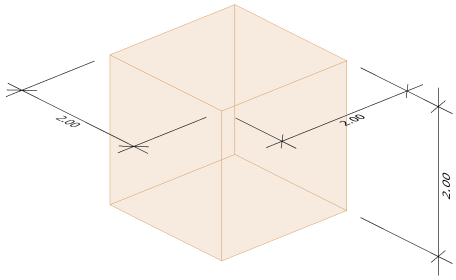

Figure 5.1 – 2x2x2 m *cuboid*

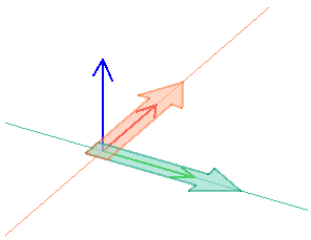

Figure 5.2 – Directions of the global coordinate system (X green, Y red, Z blue)

5.1.1.1 Uniaxial loading

In this first case uniform vertical distributed surface load was applied on the top of the cuboid element with $\sigma_z = -10$ kN/m^2 intensity (Fig. 5.3). At the bottom there is a vertical surface support. At two corner points of the bottom two other point supports were applied to ensure the statically determinated system.

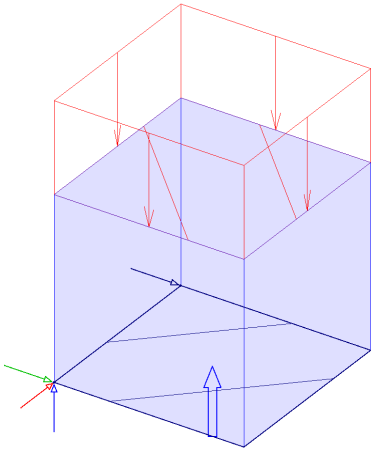

Figure 5.3 – Uniaxial compression [$\sigma_z = -10$ kN/m^2] *and applied boundary conditions*

Based on the FEM-Design calculation the following displacement results revealed (see Fig. 5.4).

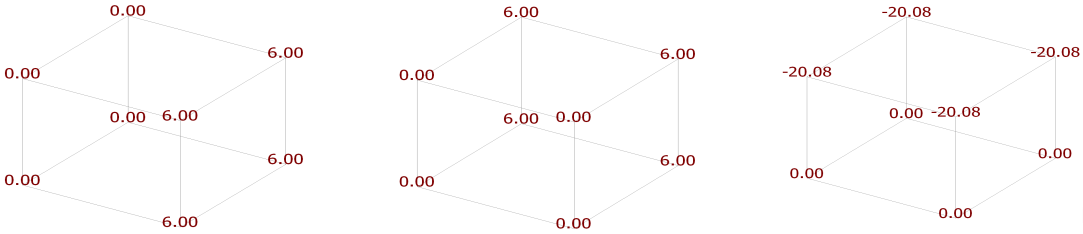

Figure 5.4 – Corner point translations in X, Y and Z directions [mm]

Based on the general Hook's law the theoretical results of these translations are the following:

$$u_z = \frac{\sigma_z l_z}{E} = \frac{-10 \cdot 2}{1000} = -0.020 \text{ m} \quad , \quad u_x = u_y = -\nu\, u_z = 0.3 \cdot 0.020 = 0.006 \text{ m} \qquad \text{(Eq. 5.1)}$$

The exact and the calculated values are very close to each other.

5.1.1.2 Shear loading

In this case shear load was applied on the cuboid element as distributed loads (see Fig. 5.5) with $\tau_{zy} = \tau_{yz} = -10$ kN/m^2 intensity. At the bottom there is a vertical surface support and horizontally also at the left and right side (see Fig. 5.5). At the front bottom edge a horizontally line support was also applied perpendicular to this edge to ensure statically determinancy.

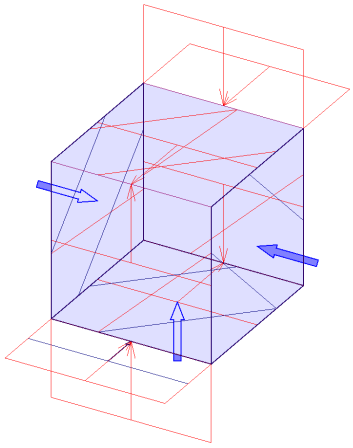

Figure 5.5 – Shear loading [$\tau_{yz} = -10$ kN/m^2] *and applied boundary conditions*

Based on the FEM-Design calculation the following diplacement results revealed (see Fig. 5.6).

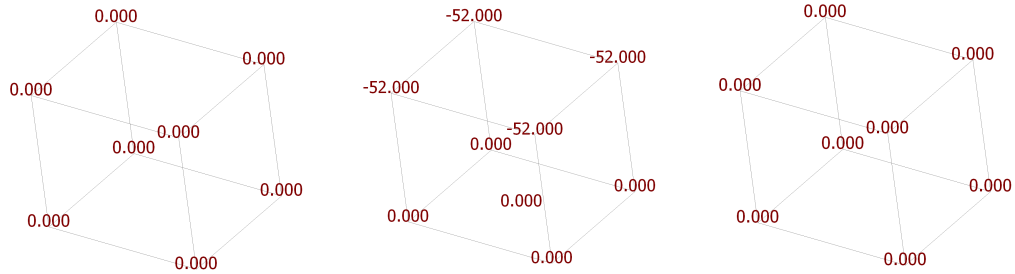

Figure 5.6 – Corner point translations in X, Y and Z directions [mm]

Based on the general Hook's law the theoretical results of these translations are the following:

$$u_x = u_z = 0\,\text{m} \quad , \qquad \text{(Eq. 5.2)}$$

according to the shear deformation and small displacement theory.

$$\gamma_{yz} = \frac{u_y}{l_z} \quad , \quad u_y = \frac{\tau_{yz}}{G} l_z = \frac{-10}{384.6} 2 = -0.052\,\text{m} \qquad \text{(Eq. 5.3)}$$

The exact and the calculated values are very close to each other.

5.1.1.3 Biaxial loading

During a biaxial pure stress state $\sigma_z = -10$ kN/m^2 vertical and $\sigma_y = -5$ kN/m^2 distributed surface loads were applied. At the bottom there is a vertical surface support and horizontally also at the left, right and rear side (see Fig. 5.7).

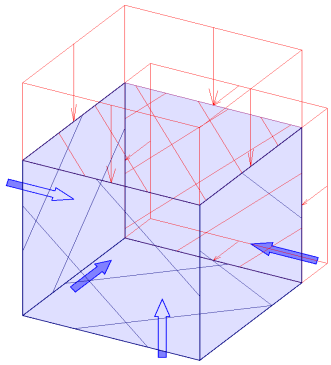

Figure 5.7 – Biaxial loading [$\sigma_z = -10$ kN/m^2 *and* $\sigma_y = -5$ kN/m^2] *and applied boundary conditions*

Based on the FEM-Design calculation the following diplacement results revealed (see Fig. 5.8).

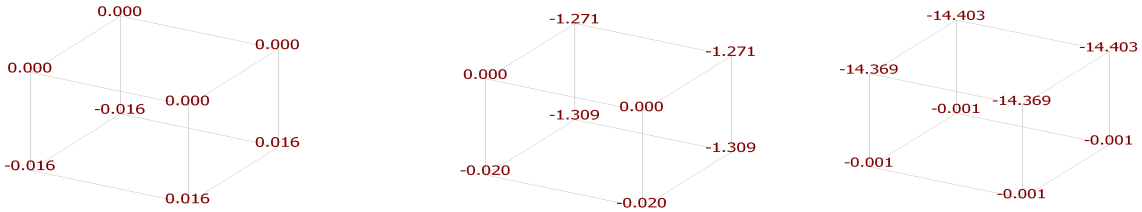

Figure 5.8 – Corner point translations in X, Y and Z directions [mm]

Based on the general Hook's law the theoretical results of these translations are the following:

$$\sigma_x = \nu(\sigma_y + \sigma_z) = 0.3((-5)+(-10)) = -4.5\,\frac{\text{kN}}{\text{m}^2} \qquad \text{(Eq. 5.4)}$$

according to the supports:

$$u_x = 0\,\text{m} \qquad \text{(Eq. 5.5)}$$

According to Hooke's law:

$$u_y = \frac{\sigma_y - \nu(\sigma_x + \sigma_z)}{E} l_y = \frac{(-5) - 0.3((-4.5)+(-10))}{1000} 2 = -0.0013\,\text{m} \qquad \text{(Eq. 5.6)}$$

$$u_z = \frac{\sigma_z - \nu(\sigma_x + \sigma_y)}{E} l_z = \frac{(-10) - 0.3((-4.5) + (-5))}{1000} 2 = -0.0143\,\text{m} \qquad \text{(Eq. 5.7)}$$

The exact and the calculated values are very close to each other.

5.1.1.4 Triaxial loading

During a triaxial pure stress state $\sigma_z = -10$ kN/m^2 vertical and $\sigma_y = -5$ kN/m^2 and $\sigma_x = -2$ kN/m^2 horizontal distributed surface loads were applied. At the bottom there is a vertical surface support and horizontally also at the right and front side (see Fig. 5.9).

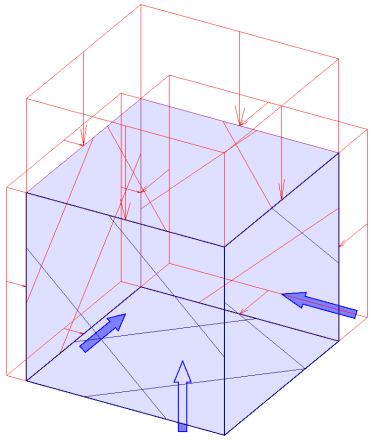

Figure 5.9 – Triaxial loading [$\sigma_z = -10$ kN/m^2 , $\sigma_y = -5$ kN/m^2 *and* $\sigma_x = -2$ kN/m^2] *and applied boundary conditions*

Based on the FEM-Design calculation the following diplacement results revealed (see Fig. 5.10).

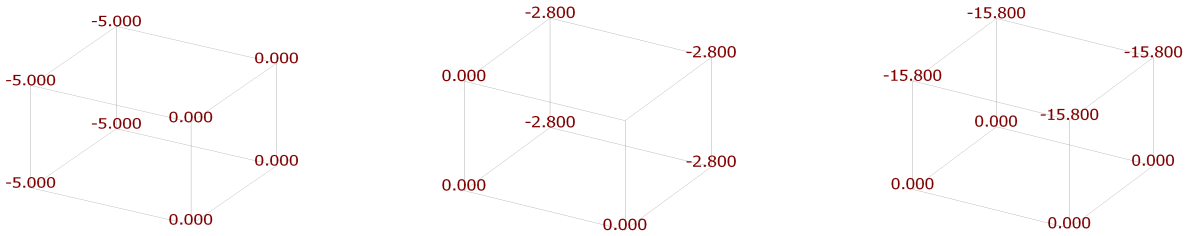

Figure 5.10 – Corner point translations in X, Y and Z directions [mm]

Based on the general Hook's law and considering the supports the theoretical results of these translations are the following:

$$u_x = -\frac{\sigma_x - \nu(\sigma_y + \sigma_z)}{E} l_x = -\frac{(-2) - 0.3((-5) + (-10))}{1000} 2 = -0.005\,\text{m} \qquad \text{(Eq. 5.8)}$$

$$u_y = \frac{\sigma_y - \nu(\sigma_x + \sigma_z)}{E} l_y = \frac{(-5) - 0.3((-2) + (-10))}{1000} 2 = -0.0028\,\text{m} \qquad \text{(Eq. 5.9)}$$

$$u_z = \frac{\sigma_z - \nu(\sigma_x + \sigma_y)}{E} l_z = \frac{(-10) - 0.3((-2) + (-5))}{1000} 2 = -0.0158\,\text{m} \qquad \text{(Eq. 5.10)}$$

The exact and the calculated values are very close to each other.

5.1.2 Infinitely smooth and rigid foundation on linear elastic soil

The investigated problem is an infinitely smooth and rigid wall foundation on the top of the ground level. The width (B = 2 m) and the height (H = 4 m) of the model space is shown in Fig. 5.11. The calculation is executed in 3D therefore the length of the soil model and footing is not relevant. In this case the length was 0.1 m. All of the vertical planes around the soil strata were fixed horizontally, the botton plane horizontally and vertically. On the top of the ground level a surface support was created and applied a uniform vertical displacement u_z = 10 mm on it to simulate a smooth rigid footing. The self-weight γ was zero, the material model was linear elastic, isotropic with E = 1333 kN/m^2 and ν = 0.333.

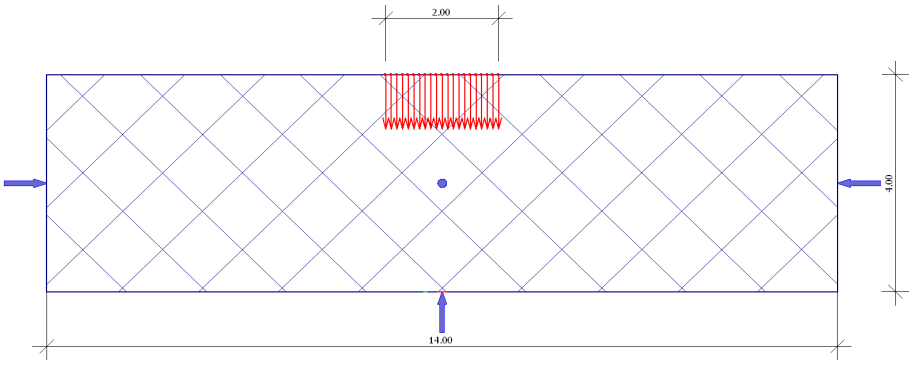

Figure 5.11 – The geometry of the problem (red arrows mean the u_z=10 mm vertical displacement load)

The finite element mesh and the displacement load is shown in Fig. 5.12. During the validation fine element group (quadratic element group) was used. The average element size was 0.10 m.

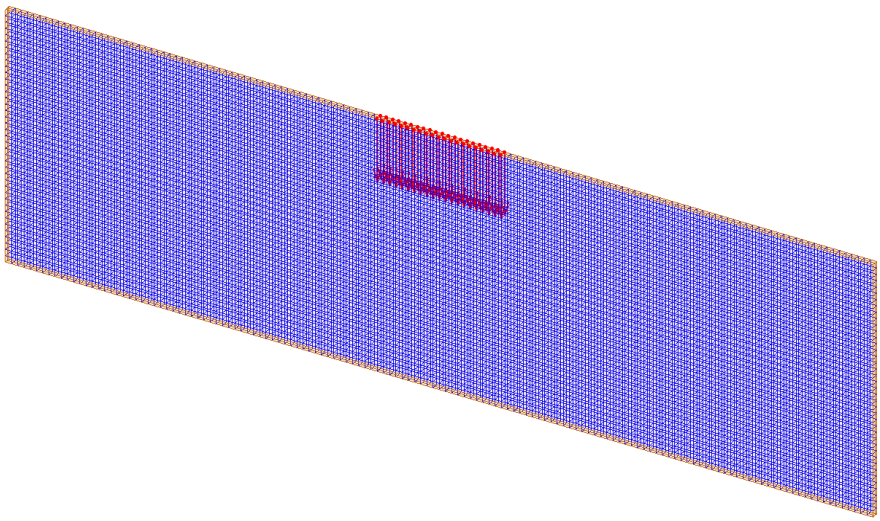

Figure 5.12 – The finite element mesh and the applied displacement load on the top of the ground level

The scaled displacements are shown in Fig. 5.13. The arising distributed forces and the resultant force under smooth rigid foundation were calculated from the finite element calculation. Namely the resultant force is F_z = 15.294 kN. A lowest value of the intensity of the distributed force in the middle of the footing is –5.03 kN/m^2 (compression). See Fig. 5.14 and 5.15 to check the distribution of the calculated forces (reaction forces) under the footing along the base width.

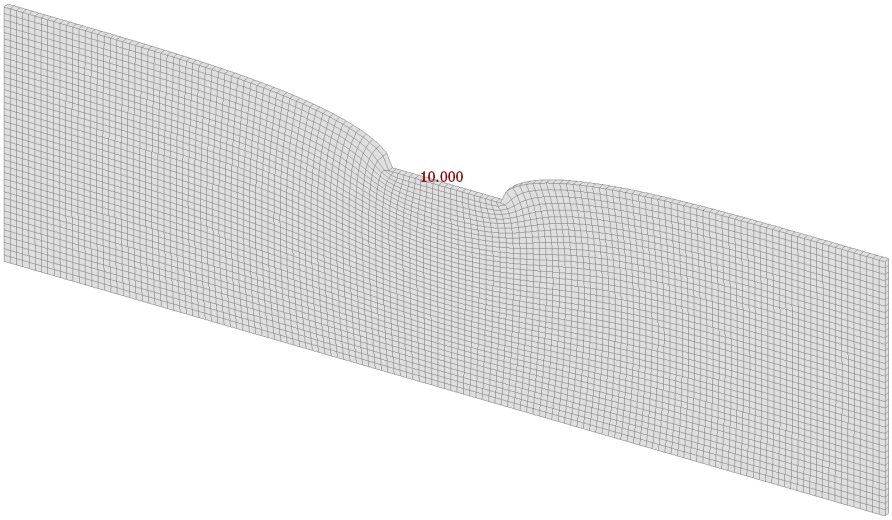

Figure 5.13 – The displacement field with the deformed mesh [mm] *(50 times scaled up)*

Based on [56] and [57] the analytical solution for the resultant force under the foundation is given with Eq. 5.11.

$$\frac{F\,\delta}{E}=u_z \qquad \text{(Eq. 5.11)}$$

where δ = 0.88 if the ratio of the $H/(0.5B)$ = 4. H and B are the mentioned depth of the soil layer and the width of the strip foundation. Based on this analytical solution this gives F = 15.15 kN resultant force. The difference (error) between the finite element calculation and the analytical solution is less than 1%.

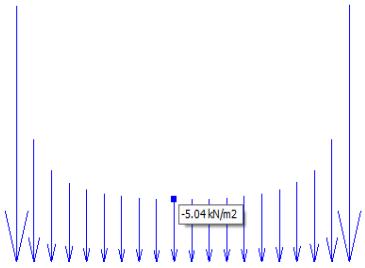

Figure 5.14 – The distribution of the forces under the foundation and the lowest value

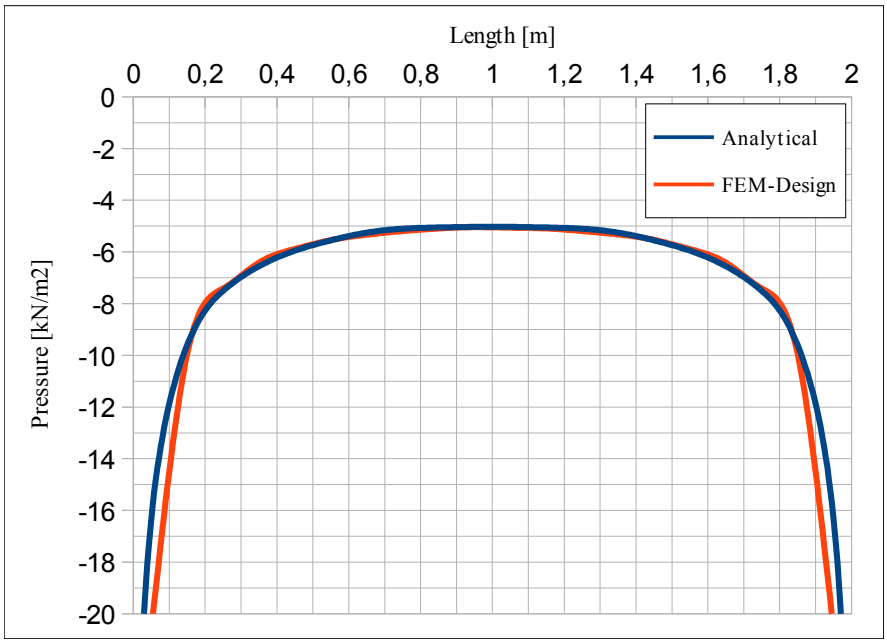

Figure 5.15 – Distribution of the forces with FE calculation and with the analytical solution

Fig. 5.16 shows the vertical stresses under the footing according to the applied uniform vertical displacement $u_z = 10$ mm.

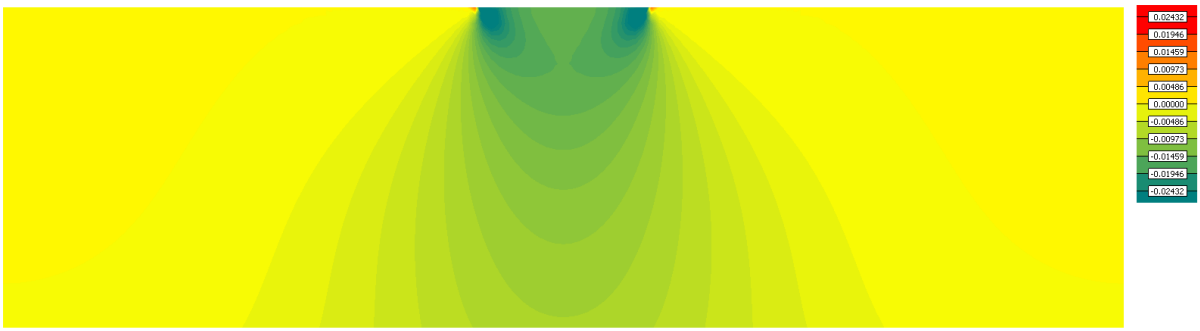

Figure 5.16 – Vertical stress distribution under the foundation [MPa]

5.1.3 Infinitely flexible wall foundation on elastic Gibson-soil

According to [56] and [58] the problem is a half-space with linearly varying Young's modulus with depth. The load is a distributed surface load on a strip with B = 2 m width (see Fig. 5.17). All of the vertical planes around the soil strata were fixed horizontally, the botton plane vertically. On the top of the ground level a uniform surface distributed load was applied with q_z = 10 kN/m^2 intensity. The self-weight γ was zero, the material model was linear elastic, isotropic with linearly increasing elastic constants. At the top of the soil layer E_{top} = 0.01 kN/m^2 and and the inrcrement according to depth was d = 299 kN/m^2/m, therefore at the botton of the strata $E_{bottom} = E_{top}+4d$ = 1196.01 kN/m^2. The Poisson's ratio was uniformly v = 0.49. See the distribution of the Young's modulus with depth in Fig 5.18.

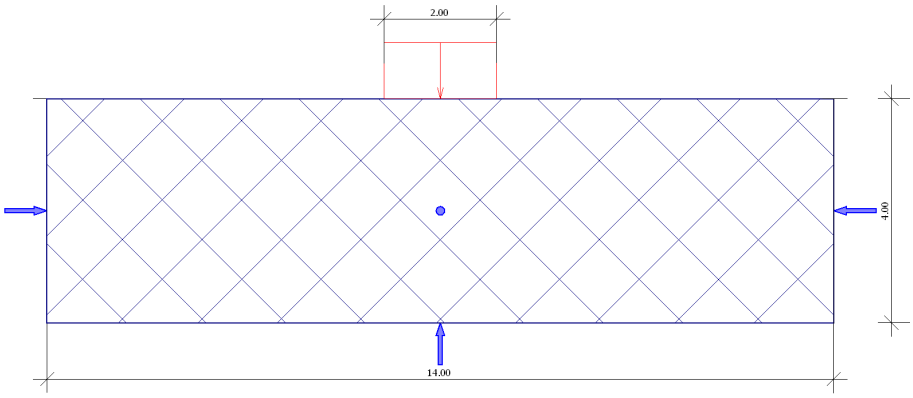

Figure 5.17 – The geometry of the problem (red arrows mean q_z=10 kN/m^2 vertical distributed load)

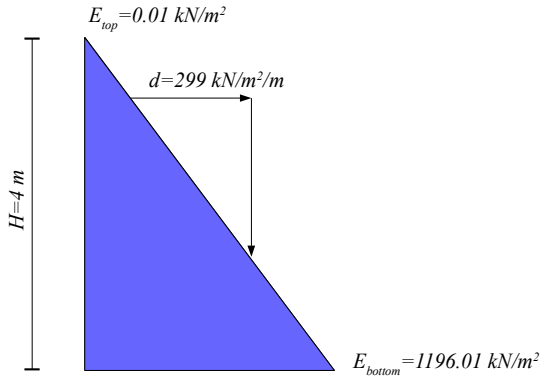

Figure 5.18 – The linearly varying Young's modulus with depth

The finite element mesh and the distributed surface load is shown in Fig. 5.19. During the validation fine element group (quadratic element group) was used. The average element size was 0.10 m.

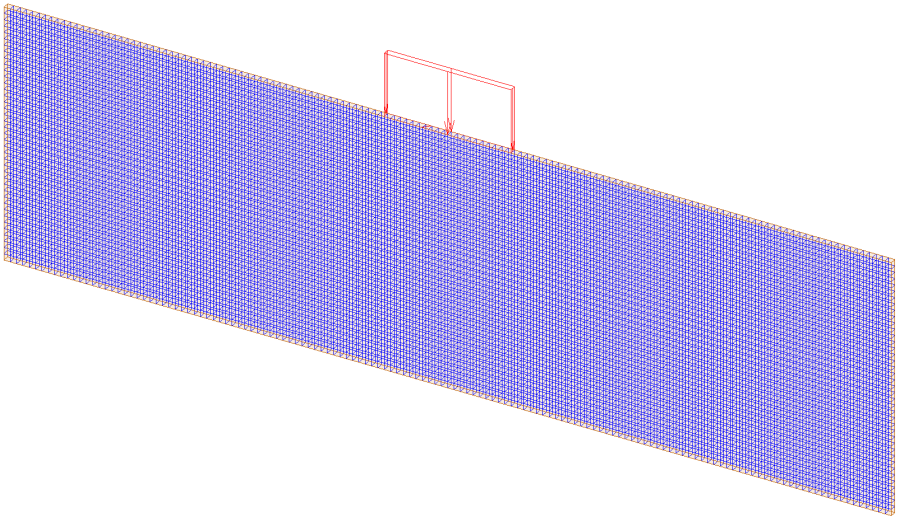

Figure 5.19 – The finite element mesh and the applied distributed load on the top of the ground level

The scaled displacements are shown in Fig. 5.20. The calculated settlement in the middle of the area of the distributed load was u_z = 47.54 mm.

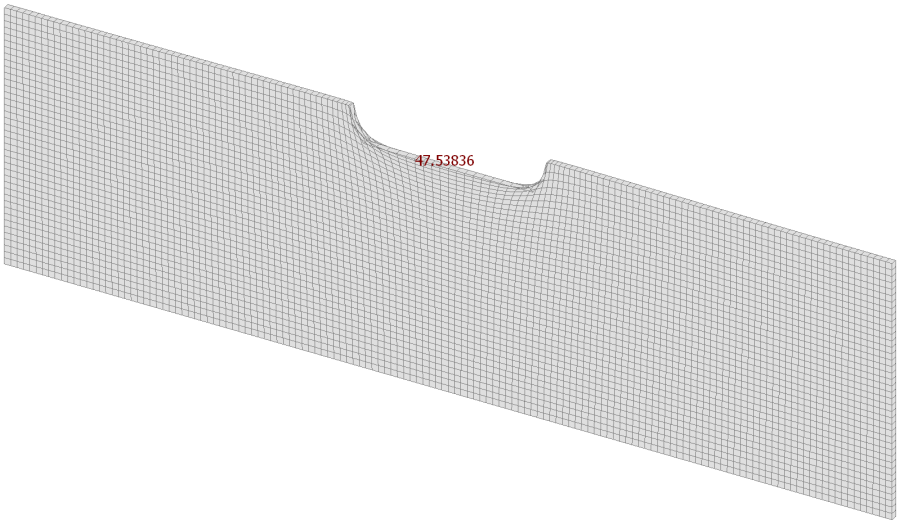

Figure 5.20 – The displacement field with the deformed mesh [mm] *(10 times scaled up)*

According to [56] and [58] the exact analytical solution is derived with ν = 0.5 but to avoid the volumetric locking [11] the allowable Poisson's ratio in FEM-Design is ν = 0.49 for solid elements. Fig. 5.20 shows that under the ditributed load the numerical calculation brought almost uniform settlement. The analytical solution is given for infinite half-space. Respect to the mentioned literatures the exact solution is given with Eq. 5.12.

$$\frac{q_z}{2\alpha} = u_z \qquad \text{(Eq. 5.12)}$$

where q_z is the intensity of the distributed load and α is the increment of the shear modulus with depth. In our case according to the given E_{top} = 0.01 kN/m^2 and E_{bottom} = 1196 kN/m^2 and with ν=0.49 the shear moduluses are G_{top} = 0.003 kN/m^2 and G_{bottom} = 401.3 kN/m^2 (see Eq. 3.1). The height of the strata was H = 4 m, therefore α = 100.

Based on tha analytical formula the settlement u_z = 50 mm. The difference (error) between the finite element calculation and the analytical solution is less than 5%. This difference comes from the incompressibility of the analytical model and the considered real infinite half-space.

Fig. 5.21 and 5.22 shows the vertical stress ditribution and the intensity and the directions of principal stresses under the distributed load from the FEM-Design calculation.

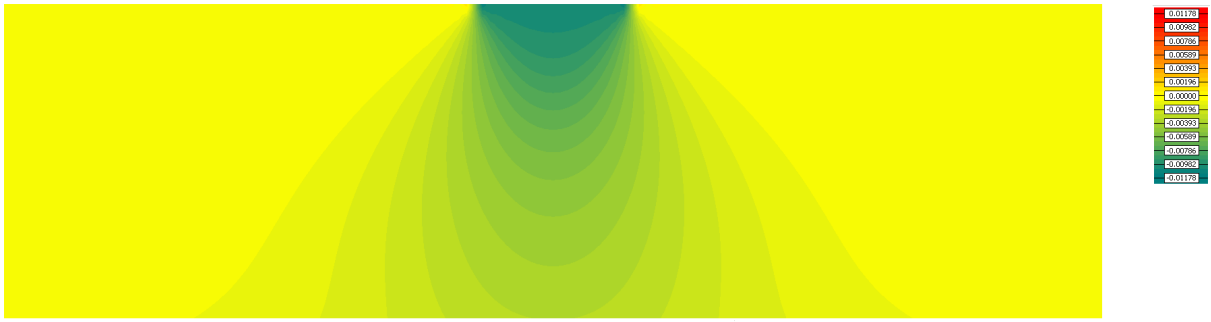

Figure 5.21 – Vertical stress distribution [MPa]

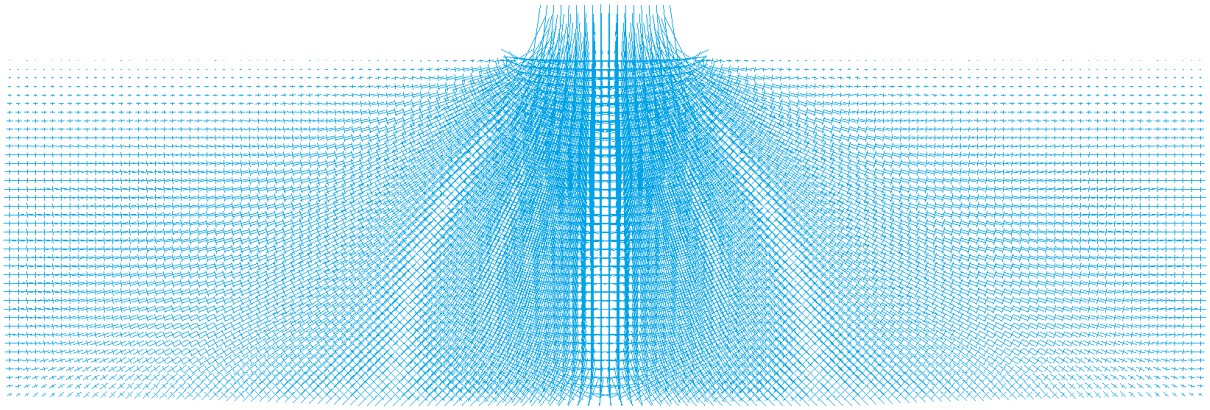

Figure 5.22 – Distribution of the intensity of the principal stresses and directions under the foundation

5.1.4 Infinitely flexible circular foundation on linear elastic soil

In this case the problem is a half-space with constant Young's modulus (the self-weight γ was zero, the material model was linear elastic, isotropic with E = 95800 kN/m^2) and a flexible circular foundation on it with R = 23.35 m radius. The dimension of the applied soil layer depends on this radius. The limit depth is $5R \approx 118$ m and the width is $10R \approx 240$ m (see Fig. 5.23). The load is a distributed surface load on a circular foundation which has zero stiffness. The intensity of the applied load is $q_z = 263.3$ *kN/m^2*. The Poisson' ratio is varying. In the first case ν = 0.49 and in the second case ν = 0.0. All of the vertical planes around the soil strata were fixed horizontally, the botton plane horizontally and vertically (see Fig. 5.23).

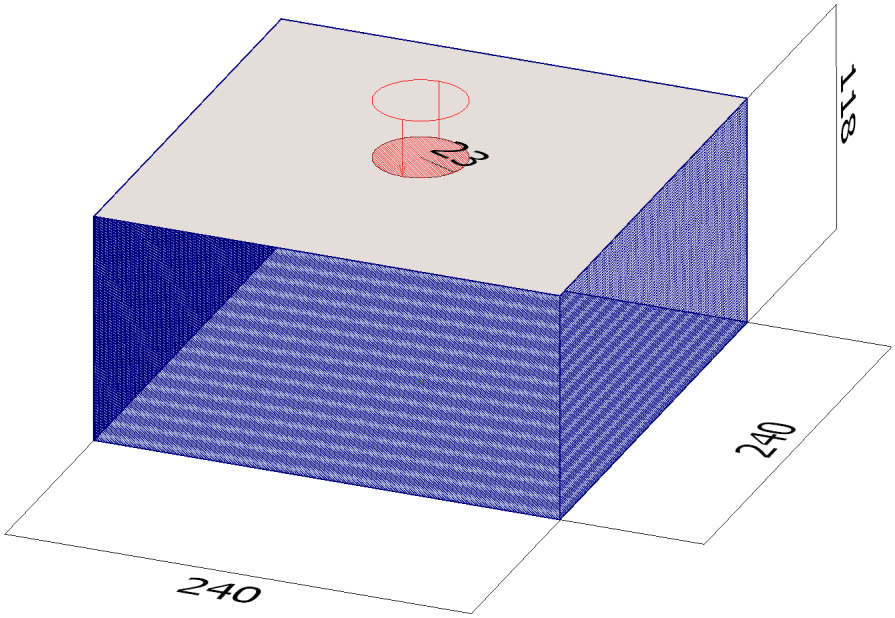

Figure 5.23 – The geometry of the problem (red arrows mean q_z=263.3 kN/m^2 vertical distributed load)

The finite element mesh and the distributed surface load is shown in Fig. 5.24. During the validation fine element group (quadratic element group) was used. The average element size was 7 m (see Fig. 5.24 about the applied 3D mesh).

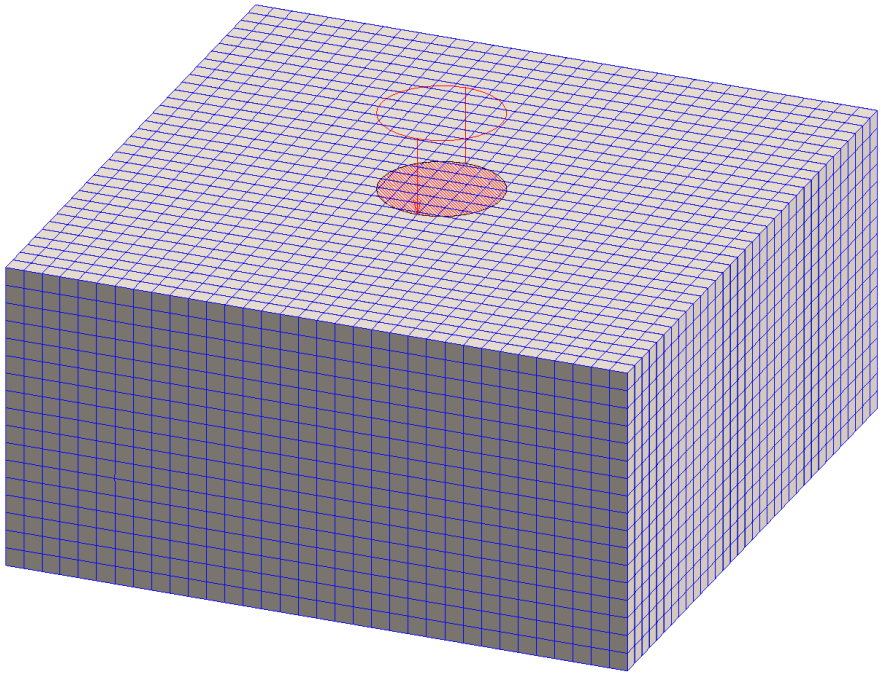

Figure 5.24 – The finite element mesh and the applied distributed load on the circular foundation

The scaled displacements are shown in Fig. 5.25 and 5.26. The calculated settlements at the center of the circle was u_z = 77.1 mm in the first case and u_z = 112 mm in the second case (see Fig. 5.25 and 5.26).

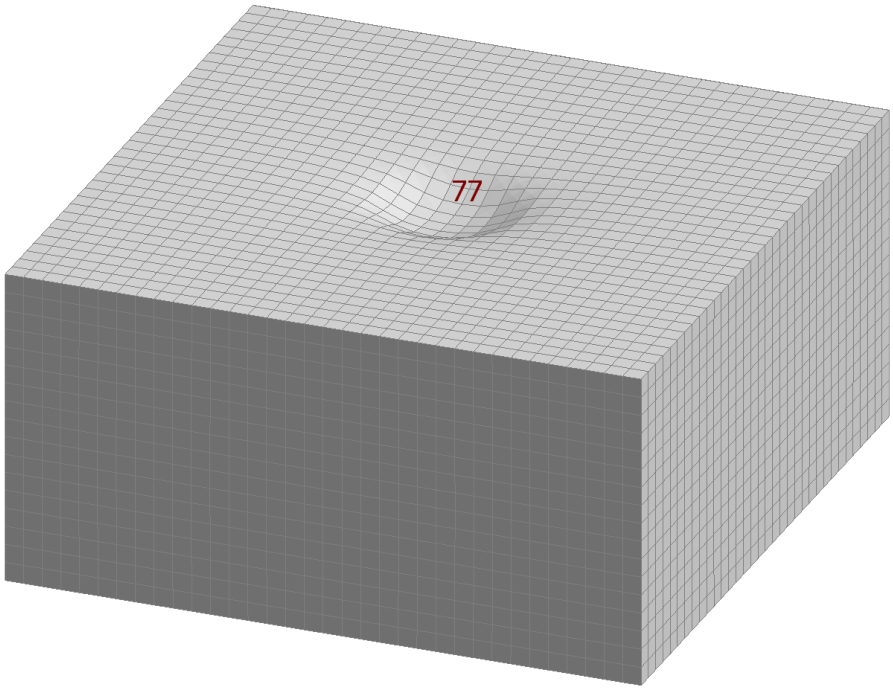

Figure 5.25 – The displacements with the deformed mesh [mm] *(150 times scaled up, v*=0.49*)*

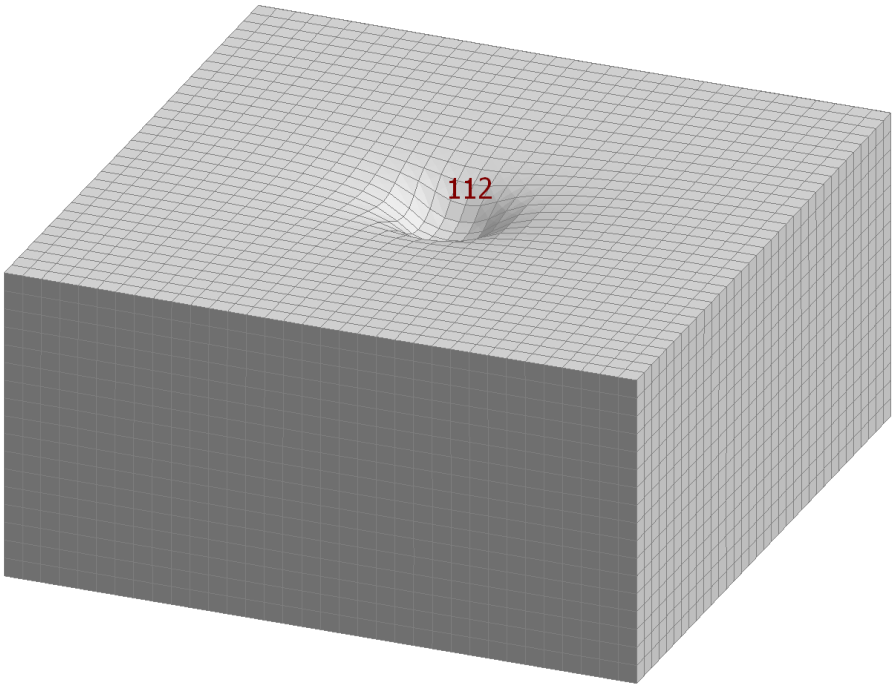

Figure 5.26 – The displacements with the deformed mesh [mm] *(150 times scaled up, v=0.0)*

Fig. 5.27 shows the vertical stress ditribution under the circle from the FEM-Design numerical calculation in the first case ($v = 0.49$).

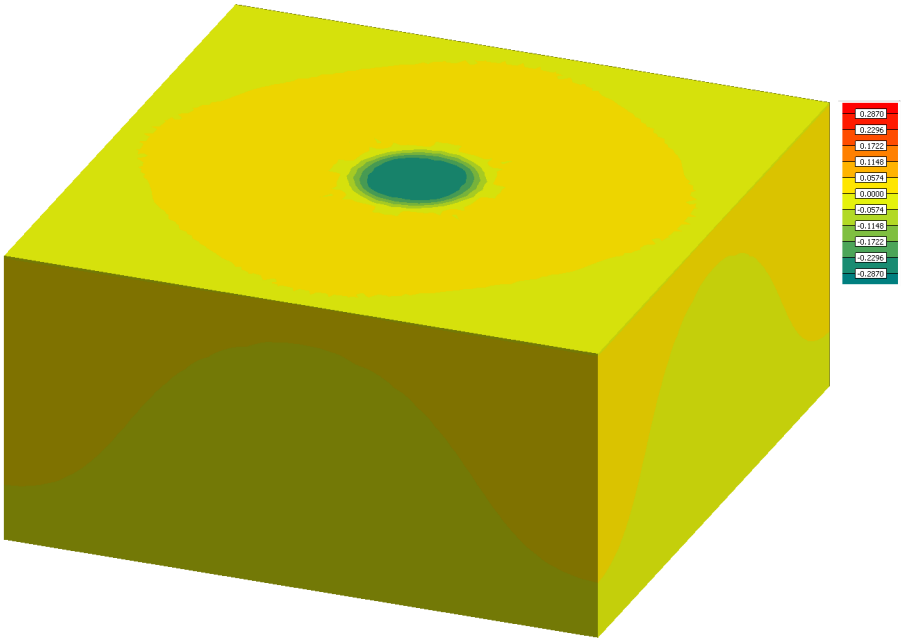

Figure 5.27 – Vertical stress distribution [MPa]

According to [56], [59] and [60] the theoretical solution of the settlement at the center of the circle is given with Eq. 5.13.

$$\frac{q_z R I_p}{E} = u_z \qquad \text{(Eq. 5.13)}$$

where q_z is the applied distributed load, R is the radius of the circle, E is the Young's modulus. I_p is the influence coefficient, which in this case if v = 0.49 equal to approximately 1.2 and if v = 0.0 equal to approximately 1.65. According to the input values this settlement is:

$$u_z = \frac{263.3 \cdot 23.35 \cdot 1.2}{95800} = 0.077\,\text{m} = 77\,\text{mm} \qquad \text{(Eq. 5.14)}$$

$$u_z = \frac{263.3 \cdot 23.35 \cdot 1.65}{95800} = 0.106\,\text{m} = 106\,\text{mm} \qquad \text{(Eq. 5.15)}$$

The difference (error) between the FEM-Design calculation and the analytical solution is less than 6 % in both case.

5.2 Verification and validation of Mohr-Coulomb material model

5.2.1 Pure stress states on a cuboid

The material model input parameters for the pure stress statas are as follows: E = 1000 kN/m^2, φ' = 20°, c' = 10 kPa, ν = 0.3. The self-weight of the soil element was set to γ = 0. The geometry of the analyzed cuboid and boundary conditions are the same as in Chapter 5.1.1 (see Fig. 5.28).

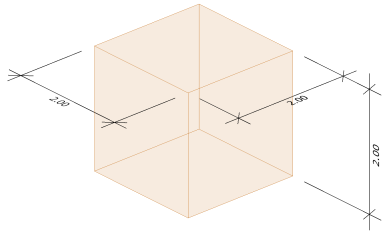

Figure 5.28 – 2x2x2 m *cuboid*

In all case in this chapter, based on the ratio between the applied normal stresses the perfectly plastic condition is arised in every integration points. In this paragraph both the fine (quadratic) and standard (linear) finite element groups are involved. According to this fact based on Chapter 2.2 the amount of integration points are different by a hexahedron element. Based on FEM-Design calculations the integration points are shown is Fig 5.29 with the red dots by fine and standard elements. These points are available after the FEM-Design calculation by the results of non-linear soil calculation results window (for further information please check „The new features guide" for this version).

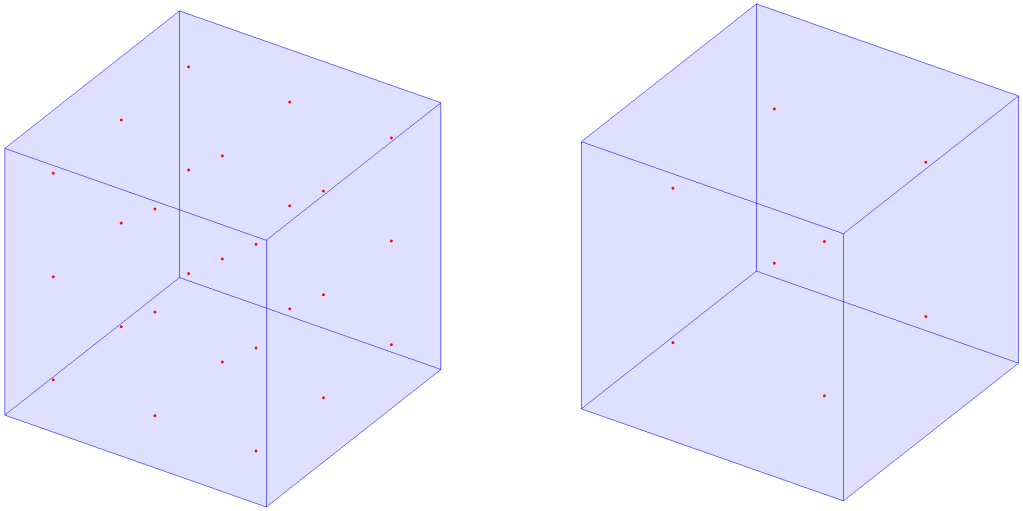

Figure 5.29 – The integration points in the analyzed element (fine and standard)

5.2.1.1 Uniaxial compression

Fig. 5.30 shows the uniaxial compression problem.

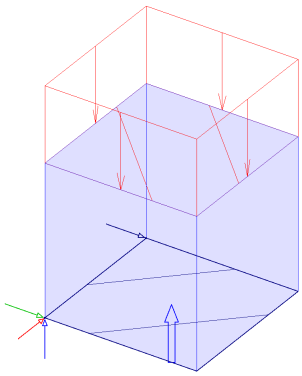

Figure 5.30 – Uniaxial compression [σ_3] and applied boundary conditions

The theoretical load-bearing capacity for this uniaxial compression problem comes from Eq. 3.18. (see below the repeated Eq. 3.18 once again). Based on the input parameters and boundary conditions, in this case: $\sigma_1' = \sigma_2' = 0$, $\sigma_3' \neq 0$.

$$0=\left(\sigma_1'-\sigma_3'\right)+\left(\sigma_1'+\sigma_3'\right)\sin\varphi'-2c'\cos\varphi' \qquad \text{(Eq. 3.18)}$$

With the substitutions of these parameters into Eq. 3.18 the following equation is revealed:

$$\sigma_3'=-2c'\frac{\cos\varphi'}{1-\sin\varphi'}=-2\cdot 10\frac{\cos 20^o}{1-\sin 20^o}=-28.56\frac{\text{kN}}{\text{m}^2} \qquad \text{(Eq. 5.16)}$$

Fig. 5.31 shows the load-displacement diagram of the cuboid in this case for fine and standard element types also. The load-bearing capacity from the numerical calculation based on Fig. 5.31 is $\sigma_3' = -28.9$ kN/m^2. There is no significante difference between fine and standard calculation in this case but this is only true by pure stress states.

When the increased distributed load reaches this $\sigma_3' = -28.9$ kN/m^2 value the displacements are increasing radically and basically at the end of the calculation infinite displacements occures.

The differences (error) between the FEM-Design calculations and the theoretical solution are less than 1.2 %.

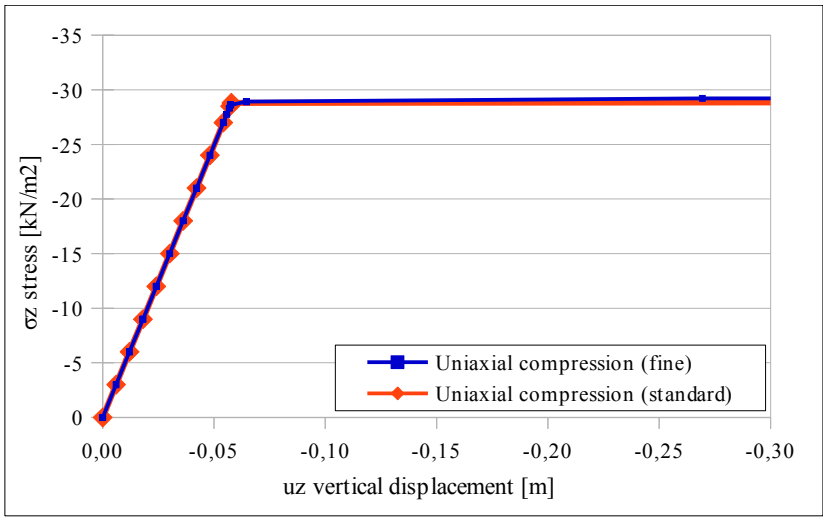

Figure 5.31 – Stress-displacement diagram

5.2.1.2 Biaxial compression

Fig. 5.32 shows the biaxial compression problem.

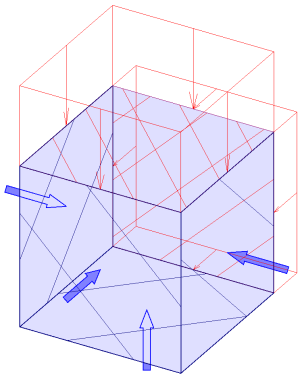

Figure 5.32 – Biaxial loading [$\sigma_3'/\sigma_1' = 3$] and applied boundary conditions

Based on the input parameters and boundary conditions, in this case: $\sigma_3'/\sigma_1' = 3$ and $\sigma_2' = \nu(\sigma_1'+\sigma_3') = 0.3\ (\sigma_3'/3 + \sigma_3') = 0.4\ \sigma_3'$. Thus in this load case the principal stresses in the function of σ_3' are as follows: $\sigma_1' = 0.3333\sigma_3'$, $\sigma_2' = 0.4\sigma_3'$ and σ_3'. With the substitutions of these parameters into Eq. 3.18 and using the material parameters also the following equation is revealed:

$$\sigma_3' = -2c'\frac{\cos\varphi'}{(1-\sin\varphi')} + \sigma_1'\frac{(1+\sin\varphi')}{(1-\sin\varphi')} = -2c'\frac{\cos\varphi'}{(1-\sin\varphi')} + 0.3333\,\sigma_3'\frac{(1+\sin\varphi')}{(1-\sin\varphi')} \quad \text{(Eq. 5.17)}$$

$$\sigma_3' = -2c'\frac{\cos\varphi'}{(1-\sin\varphi'-0.3333-0.3333\sin\varphi')} = -2\cdot 10\frac{\cos 20^\circ}{(0.6667-1.3333\sin 20^\circ)} = -89.2\,\frac{\text{kN}}{\text{m}^2} \quad \text{(Eq. 5.18)}$$

Fig. 5.33 shows the load-displacement diagram of the cuboid in this case for fine and standard element types also. The load-bearing capacity from the FEM-Design calculation based on Fig. 5.33 is $\sigma_3' = -89.6$ kN/m^2. There is no significante difference between fine and standard calculation in this pure stress case.

When the increased distributed load reaches this $\sigma_3' = -89.6$ kN/m^2 value, the displacements are increasing radically and basically at the end of the calculation infinite displacements occured.

The differences (error) between the FEM-Design calculations and the theoretical solution are less than 0.5 %.

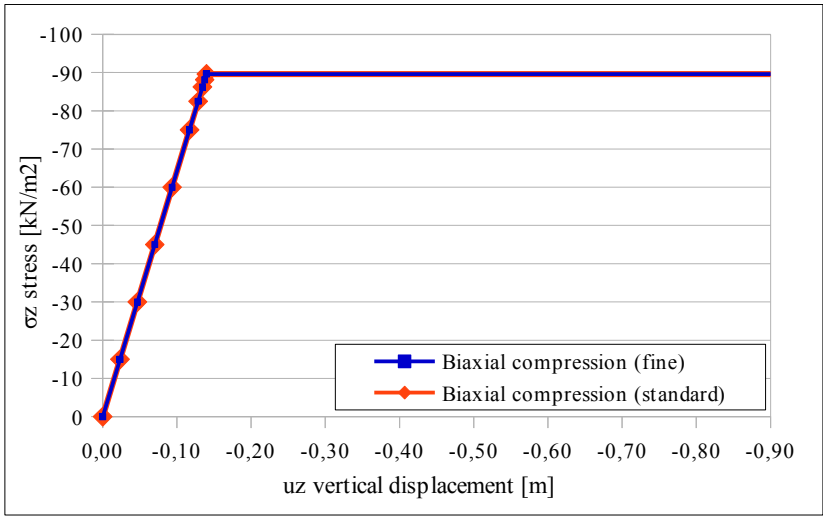

Figure 5.33 – Stress-displacement diagram

5.2.1.3 Triaxial compression

Fig. 5.34 shows the triiaxial compression problem.

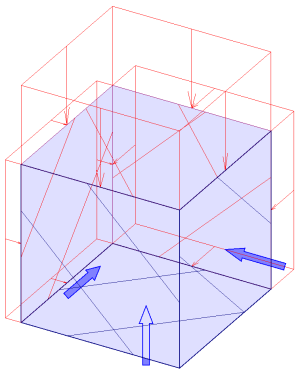

Figure 5.34 – Triaxial loading [$\sigma_3'/\sigma_2' = 2$ *and* $\sigma_2'/\sigma_1' = 2.5$] *and applied boundary conditions*

Based on the input parameters and boundary conditions, in this case: $\sigma_3'/\sigma_2' = 2$ and $\sigma_2'/\sigma_1' = 2.5$. Thus in this load case the principal stresses in the function of σ_3' are as follows: $\sigma_1' = 0.2\sigma_3'$, $\sigma_2' = 0.5\sigma_3'$ and σ_3'. With the substitutions of these parameters into Eq. 3.18 and using the material parameters also the following equation is revealed:

$$\sigma_3' = -2c'\frac{\cos\varphi'}{(1-\sin\varphi')} + \sigma_1'\frac{(1+\sin\varphi')}{(1-\sin\varphi')} = -2c'\frac{\cos\varphi'}{(1-\sin\varphi')} + 0.2\sigma_3'\frac{(1+\sin\varphi')}{(1-\sin\varphi')} \quad \text{(Eq. 5.19)}$$

$$\sigma_3' = -2c'\frac{\cos\varphi'}{(1-\sin\varphi'-0.2-0.2\sin\varphi')} = -2\cdot 10\frac{\cos 20^o}{(0.8-1.2\sin 20^o)} = -48.2\frac{\text{kN}}{\text{m}^2} \quad \text{(Eq. 5.20)}$$

Fig. 5.35 shows the load-displacement diagram of the cuboid in this case for fine and standard element types also. The load-bearing capacity from the FEM-Design calculation based on Fig. 5.35 is σ_3' = –49.2 kN/m^2. There is no significante difference between fine and standard calculation in this pure stress case.

When the increased distributed load reaches this σ_3' = –49.2 kN/m^2 value, the displacements are increasing radically and basically at the end of the calculation infinite displacements occured.

The differences (error) between the FEM-Design calculations and the theoretical solution are less than 2 %.

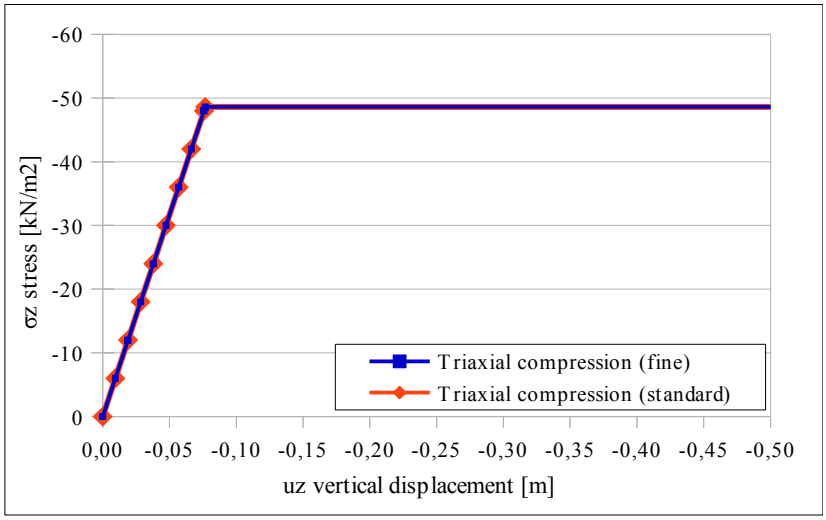

Figure 5.35 – Stress-displacement diagram

5.2.2 Load-bearing capacity of a shallow wall foundation

In real life it is a frequented occurrence when the cohesion of a clay layer increasing with depth. It is also known that the Young's modulus can increase with depth (see Chapter 5.1.2). In this chapter the theoretical load-bearing capacity will be calculated according to the linear elastic perfectly plastic Mohr-Coulomb material model for a cohesive soil.

A strip foundation will be analyzed in 3D. Due to the symmetry during the model calculation only the half of the strata and the foundation will be built. Fig 5.36 shows the applied boundary conditions. At the top of the soil a 1 m width footing is defined (the footing was rigid with E = 31000 GPa elastic stiffness). According to the symmetry it means a B = 2 m width foundation. The depth of the soil layer is H = 2 m and the width of the half model space is $4B/2$ = 4 m. Considering the symmetry condition at the left edge of the foundation the rotation around it was restricted and the horizontal displacement also perpendicular to this edge (see Fig 5.36). All of the vertical planes around the soil strata were fixed horizontally, the botton plane vertically. The material model was the Mohr-Coulomb plasticity. The ditribution of the Young's modulus and the cohesion is shown in Fig 5.37. The frictional angle is set to zero ($\varphi' = 0$) and the Poisson's ratio was ν = 0.49. To calculate the load-bearing capacity a ditributed load q_z = 15 kN/m^2 was applied on the top of the foundation (see Fig. 5.36 and 5.38). The vertical displacements in the center point of the footing were saved in every load step.

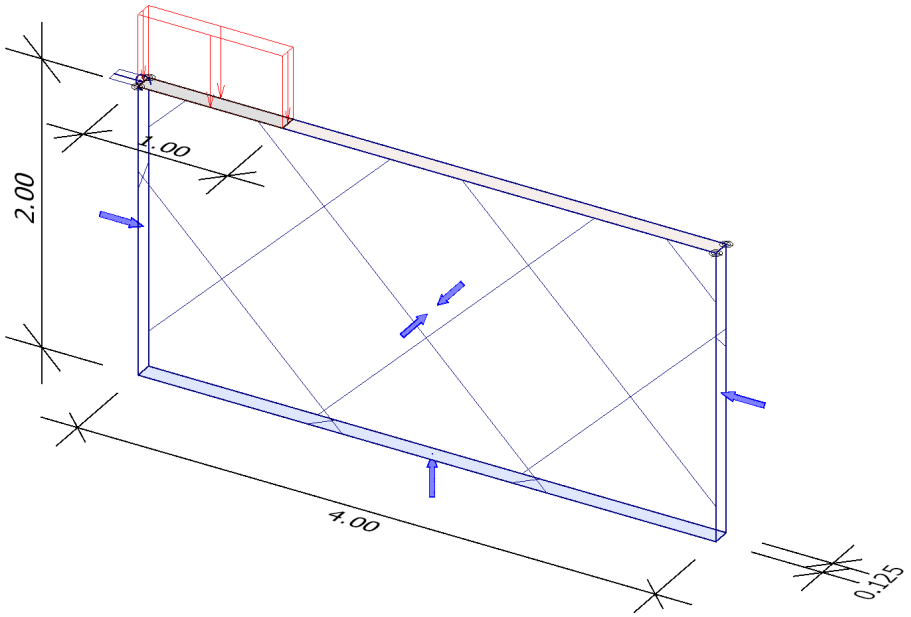

Figure 5.36 – The geometry of the problem (red arrows mean q_z vertical distributed load)

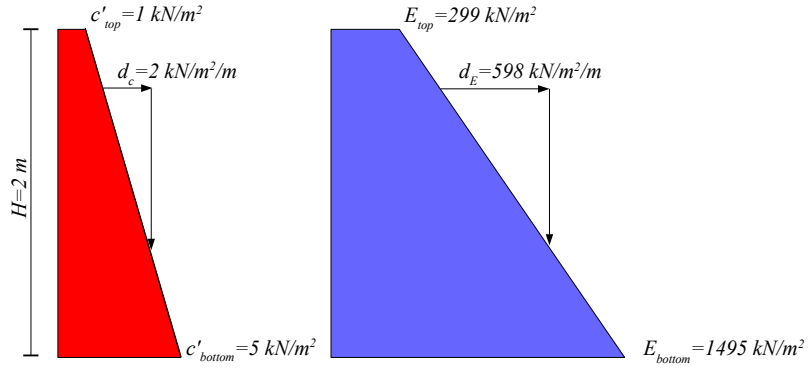

Figure 5.37 – The linearly varying cohesion and Young's modulus with depth

The finite element mesh and the distributed surface load is shown in Fig. 5.38. During the validation fine element group (quadratic element group) was used. The average element size was 0.05 m (see Fig. 5.38 about the applied 3D mesh).

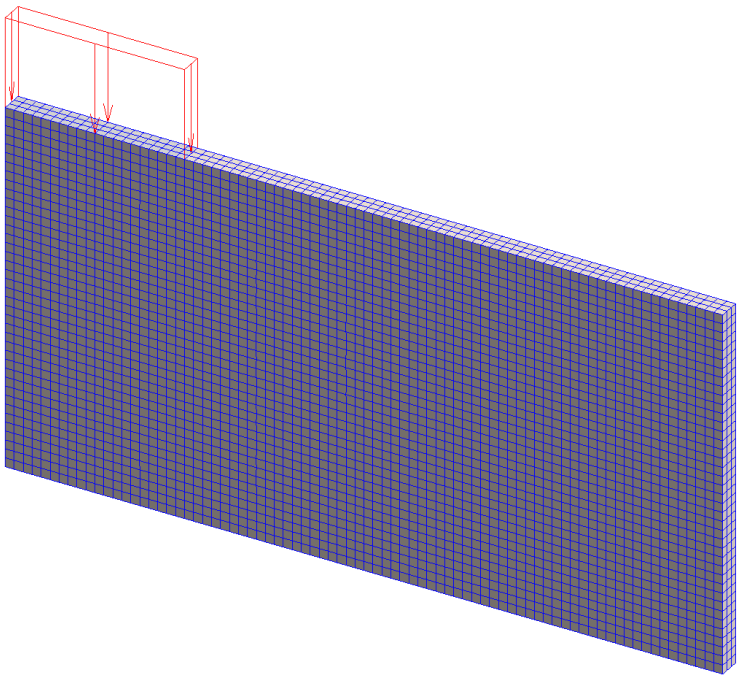

Figure 5.38 – The finite element mesh and the applied distributed load on the strip foundation

Two different cases were analyzed. In the first case simulate a rough foundation because the connection was set to rigid in all directions between the footing and the soil. In the second case the connection between the footing and the soil was rigid only in the vertical direction, thus there can be a slip between them. This case simulate a perfectly smooth foundation.

The scaled displacements are shown in Fig. 5.39 and Fig. 5.40. The calculated settlement at the center of the circle was u_z = 1193 mm in the first case (see Fig. 5.39) and u_z = 2015 mm in the second case (see Fig. 5.40). These values are large displacements considering that the half-width of the footing was *B/2 = 1* m.

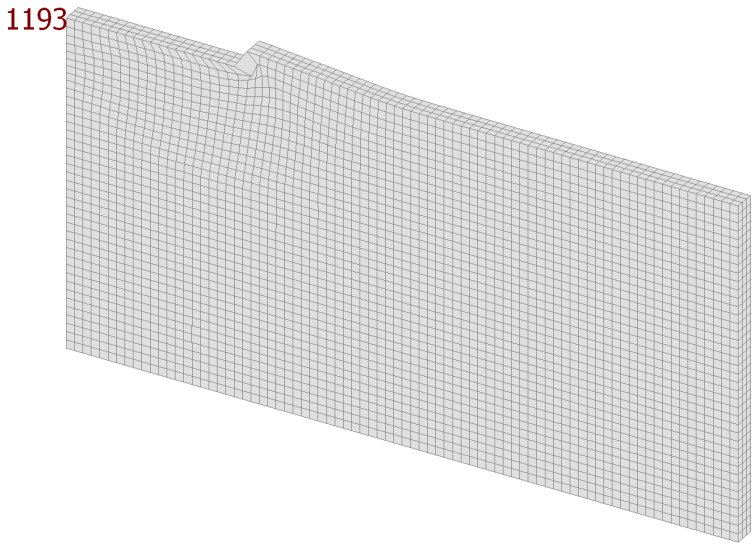

Figure 5.39 – The displacements with the deformed mesh [mm] *(rough case, 0.03 times scaled down)*

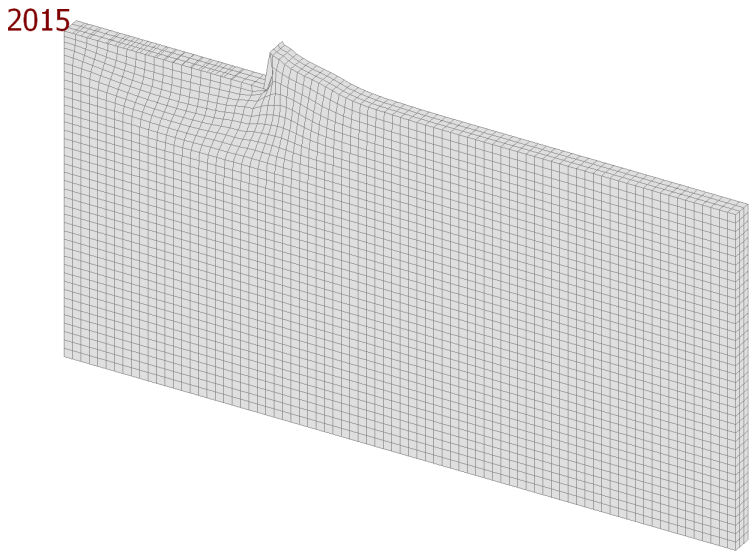

Figure 5.40 – The displacements with the deformed mesh [mm] *(smooth case, 0.03 times scaled down)*

Based on the finite element calculations the load-bearing capacity for rough foundation is $q_{z.max}$ = 10.3 kN/m^2 and for the smooth foundation $q_{z.max}$ = 8.8 kN/m^2 respectively (see Fig. 5.41). We can say that these two distributed loads are the load-bearing capacities because after these loads we get very large displacement in the center of the foundation and next to the foundation plastic regions arised (see Fig. 5.39 and 5.40). Based on the load-displacement diagrams (Fig. 5.41) these two load-bearing capacities are reasonable from the FEM-Design calculations.

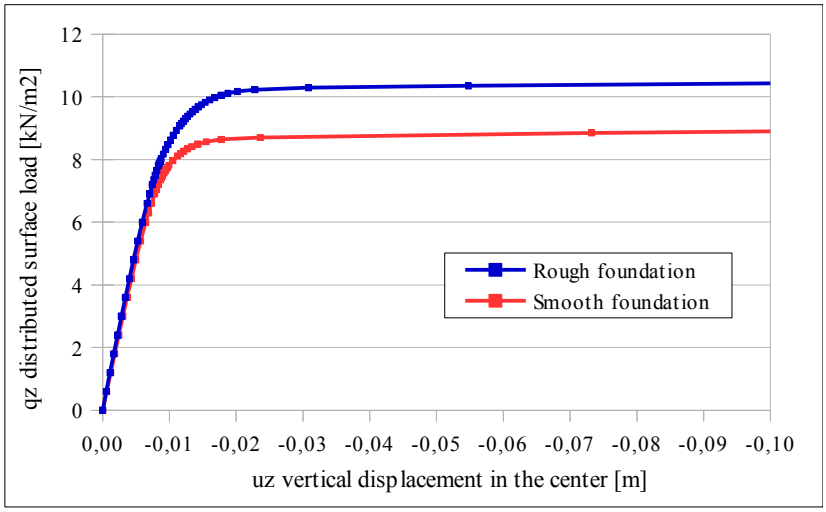

Figure 5.41 – Load-vertical displacement diagram of the two different cases

In the analyzed cases the load bearing capacities based on [56], [61] and [62] are given with Eq. 5.21.

$$q_{z.max} = \frac{F}{B} = \beta \left[(2+\pi) c_{top} + \frac{B\, d_c}{4} \right] \qquad \text{(Eq. 5.21)}$$

where $q_{z.max}$ is the load-bearing capacity in kN/m^2, c_{top} is the cohesion at the top of the ground level B is the width of the wall foundation and d_c is the increment of the cohesion with depth. β is a factor depends on the foundation roughness. In this case β equals to 1.27 and 1.48 for rough and smooth foundation. Based on the input data and Eq. 5.21 the load-bearing capacities for rough and smooth cases are $q_{z.max}$ = 9.1 kN/m^2 and $q_{z.max}$ = 7.8 kN/m^2 respectively. The differences (error) between the FEM-Design calculations and the analytical solutions are less than 12 %.

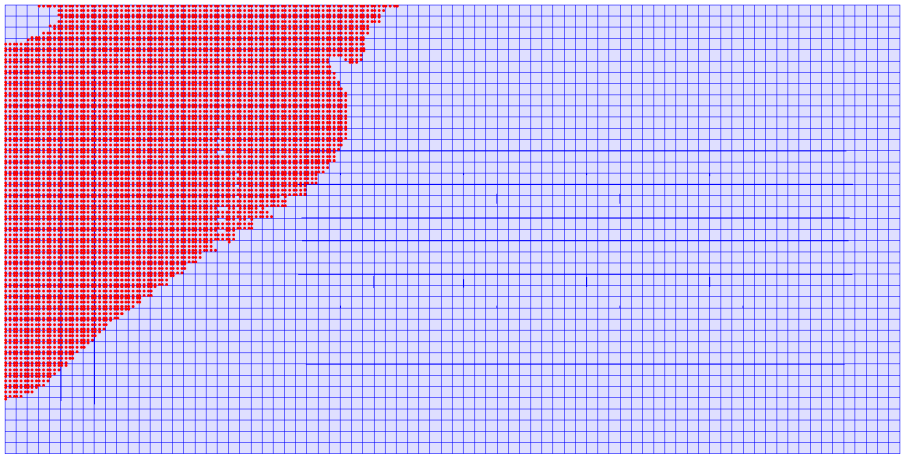

Figure 5.42 – The integration points in plastic condition at failure (rough case)

5.2.3 Load-bearing capacity of a circular isolated foundation

The material parameters: E = 2400 kPa, ν = 0.33, φ' = 30° and c' = 1.6 kPa. The self-weight of the soil was γ = 16 kN/m^3. A circular foundation was analyzed in 3D. Due to the symmetry during the model calculation only the quarter of the strata and the foundation was built. Fig 5.43 shows the applied boundary conditions. At the top of the soil a quarter circle was defined with R = 1 m radius (the footing was rigid with E = 31000 GPa elastic stiffness). The depth of the soil layer is H = *4* m and the width of the half model space is $10R/2$ = 5 m. At the symmetry conditions the rotation of the foundation around its edges was restricted and the horizontal displacement also perpendicular to these edges (see Fig 5.43). All of the vertical planes around the soil strata were fixed horizontally, the botton plane vertically. The material model was the Mohr-Coulomb plasticity. To calculate the load-bearing capacity a ditributed load q_z = 500 kN/m^2 was applied on the top of the foundation (see Fig. 5.43 and 5.44). The vertical displacements in the center point of the footing were saved in every load step.

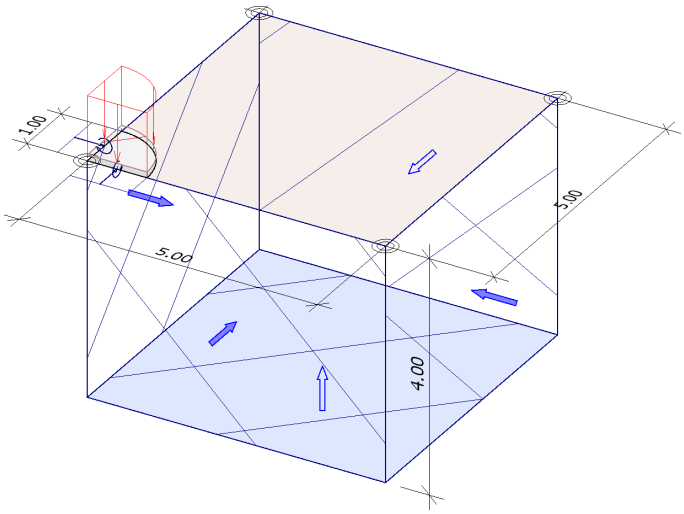

Figure 5.43 – The geometry of the problem (red arrows mean q_z vertical distributed load)

The finite element mesh and the distributed surface load is shown in Fig. 5.44. During the validation fine element group (quadratic element group) was used. The average element size was 0.45 m with a local refinement around the footing (see Fig. 5.44 about the applied 3D mesh).

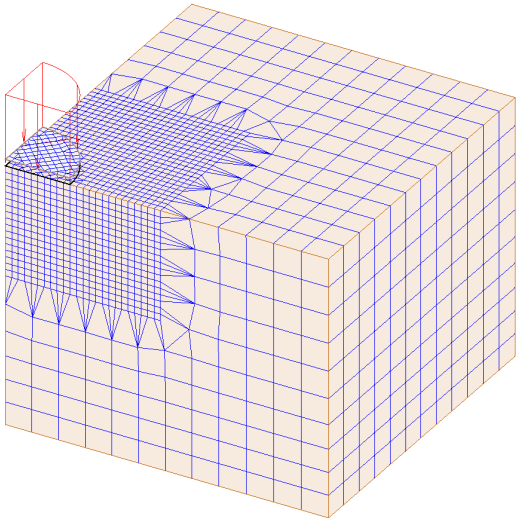

Figure 5.44 – The finite element mesh and the applied distributed load on the circular foundation

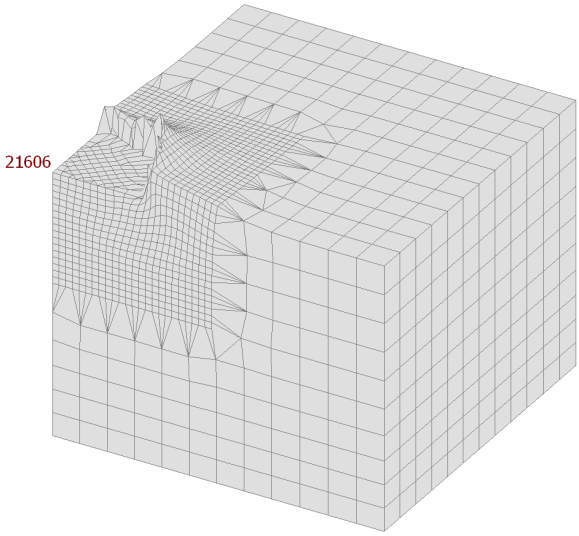

Figure 5.45 – The displacements with the deformed mesh [mm] *(0.0016 times scaled down)*

The scaled displacements are shown in Fig. 5.45 at the end of the calculation. The calculated settlement at the center of the circle was u_z = 21606 mm. This value is a large displacement therefore it means that the footing reached its load-bearing capacity before the maximum load level what was applied. Based on the finite element calculations the load-bearing capacity for rough foundation is $q_{z.max}$ = 375 kN/m^2 , see the saved load-displacement curve in Fig. 5.46. We can say that this distributed load is the load-bearing capacity because after this load-step we get very large displacement in the center of the foundation and next to the foundation plastic regions arised (see Fig. 5.46). Based on the load-displacement diagrams (Fig. 5.46) this load-bearing capacity is reasonable from the FEM-Design calculation.

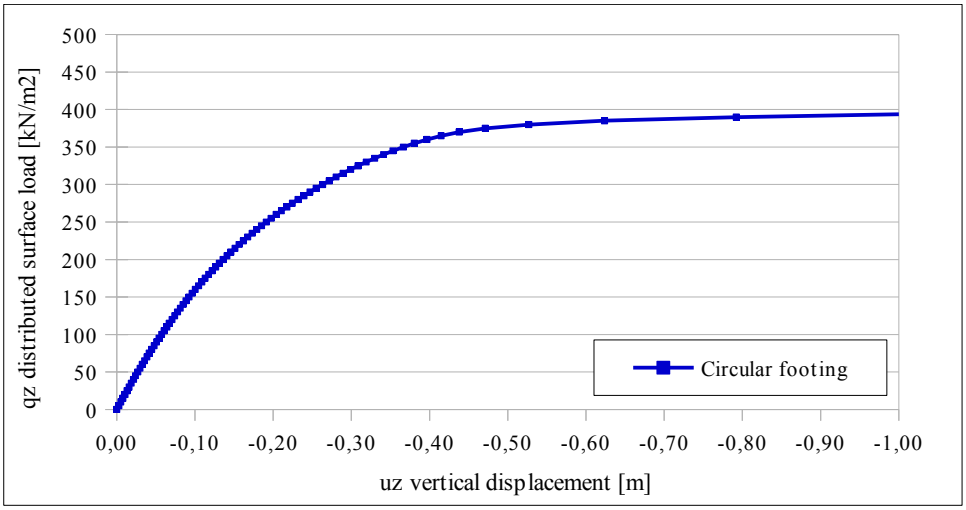

Figure 5.46 – Load-vertical displacement diagram of the footing

There is analytical solution for this problem based on Terzaghi's theory. The load-bearing capacity of the circular footing is as follows according to Terzaghi:

The load-bearing factors:

$$N_q = e^{\pi \tan(\varphi')} \tan^2\left(45^o + \frac{\varphi'}{2}\right) = e^{\pi \tan(30^o)} \tan^2\left(45^o + \frac{30^o}{2}\right) = 18.40 \quad \text{(Eq. 5.22)}$$

$$N_c = \frac{N_q - 1}{\tan\varphi'} = \frac{18.40 - 1}{\tan 30^o} = 30.14 \quad \text{(Eq. 5.23)}$$

$$N_\gamma = (N_q + 1)\tan\varphi' = (18.40 + 1)\tan 30^o = 11.20 \quad \text{(Eq. 5.24)}$$

The shape correction factors:

$$s_q = 1 + \frac{B}{L}\sin\varphi' = 1 + \frac{2}{2}\sin 30^o = 1.5 \quad \text{(Eq. 5.25)}$$

$$s_c = \frac{s_q N_q - 1}{N_q - 1} = \frac{1.5 \cdot 18.40 - 1}{18.40 - 1} = 1.847 \quad \text{(Eq. 5.26)}$$

$$s_\gamma = 1 - 0.3\frac{B}{L} = 1 - 0.3\frac{2}{2} = 0.7 \quad \text{(Eq. 5.27)}$$

Based on these data the load-bearing capacity:

$$\sigma_f = t\,\gamma\,N_q\,s_q + c\,N_c\,s_c + \gamma\,B\,N_\gamma\,s_\gamma \qquad \text{(Eq. 5.28)}$$

$$\sigma_f = 0 \cdot 16 \cdot 18.40 \cdot 1.5 + 1.6 \cdot 30.14 \cdot 1.847 + 16 \cdot 2 \cdot 11.20 \cdot 0.7 = 339.9 \frac{\text{kN}}{\text{m}^2} \qquad \text{(Eq. 5.29)}$$

Based on the finite element calculations the load-bearing capacity for the circular foundation is $q_{z.max}$ = 375 kN/m^2 (see Fig. 5.46). The differences (errors) between the FEM-Design calculations and the analytical solution is less than 11 %. For further information on this subject see [63]

5.3 Verification of soft clay models

For the verification of the soft clay material models (see Chapter 3.3) a simple soil strata was analyzed. See Fig 5.47 for the detailed geometry. The self-weight of the soil was neglected ($\gamma = 0$) and a total distributed surface load was applied on the top of the soil (see Fig. 5.47). The material model for the soil layer was over-consolidated (see Fig. 5.48). The Mohr-Coulomb failure criteria was neglected see Chapter 4.4, thus the effective frictional angle and the effective cohesion do not have any effects on the displacements. The input parameters based on Fig. 5.48 are as follows: $M_0 = 30000$ kN/m^2, $M_L = 1000$ kN/m^2, $M' = 13.4$, $p_C' = 50$ kN/m^2 ($\sigma_C' = 74.6$ kN/m^2), $p_L' = 100$ kN/m^2 ($\sigma_L' = 149.3$ kN/m^2), $\nu = 0.3$ and the applied surface load was $q_z = 300$ kN/m^2.

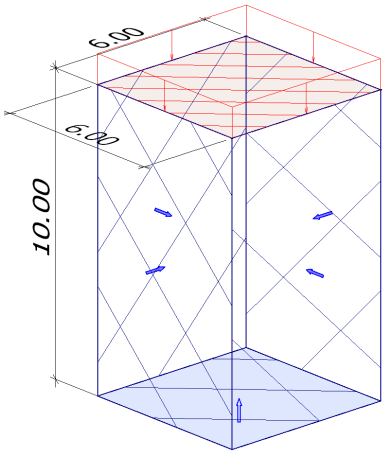

Figure 5.47 – The geometry of the problem and the boundary conditions (supports and q_z vertical surface load)

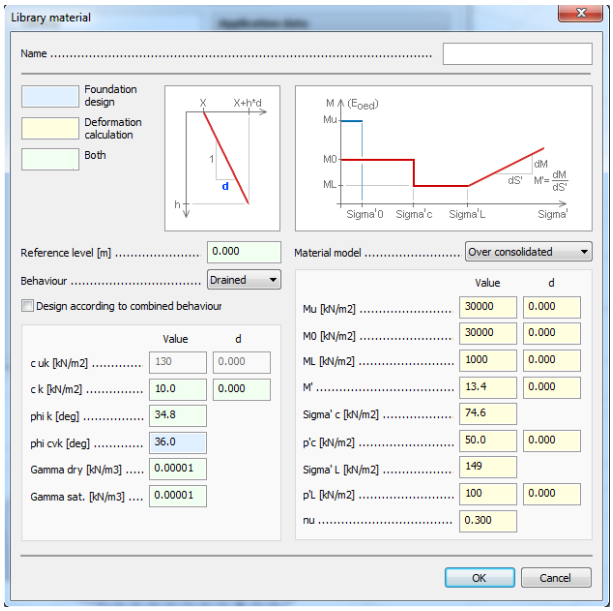

Figure 5.48 – The applied material model parameters for over-consolidated soil

Based on Chapter 3.3 until the stress state reach the mean effective preconsolidation pressure (p_C') the behaviour is linear elastic. (Be careful, the self-weight of the soil was neglected in this example.) According to the linear elastic theory (Chapter 3.1) the vertical stresses for a half-space are:

$$K_0=\frac{\nu}{1-\nu}=\frac{0.3}{1-0.3}=0.4286 \qquad \text{(Eq. 5.30)}$$

$$\sigma_x'=\sigma_y'=K_0\sigma_z'=0.4286\,\sigma_z' \qquad \text{(Eq. 5.31)}$$

$$p_C'=\frac{\sigma_x'+\sigma_y'+\sigma_z'}{3}=\frac{K_0\sigma_z'+K_0\sigma_z'+\sigma_z'}{3}=\frac{0.4286\,\sigma_z'+0.4286\,\sigma_z'+\sigma_z'}{3}=0.6191\,\sigma_z' \qquad \text{(Eq. 5.32)}$$

Based on Eq. 5.32 the pressure load (surface load) on the top of the soil can be calculeted which causes the mean effective pre-consolidation pressure:

$$\sigma_{z1}'=\frac{p_C'}{0.6191}=\frac{50}{0.6191}=80.76\frac{\text{kN}}{\text{m}^2}\ \text{(compression)} \qquad \text{(Eq. 5.33)}$$

Therefore the vertical displacement when the external load causes the mean effective preconsolidation pressure:

$$u_{z1}=\int_z^0\frac{\Delta\sigma_{z1}'}{M_0}dz=\frac{-(80.78-0)\cdot 10}{30000}=-0.02693\,\text{m} \qquad \text{(Eq. 5.34)}$$

Under further load increment the oedometer modulus depends on the stress state (see Chapter 3.3) thus until we reach the p_L' mean effective stress value the compression modulus is equal to M_L (see Fig. 5.48). Therefore the load value (pressure) when the mean effective stress reaches p_L' value is:

$$\sigma_{z2}'=\frac{p_L'}{0.6191}=\frac{100}{0.6191}=161.5\frac{\text{kN}}{\text{m}^2}\ \text{(compression)} \qquad \text{(Eq. 5.35)}$$

Therefore the vertical displacement when the external load causes this mean effective stress:

$$u_{z2}=u_{z1}+\int_z^0\frac{\Delta\sigma_{z2}'}{M_L}dz=-0.02693+\frac{-(161.6-80.78)\cdot 10}{1000}=-0.8351\,\text{m} \qquad \text{(Eq. 5.36)}$$

After this stress state the stress dependency is different (see Fig. 5.48). The connection between the mean effective stresses and compression modulus is linear in this case. Thus after p_L' mean effective stress the vertical-stress - vertical-strain relationship in this case is the following:

$$d\varepsilon_z = \frac{1}{M_L - 0.6191 M_p' \sigma_z'} d\sigma_z' \qquad \text{(Eq. 5.37)}$$

$$\varepsilon_z = \int_{\Delta\sigma_z'} \frac{1}{M_L - 0.6191 M_p' \sigma_z'} d\sigma_z' \qquad \text{(Eq. 5.38)}$$

where $M_p' = 1.5\ M' = 20$, because M' is given in the function of $\Delta\sigma_z'$ and during the calculation we need M_p' what is given in the function of $\Delta p'$ (see Fig. 5.48 and Chapter 3.3).

In this case the stress increment is equal to the difference between the value of the applied surface load (q_z = 300 kN/m^2) and surface pressure which belongs to p_L' (see Eq. 5.35). Thus this $\Delta\sigma_{z3}'$ = 300 – 161.5 = 138.5 kN/m^2 (compression).

From the stress increment the vertical strain can be calcaulted (see Eq. 5.38). To calculate the additional vertical displacements the following determinated integral must be calculated:

$$\Delta u_{z3} = \int_z^0 \varepsilon_z dz = \int_z^0 \int_{\Delta\sigma_z'} \frac{1}{M_L - 0.6191 M_p' \sigma_z'} d\sigma_z' dz \qquad \text{(Eq. 5.39)}$$

Therefore the vertical displacement when the external load reaches q_z = 300 kN/m^2:

$$u_{z3} = u_{z2} + \int_z^0 \frac{\Delta\sigma_{z3}'}{M(\sigma_z')} dz = u_{z2} + \int_z^0 \int_0^{\Delta\sigma_{z3}'} \frac{1}{M_L - 0.6191 M_p' \sigma_z'} d\sigma_z' dz = \qquad \text{(Eq. 5.40)}$$

$$= -0.8351 + \int_{-10\,\mathrm{m}}^0 \int_0^{-138.5} \frac{1}{1000 - 0.6191 \cdot 20\sigma_z'} d\sigma_z' dz = -0.8351 + \int_{-10\,\mathrm{m}}^0 (-0.08063) dz =$$

$$= -0.8351 + (-0.08063)[(0) - (-10)] = -0.8351 - 0.8063 = -1.6414\ \mathrm{m}$$

Fig. 5.49 shows the vertical load – vertical displacement diagram of the calculation with FEM-Design and the relevant values at different load values.

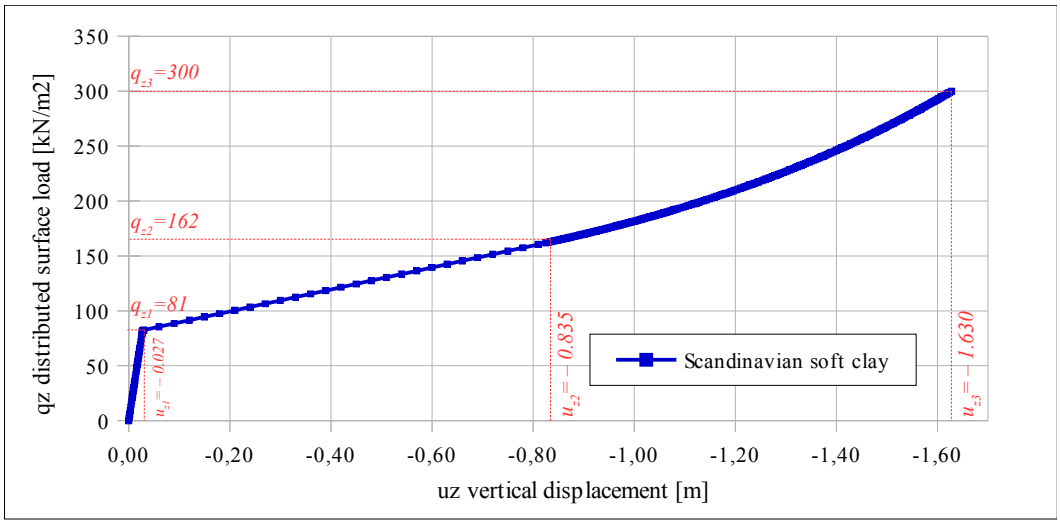

Figure 5.49 – Load-displacement curve with the significant values

The differences (error) between the FEM-Design calculations and the theoretical analytical solutions are less than 0.7 % (see Fig. 5.49 and Eq. 5.40).

5.4 Verification of the effect of water pressure and effective stresses

The following example will give information about the effect of water pressure and the calculation of effective stresses. In this case only the self-weight of the strata will be active. Thus the relevant load-combinations will contain the same load-case, namely the „soil dead load". But in the three different analyzed combinations the corresponding ground water levels (GWL) will be different. In the next figure one can see the input geometry and the three different GWL-s (Fig. 5.50).

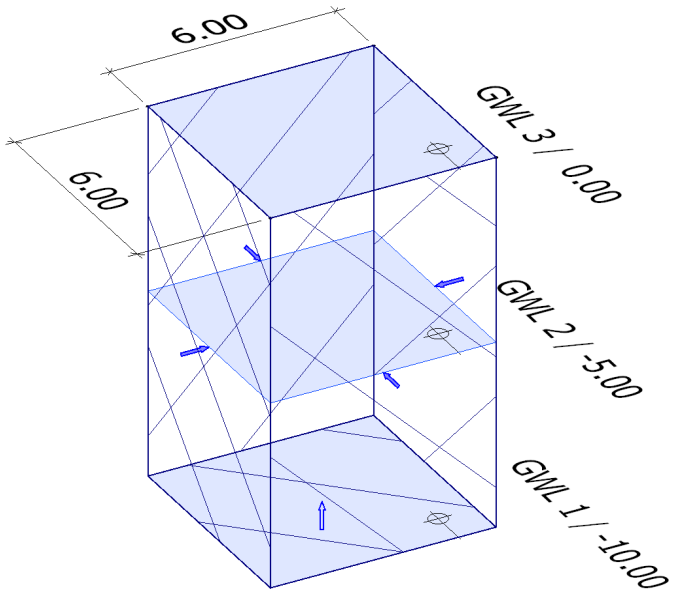

Figure 5.50 – The geometry and the three different ground water levels (GWL)

The limit depth was $z = -10$ m, GWL1 was on $z = -10$ m, GWL2 was on $z = -5$ m and GWL3 was on $z = 0$ m. The compression modulus was $M_0 = E_{oed} = 10000$ kPa, the Poisson's ratio was $\nu = 0.3$, thus the $\varphi' = 34.86^0$. The dry self-weight of the soil was $\gamma_{dry} = 18$ kN/m^3, the saturated self-weight of the soil was $\gamma_{sat} = 20$ kN/m^3. The self-weight of the water is $\gamma_w = 10$ kN/m^3.

Let's see the analytical exact solution for the stress distribution and the defomartion for this half-space problem. The coefficient of earth pressure at rest in this case (see the first footnote in Chapter 3.2.2):

$$K_0 = 1 - \sin\varphi' = \frac{\nu}{1-\nu} = 1 - \sin\left(34.85^o\right) = \frac{0.3}{1-0.3} = 0.4286 \qquad \text{(Eq. 5.41)}$$

In FEM-Design the K_0 value depends on the Poisson's ratio (see the first footnote in Chapter 3.2.2).

The effective vertical stresses by the three different ground water levels (GWL) at different heights are the following respectively. The effective vertical stress at the top is equal to zero in the three cases:

$$\sigma_{z1}'_{(z=0)}=\sigma_{z2}'_{(z=0)}=\sigma_{z3}'_{(z=0)}=0 \qquad \text{(Eq. 5.42)}$$

The effective vertical stresses at $z = -5$ m are as follows by the three different ground water levels:

$$\sigma_{z1}'_{(z=-5m)}=\gamma_{dry}(-5\,\mathrm{m})=18\cdot(-5)=-90\,\frac{\mathrm{kN}}{\mathrm{m}^2} \qquad \text{(Eq. 5.43)}$$

$$\sigma_{z2}'_{(z=-5m)}=\gamma_{dry}(-5\mathrm{m})=-90\,\frac{\mathrm{kN}}{\mathrm{m}^2} \qquad \text{(Eq. 5.44)}$$

$$\sigma_{z3}'_{(z=-5m)}=(\gamma_{sat}-\gamma_{w})(-5\mathrm{m})=10\cdot(-10)=-50\,\frac{\mathrm{kN}}{\mathrm{m}^2} \qquad \text{(Eq. 5.45)}$$

The effective vertical stresses at $z = -10$ m are as follows by the three different ground water levels:

$$\sigma_{z1}'_{(z=-10m)}=\gamma_{dry}(-10\,\mathrm{m})=18\cdot(-10)=-180\,\frac{\mathrm{kN}}{\mathrm{m}^2} \qquad \text{(Eq. 5.46)}$$

$$\sigma_{z2}'_{(z=-10m)}=\gamma_{dry}(-5\mathrm{m})+(\gamma_{sat}-\gamma_{w})(-5\mathrm{m})=18\cdot(-5)+10\cdot(-5)=-140\,\frac{\mathrm{kN}}{\mathrm{m}^2} \qquad \text{(Eq. 5.47)}$$

$$\sigma_{z3}'_{(z=-10m)}=(\gamma_{sat}-\gamma_{w})(-10\mathrm{m})=10\cdot(-10)=-100\,\frac{\mathrm{kN}}{\mathrm{m}^2} \qquad \text{(Eq. 5.48)}$$

The finite element calculation gives very close values to the exact solution for the effective vertical stresses (see Fig. 5.51).

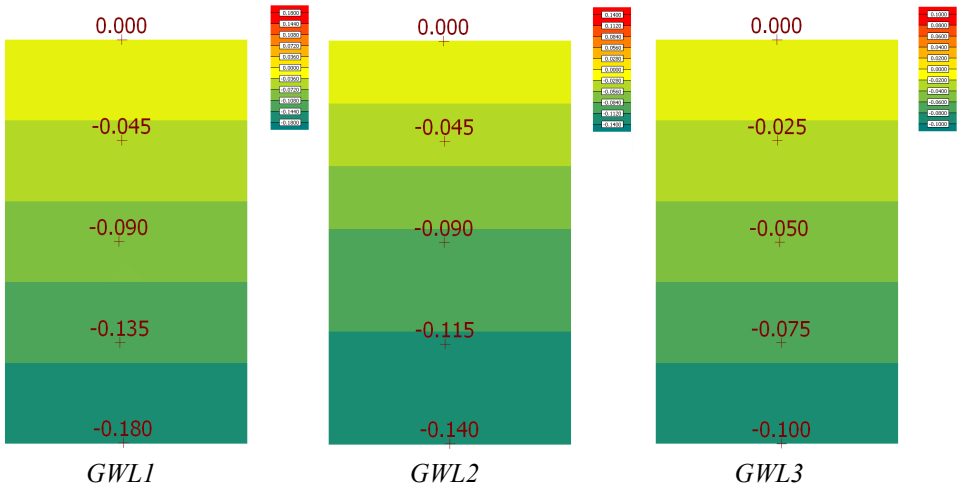

Figure 5.51 – The effective vertical stresses by the different ground water levels [MPa]

The effective horizontal stresses by the three different ground water levels (GWL) at different heights. The effective horizontal stresses at $z = 0$ m are equal to zero:

$$\sigma_{x1}'_{(z=0)} = \sigma_{x2}'_{(z=0)} = \sigma_{x3}'_{(z=0)} = 0 \qquad \text{(Eq. 5.49)}$$

The effective horizontal stresses at $z = -5$ m are as follows by the three different ground water levels:

$$\sigma_{x1}'_{(z=-5m)} = K_0 \sigma_{z1}'_{(z=-5m)} = 0.4286 \cdot (-90) = -38.57 \frac{\text{kN}}{\text{m}^2} \qquad \text{(Eq. 5.50)}$$

$$\sigma_{x2}'_{(z=-5m)} = K_0 \sigma_{z2}'_{(z=-5m)} = 0.4286 \cdot (-90) = -38.57 \frac{\text{kN}}{\text{m}^2} \qquad \text{(Eq. 5.51)}$$

$$\sigma_{x3}'_{(z=-5m)} = K_0 \sigma_{z3}'_{(z=-5m)} = 0.4286 \cdot (-50) = -21.43 \frac{\text{kN}}{\text{m}^2} \qquad \text{(Eq. 5.52)}$$

The effective horizontal stresses at $z = -10$ m are as follows by the three different ground water levels:

$$\sigma_{x1}'_{(z=-10m)} = K_0 \sigma_{z1}'_{(z=-10m)} = 0.4286 \cdot (-180) = -77.14 \frac{\text{kN}}{\text{m}^2} \qquad \text{(Eq. 5.53)}$$

$$\sigma_{x2}'_{(z=-10m)} = K_0 \sigma_{z2}'_{(z=-10m)} = 0.4286 \cdot (-140) = -60.00 \frac{\text{kN}}{\text{m}^2} \qquad \text{(Eq. 5.54)}$$

$$\sigma_{x3}'_{(z=-10m)} = K_0 \sigma_{z3}'_{(z=-10m)} = 0.4286 \cdot (-100) = -42.86 \frac{\text{kN}}{\text{m}^2} \qquad \text{(Eq. 5.55)}$$

The finite element calculation gives very close values to the exact solution for the effective horizontal stresses (see Fig. 5.52).

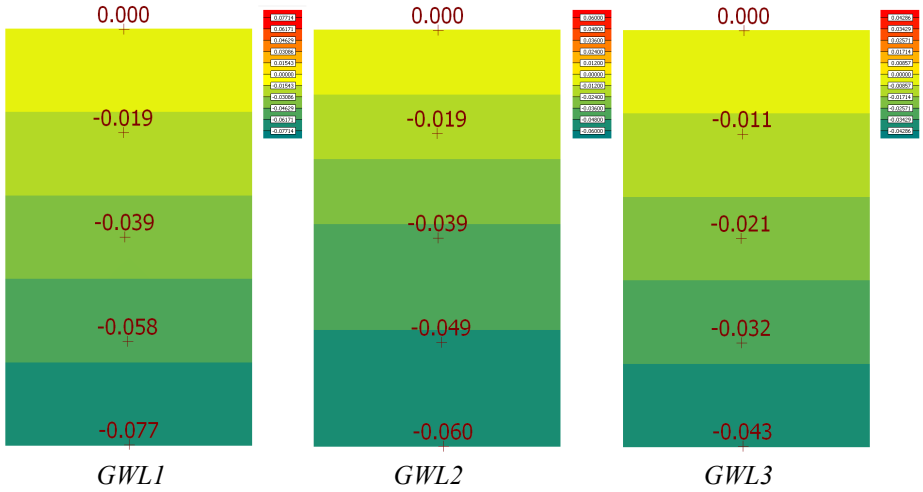

Figure 5.52 – The effective horizontal stresses by the different ground water levels [MPa]

The pressure on sidewalls (reactions at surface support) is equal to the total stresses in the soil. The total horizontal pressure comes from the effective horizontal earth pressure plus water pressure. The total horizontal pressure values by the different ground water levels at different heights:

The total horizontal stresses at $z = 0$ m are equal to zero.

$$\sigma_{x1(z=0)} = \sigma_{x2(z=0)} = \sigma_{x3(z=0)} = 0 \qquad \text{(Eq. 5.56)}$$

The total horizontal stresses at $z = -5$ m are as follows by the three different ground water levels:

$$\sigma_{x1(z=-5\,\mathrm{m})} = \sigma_{x1}{}'_{(z=-5m)} + \gamma_w(0\mathrm{m}) = -38.57 + 0 = -38.57\,\frac{\mathrm{kN}}{\mathrm{m}^2} \qquad \text{(Eq. 5.57)}$$

$$\sigma_{x2(z=-5\,\mathrm{m})} = \sigma_{x2}{}'_{(z=-5m)} + \gamma_w(0\mathrm{m}) = -38.57 + 0 = -38.57\,\frac{\mathrm{kN}}{\mathrm{m}^2} \qquad \text{(Eq. 5.58)}$$

$$\sigma_{x3(z=-5\,\mathrm{m})} = \sigma_{x3}{}'_{(z=-5m)} + \gamma_w(-5\mathrm{m}) = -21.43 + (-50) = -71.43\,\frac{\mathrm{kN}}{\mathrm{m}^2} \qquad \text{(Eq. 5.59)}$$

The total horizontal stresses at $z = -10$ m are as follows by the three different ground water levels:

$$\sigma_{x1(z=-10\,\mathrm{m})}=\sigma_{x1}{}'_{(z=-10m)}+\gamma_w(0\mathrm{m})=-77.14+0=-77.14\,\frac{\mathrm{kN}}{\mathrm{m}^2} \quad \text{(Eq. 5.60)}$$

$$\sigma_{x2(z=-10\,\mathrm{m})}=\sigma_{x2}{}'_{(z=-10m)}+\gamma_w(-5\mathrm{m})=-60.0+(-50)=-110.0\,\frac{\mathrm{kN}}{\mathrm{m}^2} \quad \text{(Eq. 5.61)}$$

$$\sigma_{x3(z=-10\,\mathrm{m})}=\sigma_{x3}{}'_{(z=-10m)}+\gamma_w(-10\mathrm{m})=-42.86+(-100)=-142.9\,\frac{\mathrm{kN}}{\mathrm{m}^2} \quad \text{(Eq. 5.62)}$$

The total vertical stresses at $z = -10$ m are as follows by the three different ground water levels:

$$\sigma_{z1(z=-10\,\mathrm{m})}=\sigma_{z1}{}'_{(z=-10m)}+\gamma_w(0\mathrm{m})=-180+0=-180\,\frac{\mathrm{kN}}{\mathrm{m}^2} \quad \text{(Eq. 5.63)}$$

$$\sigma_{z2(z=-10\,\mathrm{m})}=\sigma_{z2}{}'_{(z=-10m)}+\gamma_w(-5\mathrm{m})=-140+(-50)=-190.0\,\frac{\mathrm{kN}}{\mathrm{m}^2} \quad \text{(Eq. 5.64)}$$

$$\sigma_{z3(z=-10\,\mathrm{m})}=\sigma_{z3}{}'_{(z=-10m)}+\gamma_w(-10\mathrm{m})=-100+(-100)=-200\,\frac{\mathrm{kN}}{\mathrm{m}^2} \quad \text{(Eq. 5.65)}$$

The finite element calculation gives very close values to the exact solution for the total horizontal and vertical pressures (see Fig. 5.53).

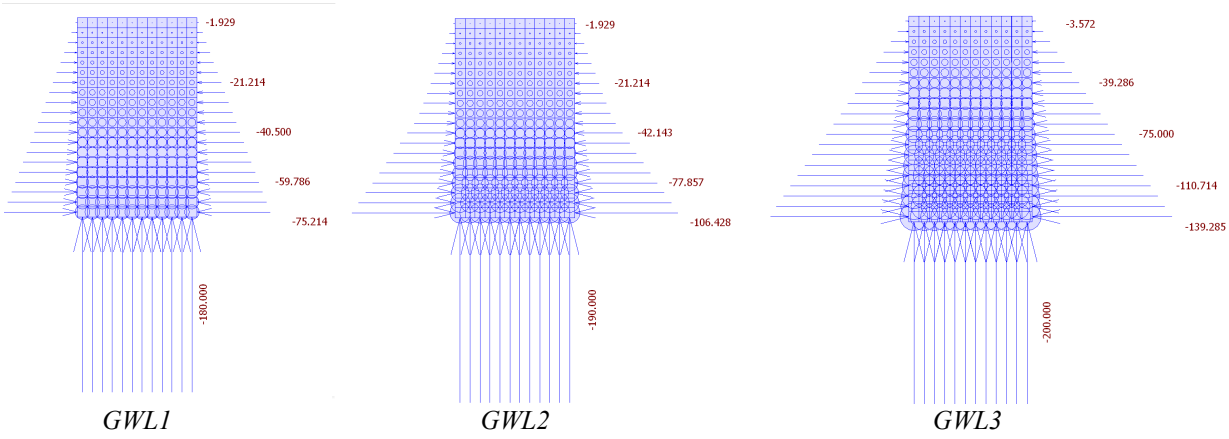

Figure 5.53 – The total horizontal pressures (surface reactions) by the different ground water levels [kPa]

The settlements caused by the self-weight of the soil comes from the effective stresses. The vertical settlements are as follows at the top of the soil by the three different GWL-s.

$$u_{z\,max1}=\int_z^0 \frac{\sigma_z{}'}{M_0}dz=\int_z^0 \frac{\gamma_{dry}\,z}{M_0}dz=\frac{\gamma_{dry}}{M_0}\left[\frac{z^2}{2}\right]_{-10}^{0}=\frac{18}{10000}\left[\frac{0^2}{2}-\frac{(-10)^2}{2}\right]=-0.090\,\mathrm{m} \quad \text{(Eq. 5.66)}$$

$$u_{z\,max2}=\int_{z}^{0}\frac{\sigma_z'}{M_0}dz=\int_{-5}^{0}\frac{\gamma_{dry}z}{M_0}dz+\int_{-10}^{-5}\left(\frac{(\gamma_{sat}-\gamma_w)z-5(\gamma_{dry}-(\gamma_{sat}-\gamma_w))}{M_0}\right)dz= \qquad \text{(Eq. 5.67)}$$

$$=\frac{18}{10000}\left[\frac{z^2}{2}\right]_{-5}^{0}+\frac{1}{10000}\left[\frac{10z^2}{2}-40z\right]_{-10}^{-5}=$$

$$=\frac{18}{10000}\left[\frac{0^2}{2}-\frac{(-5)^2}{2}\right]+\frac{1}{10000}\left[10\left(\frac{(-5)^2}{2}-\frac{(-10)^2}{2}\right)-40\left((-5)-(-10)\right)\right]=-0.080\,\text{m}$$

$$u_{z\,max3}=\int_{z}^{0}\frac{\sigma_z'}{M_0}dz=\int_{z}^{0}\frac{(\gamma_{sat}-\gamma_w)z}{M_0}dz=\frac{(\gamma_{sat}-\gamma_w)}{M_0}\left[\frac{z^2}{2}\right]_{-10}^{0}=\frac{10}{10000}\left[\frac{0^2}{2}-\frac{(-10)^2}{2}\right]=-0.050\,\text{m}$$

(Eq. 5.68)

The finite element calculation gives very close values to the exact solution for the vertical settlements also (see Fig. 5.54).

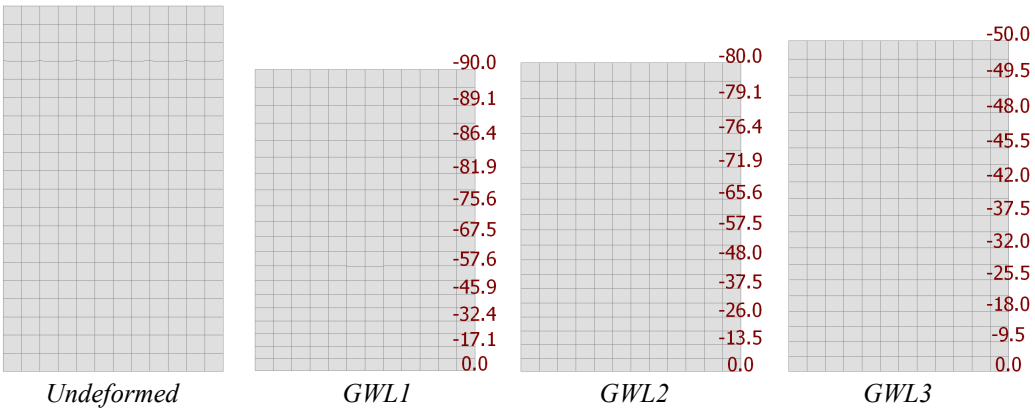

Figure 5.54 – The undeformed sideview and the vertical settlements by the different ground water levels [mm]

5.5 Verification of the effect of lateral pressures on basement walls

The limit depth was $z = -10$ m, GWL1 was on $z = -10$ m, GWL2 was on $z = -7.5$ m , GWL3 was on $z = -2.5$ m and GWL 4 was on $z = 0.0$ m. The compression modulus was $M_0 = E_{oed} = 10000$ kPa, the Poisson's ratio was $\nu = 0.3$. The self-weight of the soil was $\gamma_{dry} = 18$ kN/m^3, the saturated self-weight of the soil was $\gamma_{sat} = 20$ kN/m^3. The self-weight of the water is $\gamma_w = 10$ kN/m^3. In the middle of the modelled soil space a foundation slab (thickness equal to 1.0 m) was created but the level of the slab was under the top of the ground level ($z = -5$ m, see Fig. 5.55 and 5.56). There are four vertical basement walls (thickness equal to 20 cm) at the edge of the foudation slab and at different levels there are three plates (thickness equal to 20 cm) between the walls, see also the figures about the geometry. All of these mentioned planar parts were modelled with $\gamma_{RC} = 25$ kN/m^3 and C25/30 concrete material.

In FEM-Design the friction between the basement walls and the soil is neglected. Based on this approximation with a hand calculation we will show the analytical results of the earth pressure and water pressure which have affect on the basement walls and the finite element calculation with FEM-Design according to the different ground water levels.

In this example the average element size was 1.0 m and fine (quadratic) element group was applied during the finite element calculations (see Fig. 5.57).

The considered load-combination contains the dead load of the soil with the indicated self-weights and the self-weight of the mentioned structure (see Fig. 5.55 and 5.56). The load-combination calculation was considered with non-linear soil calculation without uplift (see the „New features guide” for more details).

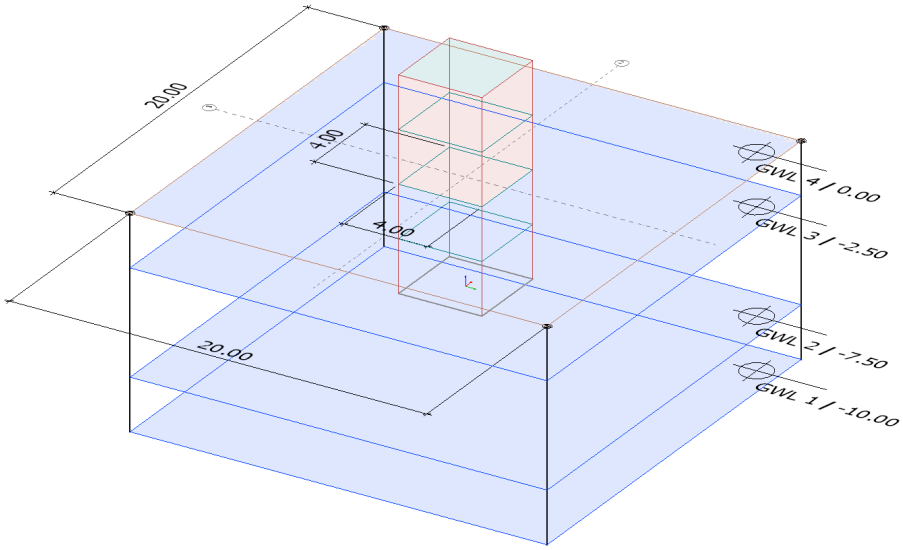

Figure 5.55 – The geometry and the four different ground water levels (GWL)

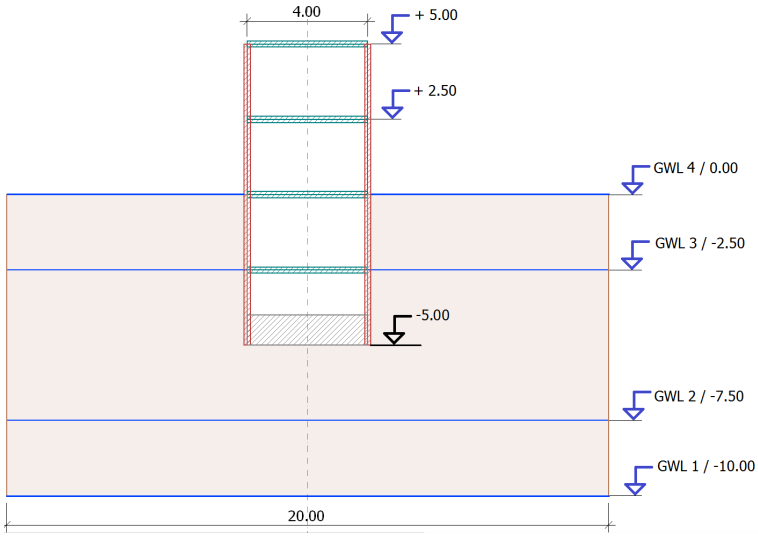

Figure 5.56 – The geometry and the four different ground water levels (GWL) in section view

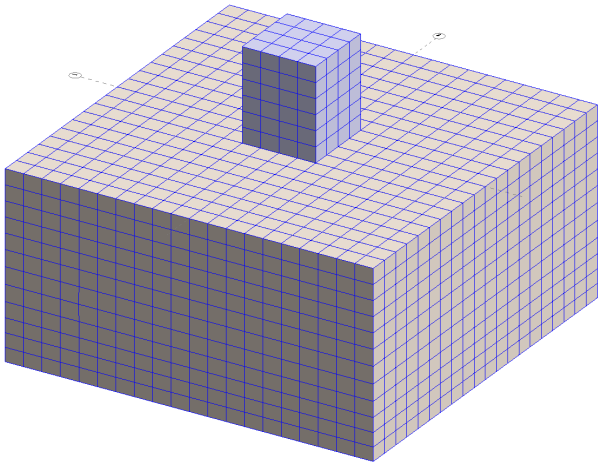

Figure 5.57 – The finite element mesh (*average element size:* 1.0 m)

By the hand calculation of the horizontal pressure on the basement walls the rest earth pressure was assumed because the rigidity of the modelled building is quite great. Thus the coefficient of earth pressure at rest (see the first footnote in Chapter 3.2.2):

$$K_0 = 1 - \sin\varphi' = \frac{\nu}{1-\nu} = \frac{0.3}{1-0.3} = 0.4286 \qquad \text{(Eq. 5.69)}$$

In FEM-Design the K_0 value depends on the Poisson's ratio (see the first footnote in Chapter 3.2.2).

Fig. 5.58 shows the results of the hand calculation without details for GWL 1 and GWL 2. The first diagram shows the total vertical stress (σ_V) next to the basement walls considering the water

level and the dry and saturated self-weight of the soil. The second shows the water pressure considering the level of the water in the soil (σ_W in case of GWL 1 and GWL 2 are zero because the level of the water is lower than the level of the foundation slab, see Fig. 5.56). The third diagram is the effective vertical stress (σ'_V) which is the difference between the total vertical stress and water pressure (see Chapter 1.3). The fourth one shows the effective horizontal stress (σ'_H) based on K_0 and σ'_V. The fifth diagram is the total horizontal stress (σ_H) which comes from the effective horizontal stress plus the water pressure. The last result on Fig. 5.58 shows the position and the amount of the resultant force from total horizontal stress.

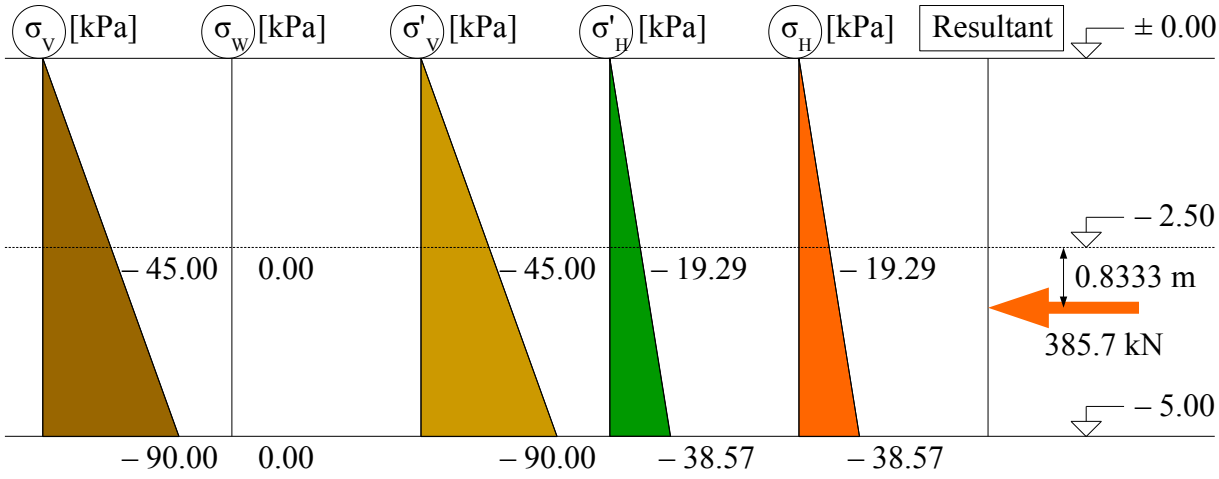

Figure 5.58 – The hand calculation of the horizontal wall pressures and resultant in case of GWL 1 and GWL 2

With the same theory and calculation method Fig. 5.59 shows the analytical results for GWL 3. The notation and the order of the diagram is equivalent with the former one.

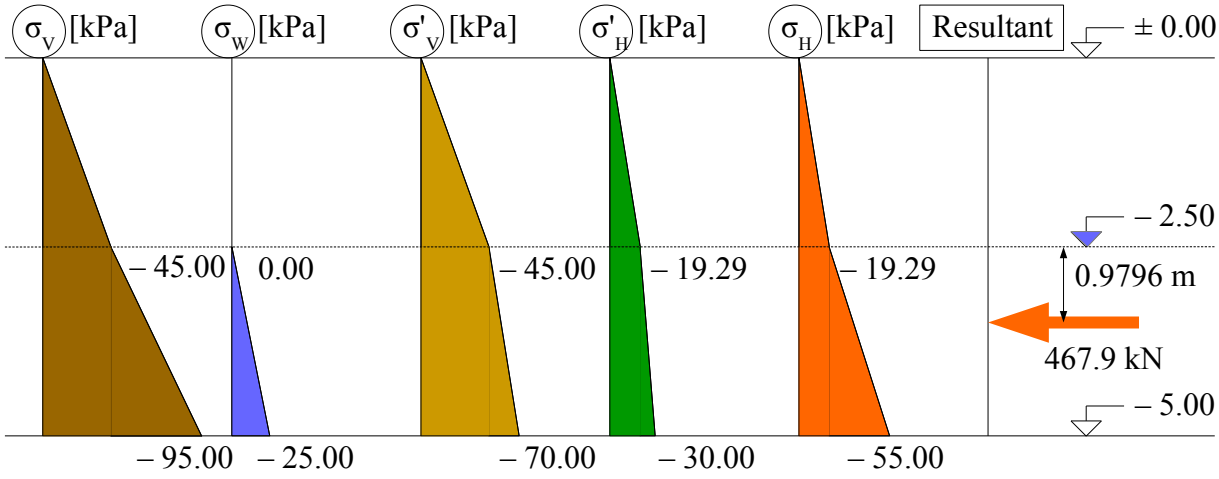

Figure 5.59 – The hand calculation of the horizontal wall pressures and resultant in case of GWL 3

With the same theory and calculation method Fig. 5.60 shows the analytical results for GWL 4

when the water level is at the top of the soil layer. The notation and the order of the diagram is equivalent with the former ones.

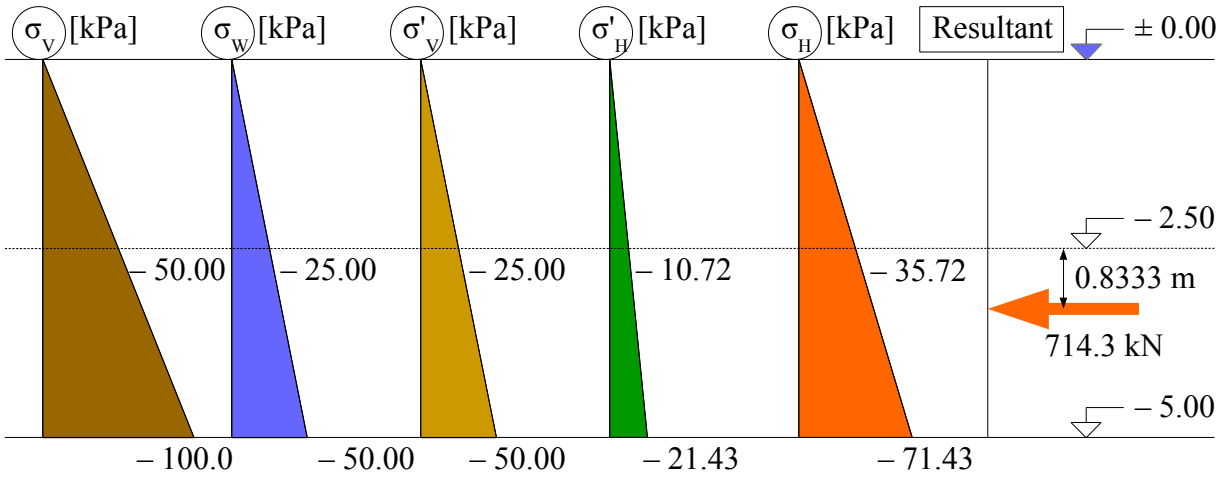

Figure 5.60 – The hand calculation of the horizontal wall pressures and resultant in case of GWL 4

Next figures (Fig. 5.61 and 5.62) show the results of the FEM-Design calculation. The results of the connection forces next to the basement walls give the total horizontal pressures which comes from the effective earth pressure plus the adequate water pressure.

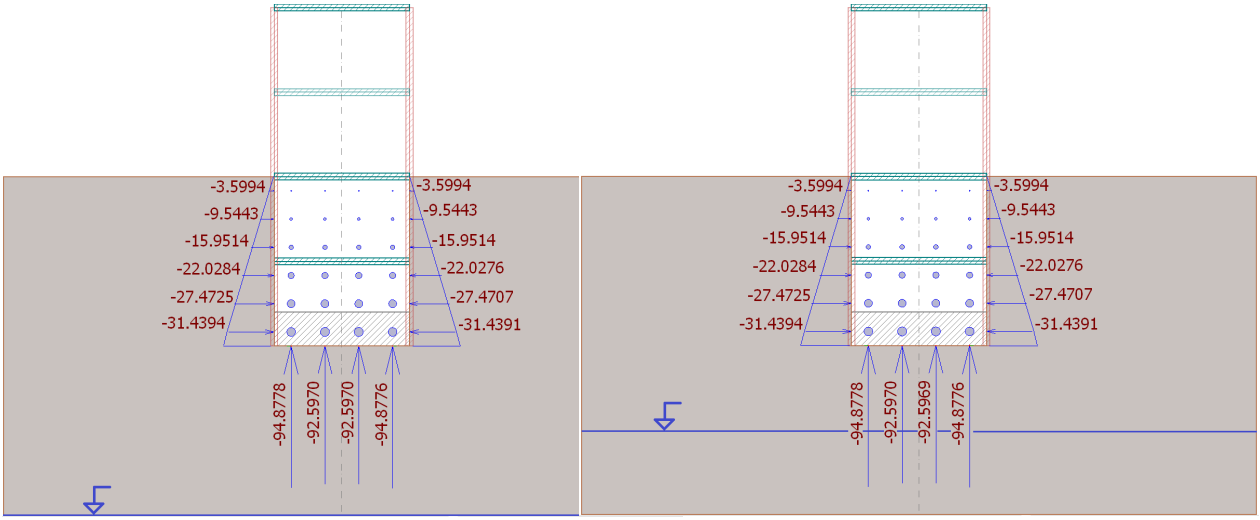

Figure 5.61 – The total horizontal pressures (connection forces) on the walls in [kPa]
GWL 1 left side, GWL 2 right side

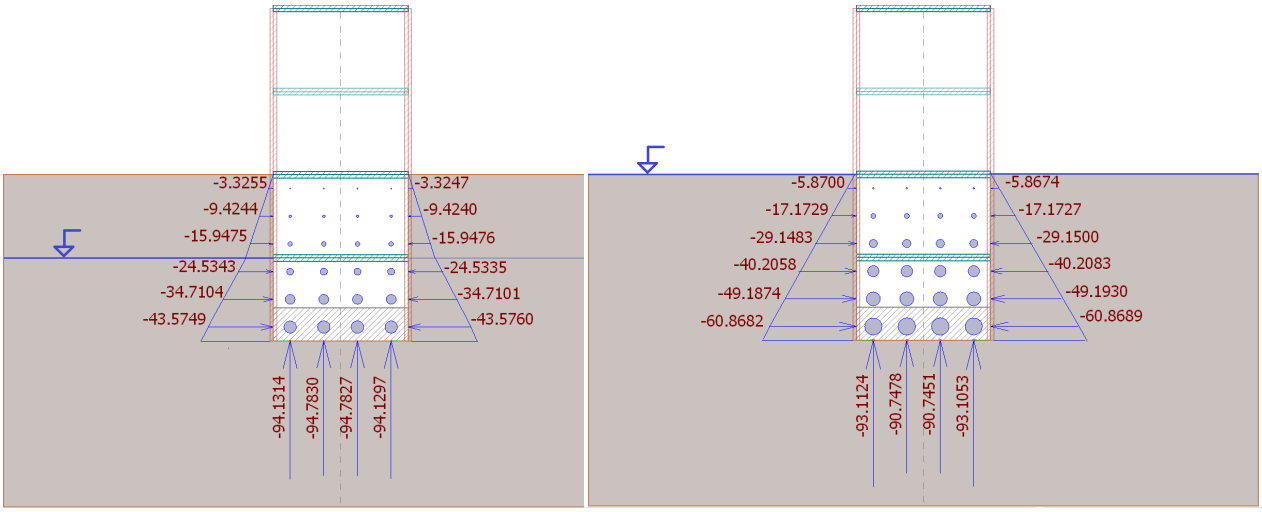

Figure 5.62 – The total horizontal pressures (connection forces) on the walls in [kPa]
GWL 3 left side, GWL 4 right side

Table 3 shows a comparison between the mentioned hand calculation and the FEM-Design calculation for the different ground water levels. The differences (error [%]) also included. The maximum difference is 14.13 %. The finite element results are in good agreement with the hand calculation. Do not forget that the stresses and pressures are the slave (secondary) variables of the FE technique, thus the results could be better if the finite element mesh is finer (more dense), see also Chapter 1.

Comparison	GWL 1 and GWL 2			GWL 3			GWL 4		
	Hand calculation	FEM-Design	Error [%]	Hand calculation	FEM-Design	Error [%]	Hand calculation	FEM-Design	Error [%]
Wall pressure at z = – 2.5 m [kPa]	– 19.29	– 18.99	1.555	– 19.29	– 18.99	1.555	– 35.72	– 34.68	2.912
Wall pressure at z = – 5.0 m [kPa]	– 38.57	– 33.42	13.35	– 55.00	– 48.01	12.71	– 71.43	– 66.71	6.608
Resultant force [kN]	385.7	363.6	5.730	467.9	435.5	6.925	714.3	669.2	6.314
Moment about z = – 2.5 m [kNm]	321.4	276.0	14.13	458.4	401.6	12.39	595.2	539.9	9.291
Position of the resultant [m] below z = – 2.5 m	0.8333	0.7591	8.904	0.9796	0.9222	5.860	0.8333	0.8068	3.180

Table 3 – The comparison of the hand and finite element calculation to the pressures on the basement walls

During a non-linear soil caculation the material model represent the connection between strains and effective stresses (see Chapter 1.3). Therefore check the stress results in the soil layer after the calculation in respect to the ground water levels. In the new geo module FEM-Design calcultes the displacements and strains with the effective stresses and at the results the solid stresses are always effective stresses.

In this example beyond the soil dead load the structural self-weight was considered. The sum of the dead load of the structures with the indicated geometry and materials is R = 1520 kN. It means that the average total vertical stress under the very stiff foundation slab must be:

$$\sigma_A = -\frac{R}{A} = \frac{1520\,\text{kN}}{16\,\text{m}^2} = -95\,\frac{\text{kN}}{\text{m}^2} \qquad \text{(Eq. 5.70)}$$

The reactions under the foundation slab almost equal to this average value in all case (by the four GWL-s), see Fig. 5.61 and 5.62. But this value contains the effect of the water levels if the ground water level is above the foundation slab. It means that the effective stresses in the soil under the foundation slab depends on the considered ground water levels.

Fig. 5.63 shows the vertical effective stresses in the soil in case of GWL 1 and GWL 2. It is obvious that the effective vertical stresses are the same above the two ground water level but at the limit depth they are different because the GWL-s were not the same. In both case the GWL-s were below the foundation slab therefore the stresses under the slab almost equal to the average hand calculated stress (see Eq. 5.70). Fig. 5.63 shows that this effective vertical stress value equal to – 91.3 kPa. The difference comes from tha mentioned fact that the stresses are the slave variables of FE technique but the difference is less than 4 %.

Fig. 5.64 shows the vertical effective stresses in the soil in case of GWL 3 and GWL 4. In both case the GWL-s were above the foundation slab therefore the stresses in the soil under the slab not equal to the average total vertical stress (see Eq. 5.70) because the effective stress in the soil depends on the water level. Fig. 5.64 shows the effective vertical stress values.

From the total stress value (Eq. 5.70) the lift force from the water (water pressure) must be substracted. In case of GWL 3 the water pressure is – 25 kPa (see Fig 5.59). Thus the average effective vertical stress under the slab must be – 95 – (–25) = – 70 kPa. In case of GWL 4 the water pressure is – 50 kPa (see Fig 5.60). Thus the average effective vertical stress under the slab must be – 95 – (–50) = – 45 kPa.

Fig. 5.64 shows the effective vertical stress in case of GWL 3 and GWL 4. Under the foundation slab these stress values are – 68.6 kPa and – 42.0 kPa based on the FE calculation in case of GWL 3 and GWL 4 respectively. The differences between the analytical results and finite element results are less than 7%.

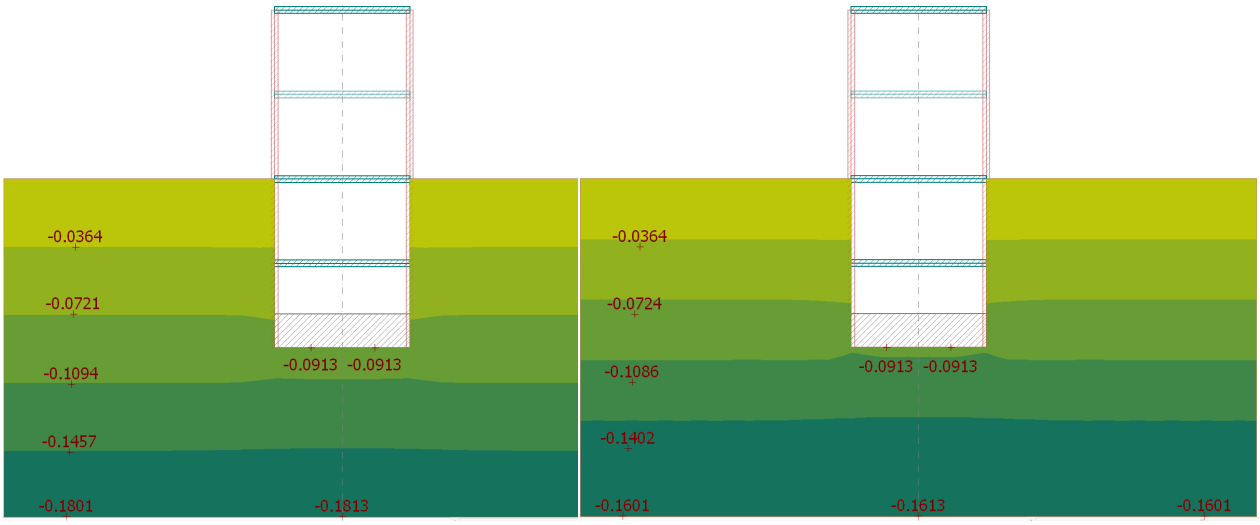

Figure 5.63 – The effective vertical stresses in [MPa]
GWL 1 left side, GWL 2 right side

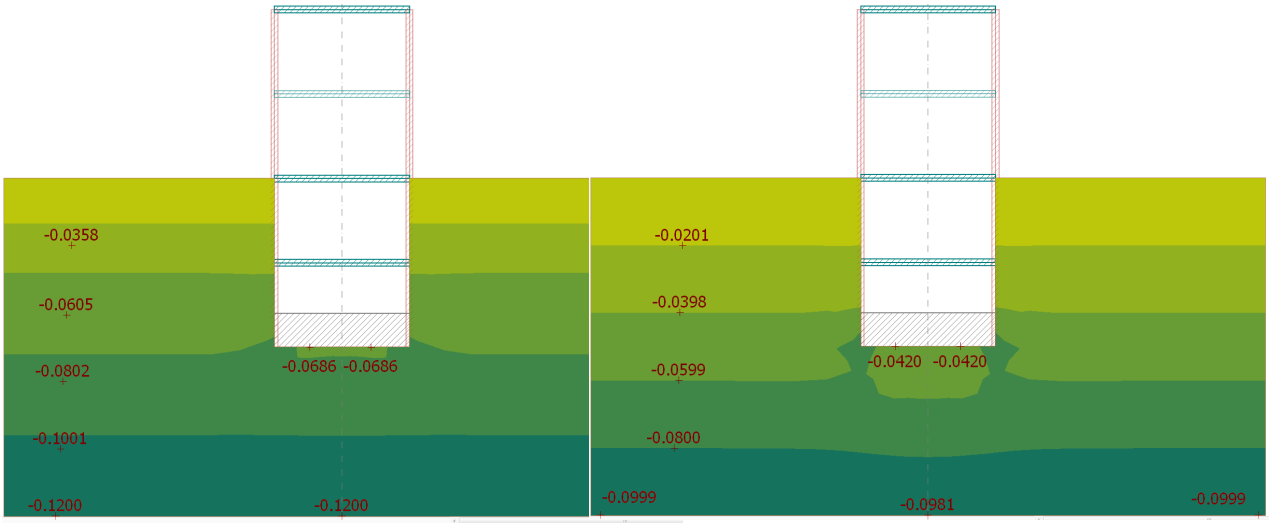

Figure 5.64 – The effective vertical stresses in [MPa]
GWL 3 left side, GWL 4 right side

According to the elasticity theory there is a unequivocal connection between the effective vertical and effective horizontal stresses. Therefore Fig. 5.65 and 5.66 show the effective vertical stresses in a section view of the modell. The comparison between these results and Fig 5.58-5.60 effective horizontal stress results by different GWL cases give quite close agreement. See also Table 4.

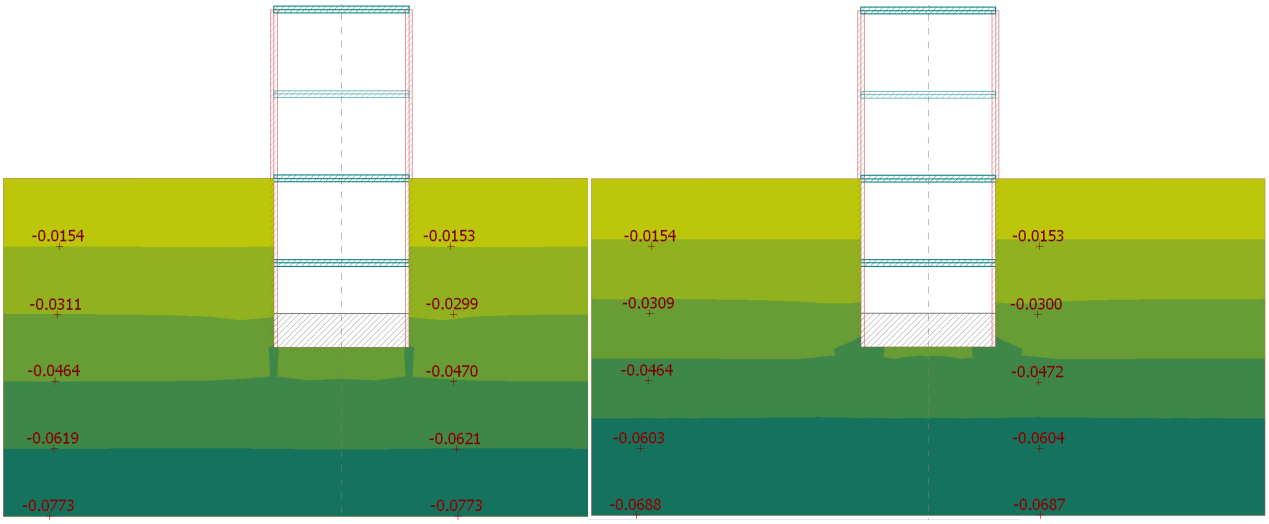

Figure 5.65 – The effective horizontal stresses in [MPa]
GWL 1 left side, GWL 2 right side

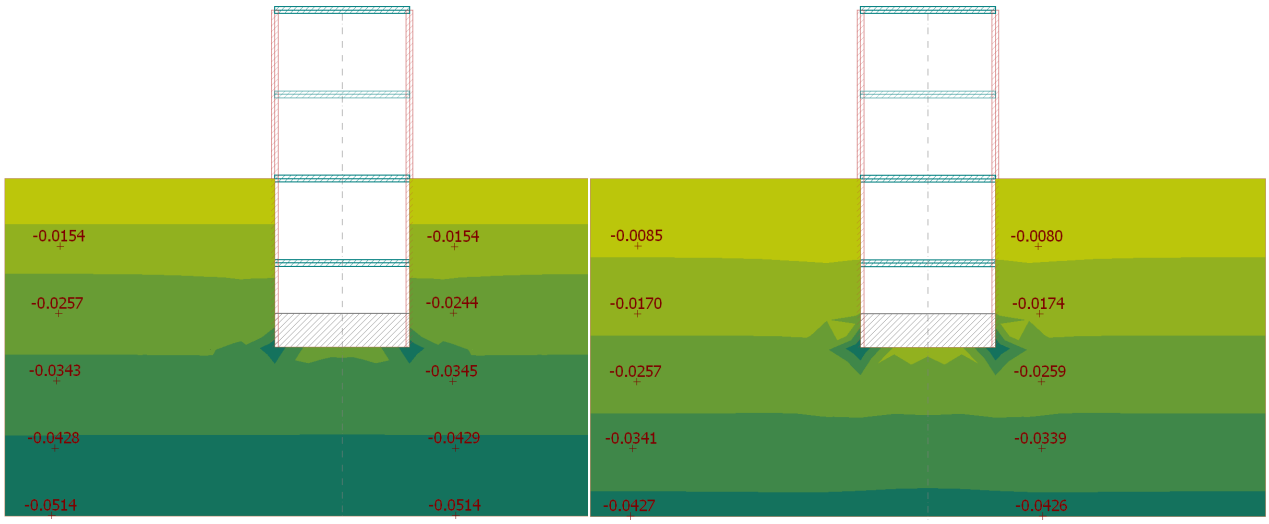

Figure 5.66 – The effective horizontal stresses in [MPa]
GWL 3 left side, GWL 4 right side

Comparison	GWL 1 and GWL 2			GWL 3			GWL 4		
	Hand calculation	FEM-Design	Error [%]	Hand calculation	FEM-Design	Error [%]	Hand calculation	FEM-Design	Error [%]
Effective horizontal stress at z = – 2.5 m [kPa]	– 19.29	– 19.23	0.3110	– 19.29	– 19.31	0.1037	– 10.72	– 10.34	3.545
Effective horizontal stress at z = – 5.0 m [kPa]	– 38.57	– 39.16	1.530	– 30.00	– 32.55	8.500	– 21.43	– 20.58	3.966

Table 4 – The comparison of the hand and finite element calculation to the effective horizontal stresses

All of the mentioned results depends on the stiffnesses of the structure and the amount of the applied loads. Now we get quite good agreements with the hand calculation (coefficient of earth pressure at rest Eq. 5.69) because the structure in the soil was quite rigid compared to the soil layer. According to the earth pressure theory (Chapter 3.2.2) the horizontal pressures depend on the movement of the structure towards or backwards to the soil which depend on the stiffnesses of the soil-structure interaction.

Fig. 5.67 shows the bending moment diagram of the basement walls and the foundation slab in a section which are in the soil in case of GWL 1 and GWL 4. The wall and the slab are surface elements thus the mentioned bending moments are those bending moments which have the bending moment vectors are perpendicular to the section (see Fig. 5.67). The total horizontal pressure on the basement walls are larger in case of GWL 4 than in GWL 1 therefore the bending moments in the walls are larger too in case of GWL 4 than GWL 1. This effect causes an opposite behaviour respect to the moments in the foundation slab.

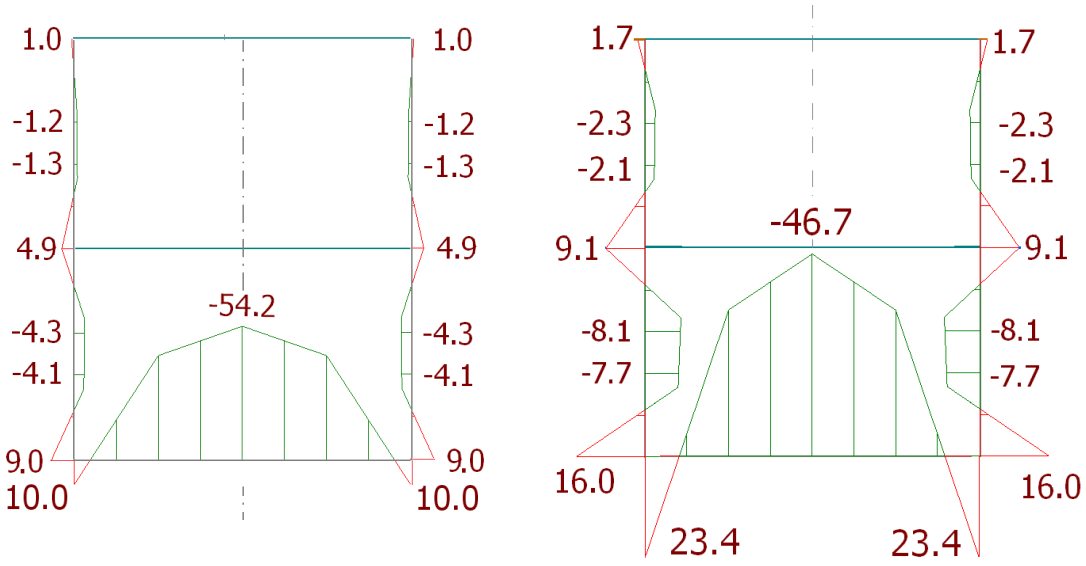

Figure 5.67 – The bending moments in the basement walls and in the foundation slab, the moment vectors are perpendicular to the section and the unit is [kNm/m]
GWL 1 left side, GWL 4 right side

5.6 Cantilever wall

In this chapter a cantilever wall was analyzed. The wall was bedded in the soil and the levels of the soil were different on the two sides of the wall (see Fig. 5.68). The difference between the two top levels of the soil was H = 3 m. The friction angle of the soil was $\varphi' = 20^o$, the self-weight of the soil was γ = 20 kN/m^2. Fig. 5.68 shows the input geometry and the material parameters.

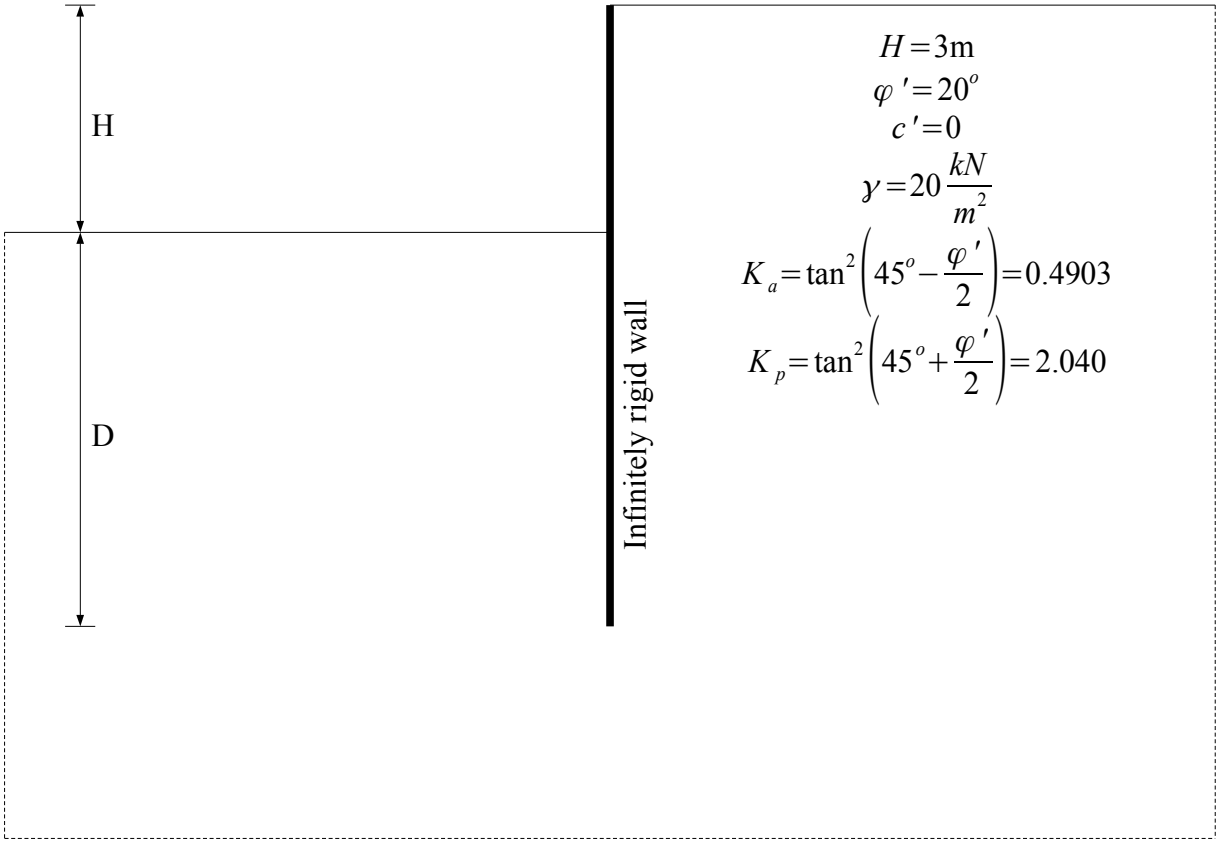

Figure 5.68 – The cantilever wall with the different soil levels on the left and right side and the input parameters

The minimal D depth of the wall is depends on the soil material parameters and the H height. Therefore the D depth is not known. By the calculation of D the active and passive earth pressure need to be considered on both sides of the wall. The wall will rotate around a point which is z distance from the bottom of the wall (see Fig. 5.69). The active and passive earth pressure ditributions are also shown in Fig. 5.69 based on the assumed rotation point. Thus based on these conditions there are two unknowns namely the D depth of the wall and the z position of the rotation point. Actually the mentioned earth pressures on the wall must be in equilibrium state which means that the sum of the forces on the wall in horizontal direction is zero and the sum of the moments in the considered plain is also zero. From these two equations the two unknowns can be calculated.

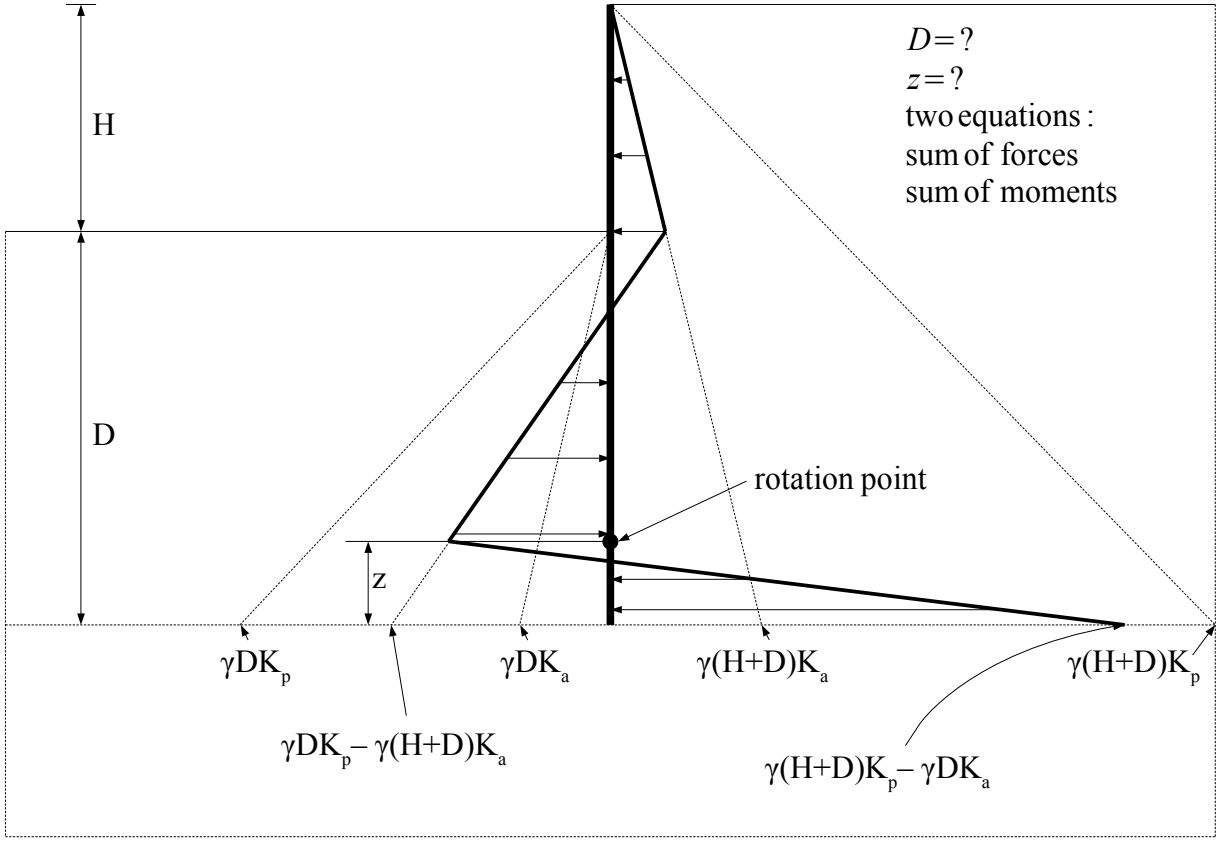

Figure 5.69 – Sum of the effect of active and passive earth pressures on the wall

Without the detailed calculations from the first equation (sum of forces) the solution for z in terms of D:

$$z=\frac{D^2 K_p-(H+D)^2 K_a}{(K_p-K_a)(H+2D)} \quad . \qquad \text{(Eq. 5.71)}$$

And from the second equation (sum of moments) we get the following equation using and substitute Eq. 5.71 into this equation:

$$(H+D)^3 K_a-D^3 K_p+\frac{(D^2 K_p-(H+D)^2 K_a)^2}{(K_p-K_a)(H+2D)}=0 \qquad \text{(Eq. 5.72)}$$

This is a fourth order polinom in terms of D. The physically possible solution for D and based on this value for z:

$$D=5.173\,\text{m}$$
$$z=1.056\,\text{m} \qquad \text{(Eq. 5.73)}$$

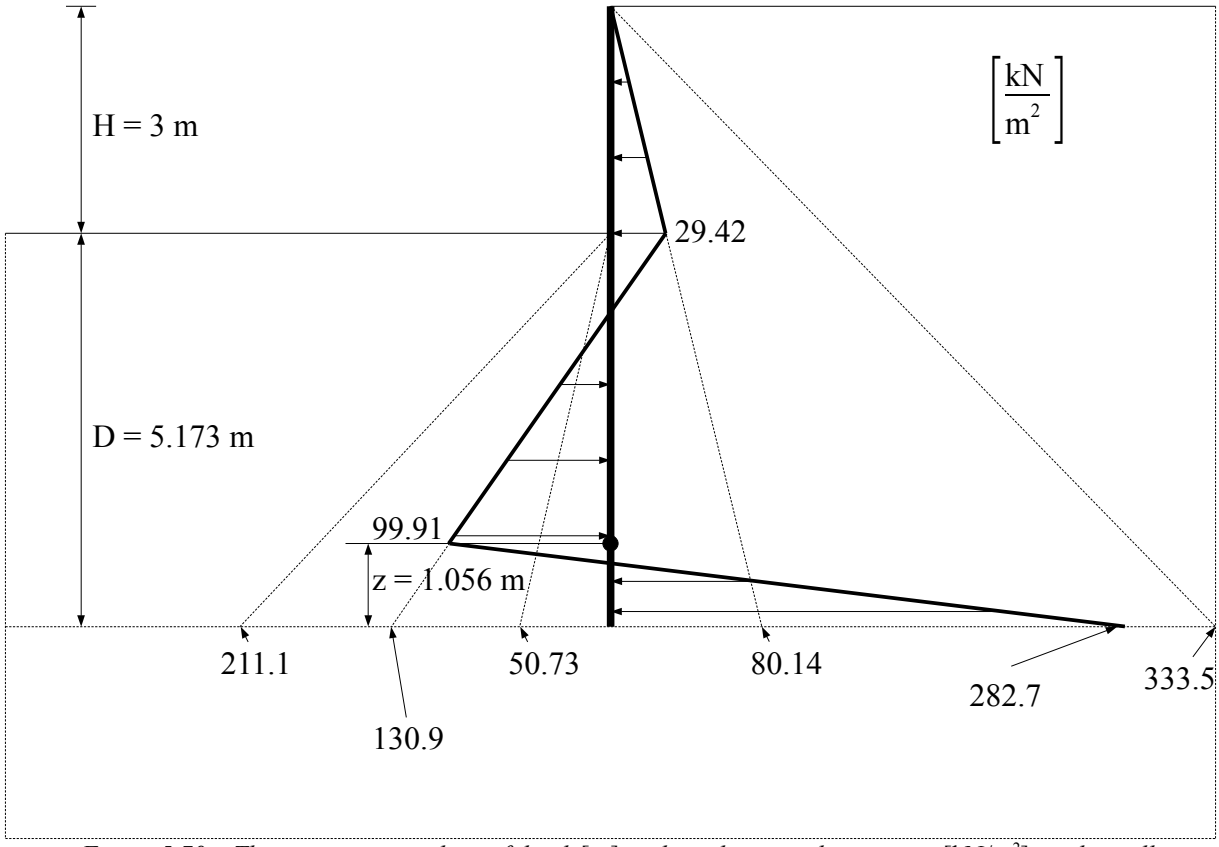

Figure 5.70 – The quantitative values of depth [m] *and resultant earth pressures* [kN/m^2] *on the wall*

Based on these values the quantitative sum of the resultant earth pressures on the wall can be calculated. Fig. 5.70 shows these calculeted values in [kN/m^2]. From the calculation method according to the active and passive earth pressures the wall is in equilibrium state, therefore it can also be thought as a plate with these external loads (pressures). Based on these pressures (Fig. 5.70) the relevant shear forces and moments can be calculated in the plate using static knowledge. The analytically calculated internal forces, namely the relevant shear forces and bending moments are shown in Fig. 5.71. Fig. 5.71 also shows the positions of the important points (roots and extremums). The black dots show the inflexion points.

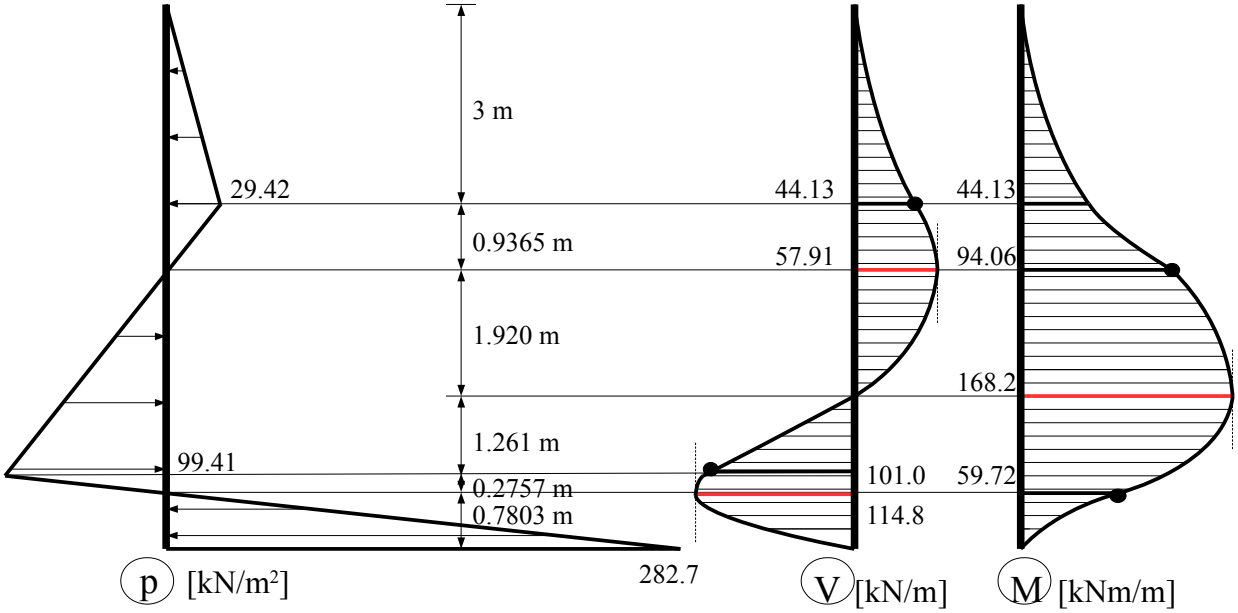

Figure 5.71 – The pressure, shear force and bending moment diagrams of the wall

After the analytical solution an FE model was built in FEM-Design based on the input geometry and the received parameters (H + D). The material model was the nonlinear Mohr-Coulomb material with the input parameters (see Fig. 5.68). The geometry of the built FE model can be seen in Fig 5.72. According to the fact that it can be considered as a 2D problem the width of the model is not relevant thus in the 3D model the width of the model was 0.4 m (see Fig. 5.72). The model space was 10-10 m in both directions from the wall and the limit depth was also 10 m.

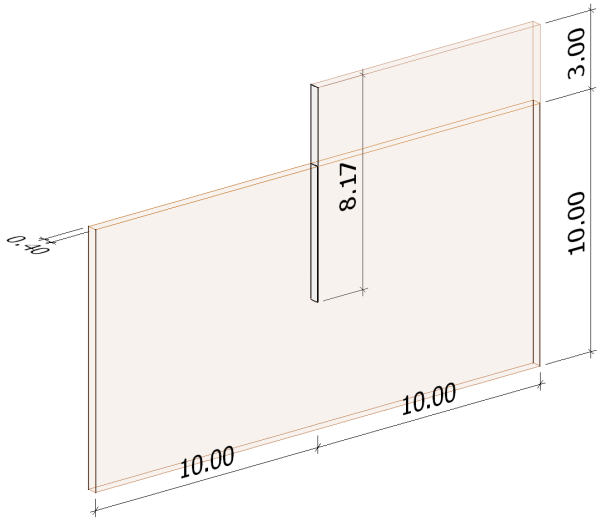

Figure 5.72 – The geometry of the problem [m]

The average mesh size in this problem was 0.20 m. The automatically generated mesh in two different view can be seen in Fig. 5.73.

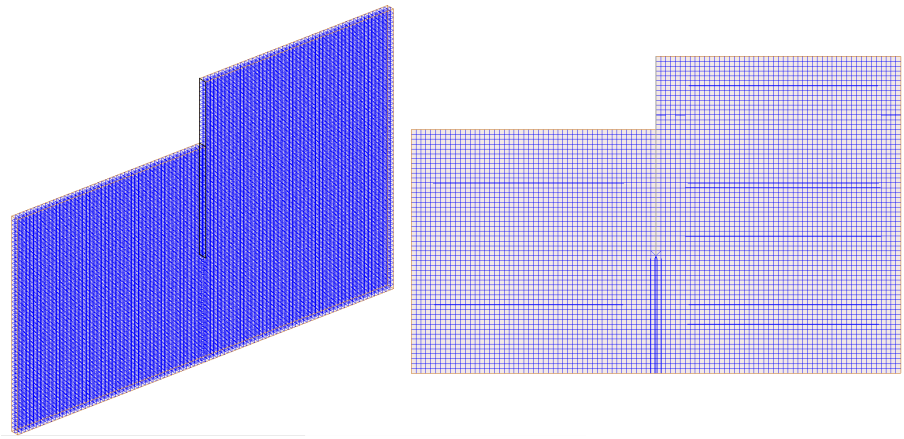

Figure 5.73 – The finite element mesh in two different views

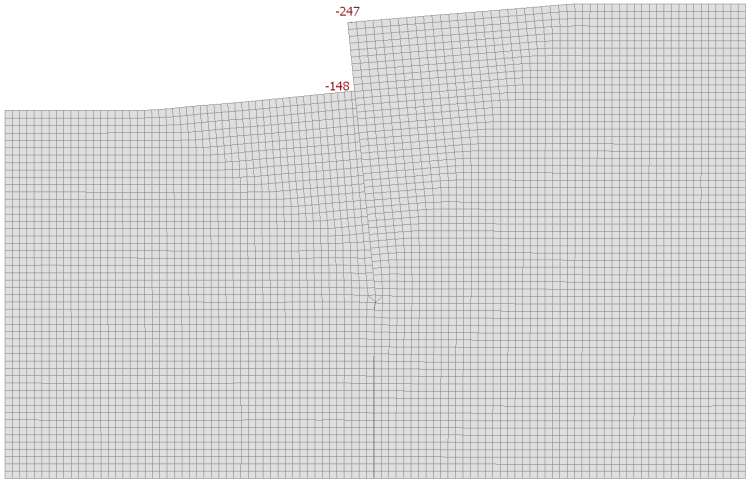

Figure 5.74 – The displacements with the deformed mesh [mm] *(3 times scaled up)*

During the computation in the nonlinear soil calculation only the self-weight of the soil was considered. Fig. 5.74 shows the total displacements based on the nonlinear calculation. More relevant information is the connection forces (pressures) on the wall based on the active and passive earth pressures with the FE calculation (Fig. 5.75). The comparison between Fig. 5.71 and 5.75 shows that the hand calculation and the FE calculation are in good agreement. The shape and the values of the resultant connection forces on the wall are almost equal to the analytical solution.

By the design of the wall the internal forces are very important. The relevant bending moments and shear forces of the wall can be seen in Fig. 5.76. and 5.77. The position of the roots and extremums are also indicated in Fig. 5.76. and 5.77.

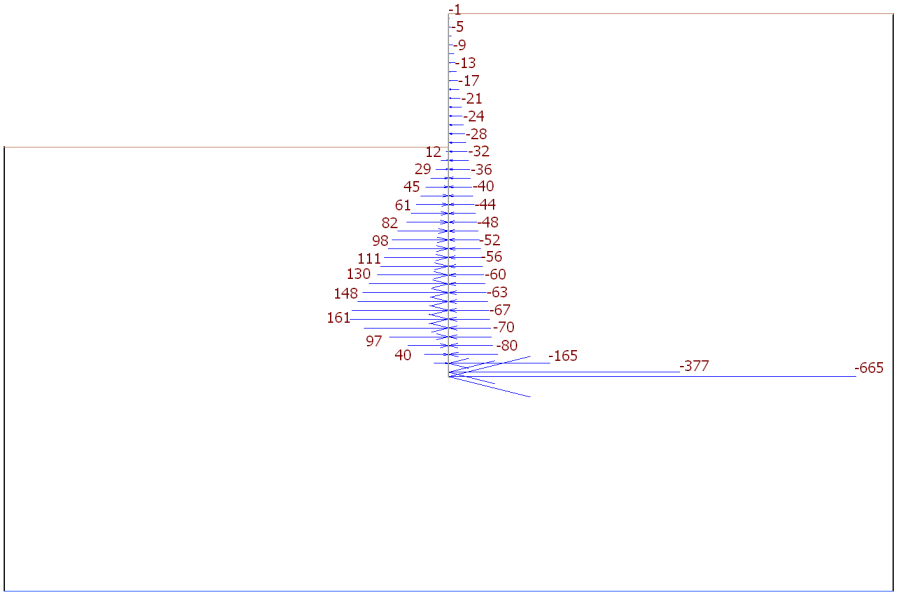

Figure 5.75 – The connection forces (pressures) [kN/m^2] *on the left and right side of the wall*

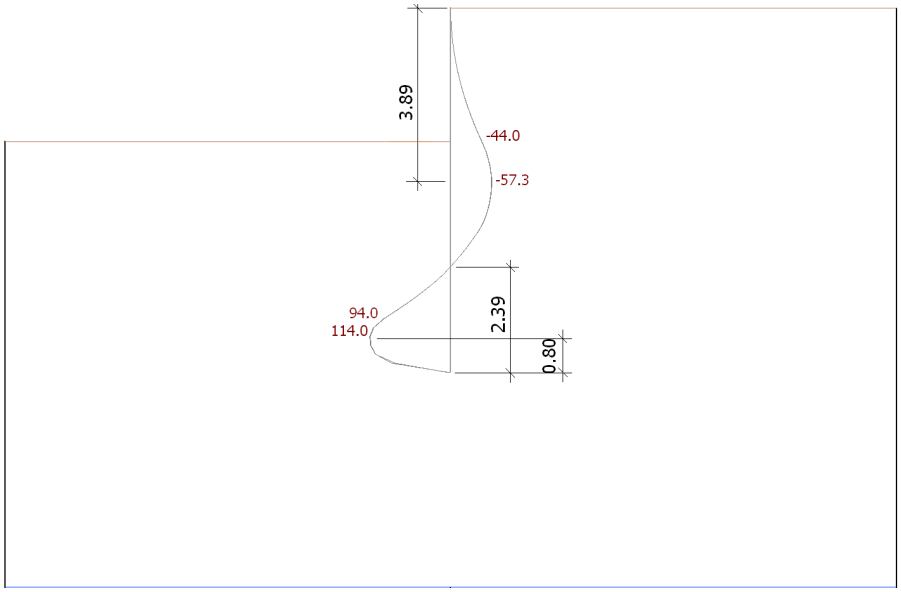

Figure 5.76 – The shear force diagram of the wall based on the NONLINEAR calculation – t_{xz} [kN/m]

The extremums of the shear forces of the wall from the analytical calculation were t_{1a} = 57.91 kN/m and t_{2a} = 114.8 kN/m (see Fig. 5.71). The FE calculation gave t_{1FE} = 57.3 kN/m and t_{2FE} = 114.0 kN/m (Fig. 5.76). The differences between the FEM-Design calculations and the analytical solutions are less than 1 %. The position of these extremums were z_{1a} = 3.937 m from the top of the wall and z_{2a} = 0.7803 m from the bottom of the wall by the hand calculation (Fig. 5.71). The position of these extremums were z_{1FE} = 3.89 m from the top of the wall and z_{2FE} = 0.80 m from the bottom of the wall by the FE calculation (Fig. 5.76).

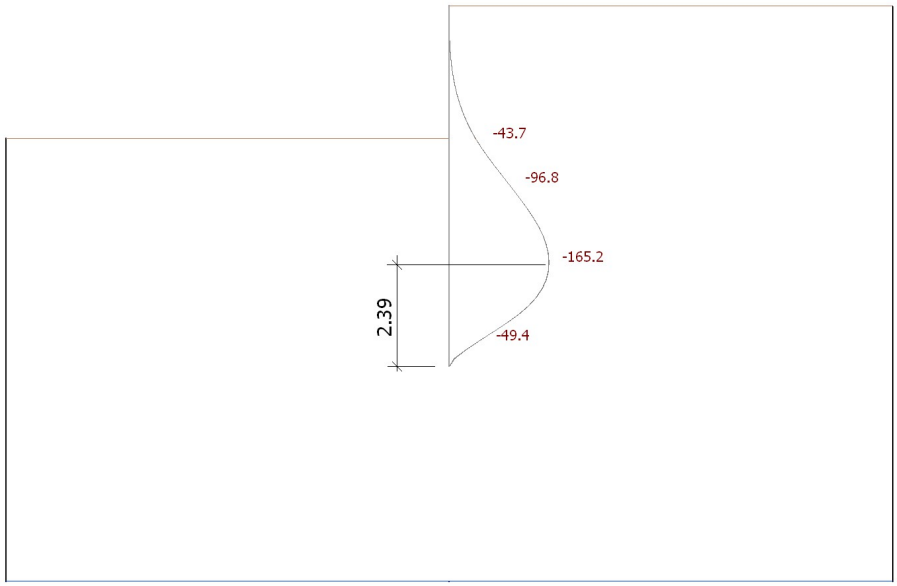

Figure 5.77 – The bending moment diagram of the wall based on the NONLINEAR calculation – m_x [kNm/m]

The extremum of the bending moment of the wall from the analytical calculation was m_{1a} = 168.2 kNm/m (see Fig. 5.71). The FE calculation gave m_{1FE} = 165.2 kNm/m (Fig. 5.77). The difference between the FEM-Design calculation and the analytical solution is less than 2 %. The position of this extremum was z_{3a} = 2.317 m from the bottom of the wall by the hand calculation (Fig. 5.71). The position of this extremum was z_{3FE} = 2.39 m from the bottom of the wall by the FE calculation (Fig. 5.77).

Based on the active and passive earth pressures the soil is in plastic condition on the left and right sides of the wall (see Chapter 3.2.2). By the load-combination results the „soil plastic condition" shows us the elements (integration points) which are in plastic conditions (see Fig. 5.78).

Figure 5.78 – The finite elements (integration points) in plastic condition (active and passive side)

In the FE calculation we modelled the depth of the wall based on the analytical solution. Let's check the effect of the length of the wall. In our FE models we modified the length of the wall (*D* depth) but the *H* value was constant. Fig. 5.79 shows the maximum total displacements in the function of $H + D$ wall length. The diagram shows that if we apply longer wall than what we calculated from the analytical solution the total displacements will be smaller and smaller, but if we apply smaller wall length than $H + D = 3 + 5.173 = 8.173$ m the total displacements increasing exponentially which means that according to the plastic states and the end of the shear capacity of the soil, the equilibrium is not possible (not adequate) see Fig. 5.79a. For the illustration of large displacements below the minimum wall length the vertical axis of the diagram in Fig. 5.79b is in logarithmic scale.

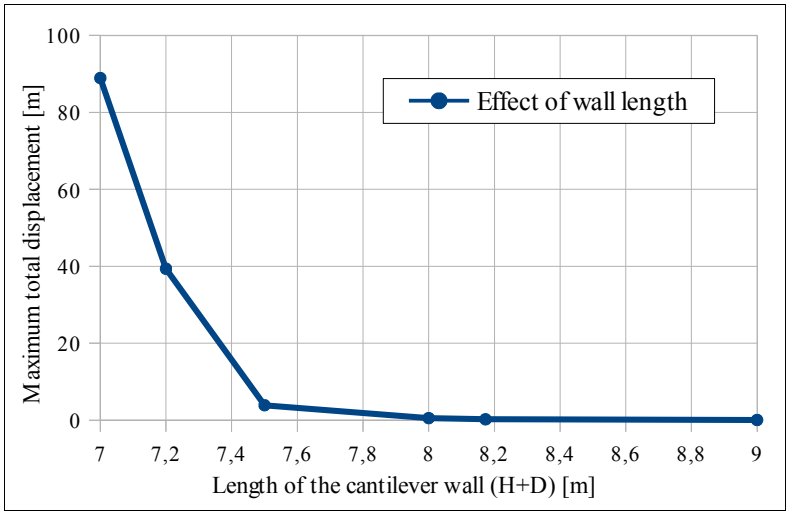

a)

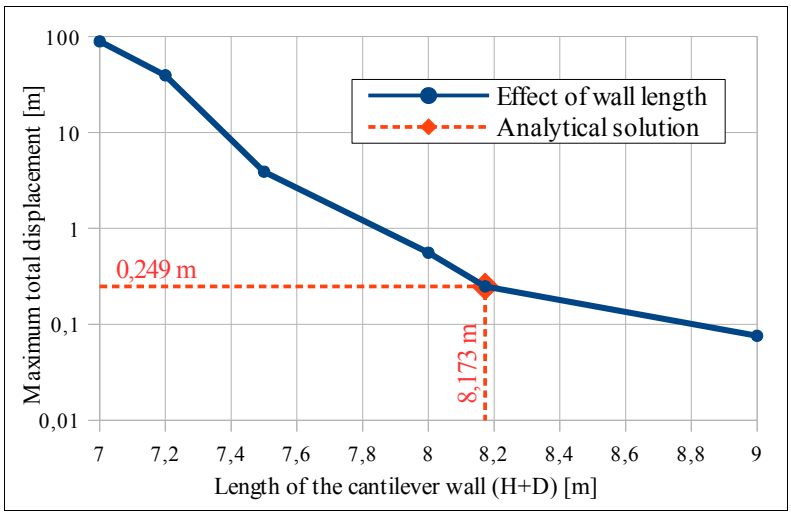

b)

Figure 5.79 – The effect of the length of the cantilever wall on the maximum total displacements with the finite element calculation: a) normal scale; b) logaritmic scale

WARNING: As an interesting thing we draw attention to the fact that the linear calculation in this case leads to completely different false results. It comes from the fact that basically the soil is not a linear elastic material. The shear force and the bending moment diagrams based on the linear calculation can be seen in Fig. 5.80 and 5.81. The values are much smaller and they are on the opposite side than by the nonlinear calculation. It means that by this problem the linear elastic-perfectly plastic Mohr-Coulomb material model leads to an adequate result but the linear calculation leads a wrong solution.

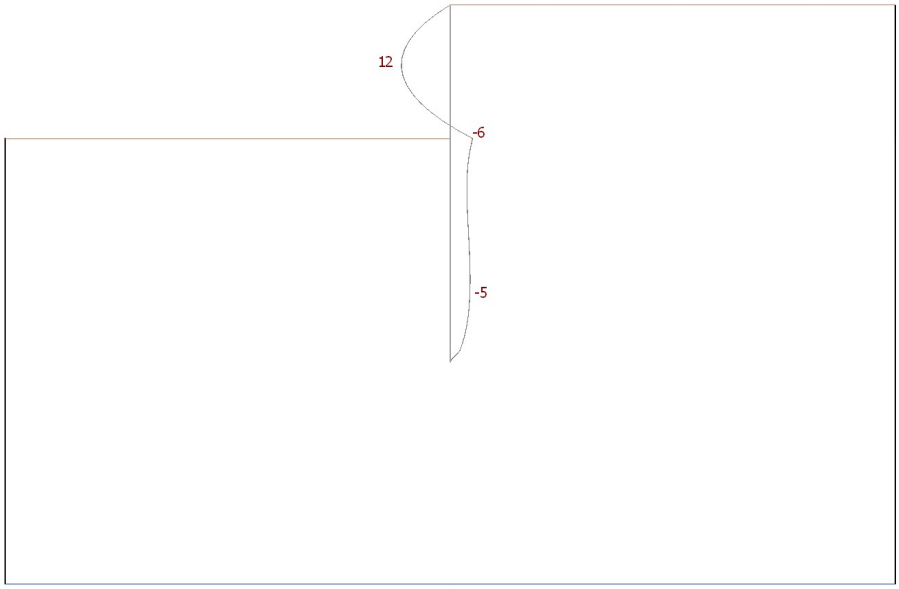

Figure 5.80 – The shear force diagram of the wall based on the LINEAR calculation – t_{xz} [kN/m]

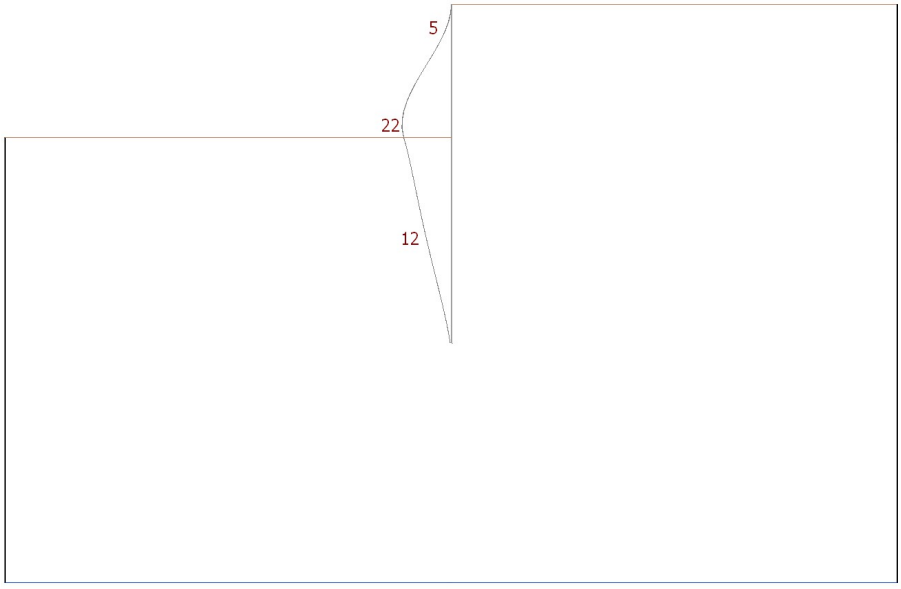

Figure 5.81 – The bending moment diagram of the wall based on the LINEAR calculation – m_x [kNm/m]

5.7 Slope stability

In this chapter the following slope was analyzed (Fig. 5.82). The width and the height of the slope with the considered material parameters also shown in Fig. 5.82. The problem was modelled in FEM-Design based on the Mohr-Coulomb material model. Beyond the self-weight of the soil an external vertical total load (see Fig. 5.83) or an external vertical partial load (see Fig. 5.93) were considered. In Chapter 5.7.1 the reduction factor of φ'-c' was analyzed according to the self-weight of the soil. The φ'-c' reduction factor was calculated which leads to the failure of the slope due to the self-weight of the soil. In Chapter 5.7.2 the same slope was analyzed with an additional total distributed load on the top of the slope. In Chapter 5.7.3 the same slope was analyzed with an additional partial distributed load on the top of the slope.

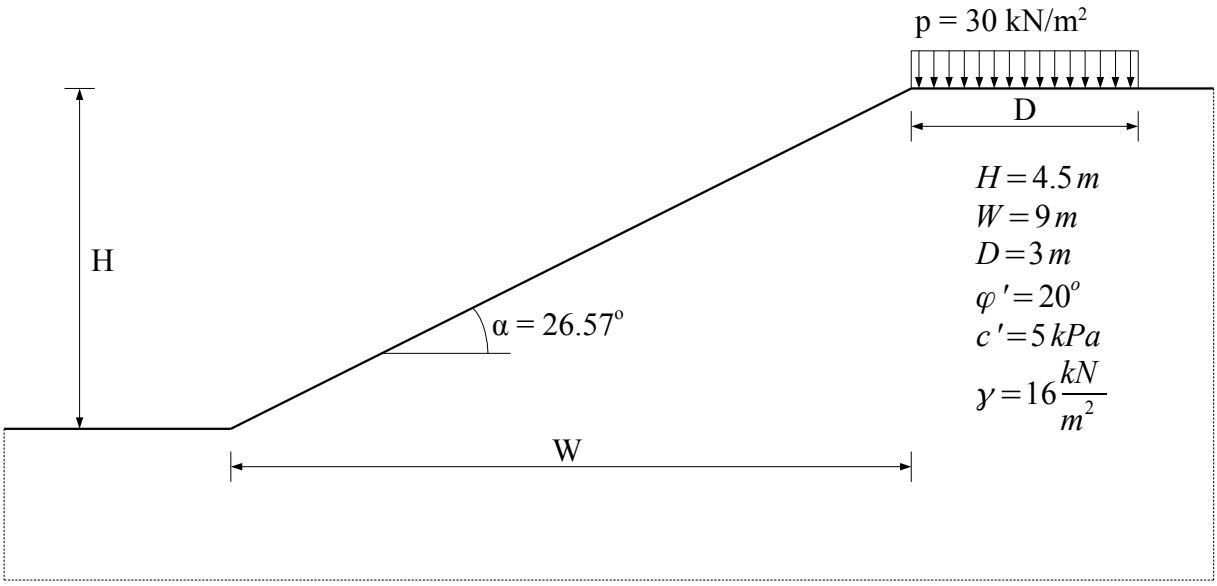

Figure 5.82 – The geomtery of the slope and the input data

5.7.1 Slope stability due to the self-weight of the soil

In Chapter 5.7.1 and 5.7.2 the model space and the finite element mesh were the same but the considered loads (self-weight and external loads) were different. The physical model space in FEM-Design for these two chapter can be seen in Fig. 5.83. The default soil supports in FEM-Design around the soil restrict the translation perpendicular to the boundary plain of the soil. Due to the slope stability problem an additional horizontal surface support needed at the bottom of the soil strata (see Fig. 5.83). Fig. 5.84 shows the automatically generated 3D finite element mesh with 0.5 m average element size.

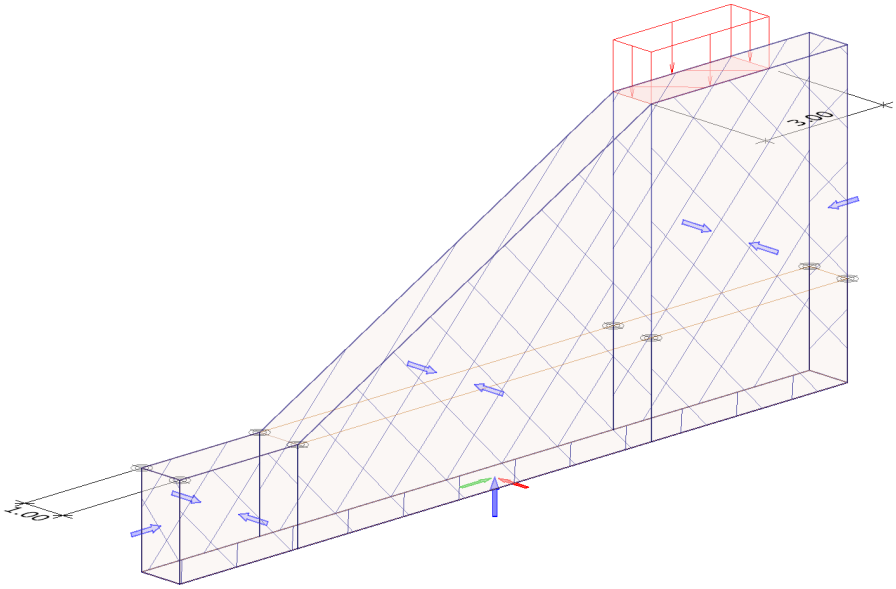

Figure 5.83 – The geomtery of the slope and the physical model with the total load

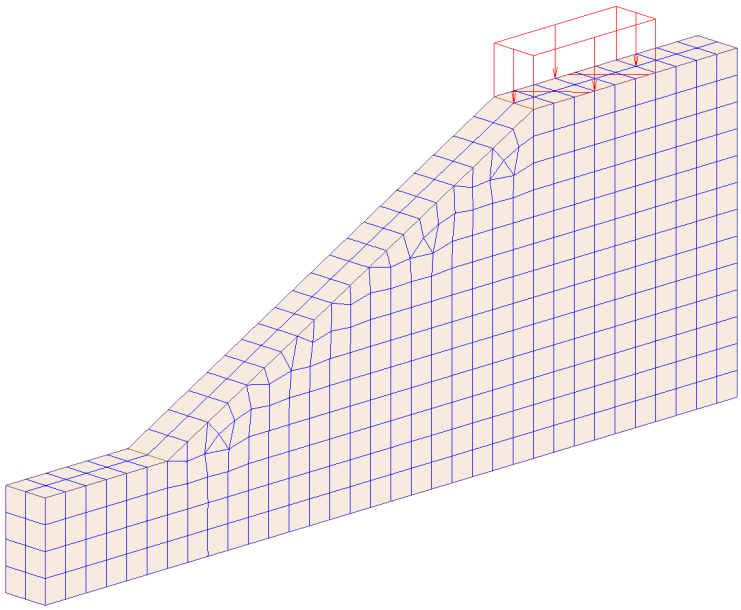

Figure 5.84 – The mesh of the slope and the external vertical load q_z = 30 kN/m^2

In this chapter the reduction factor of φ'-c' was analyzed according to the self-weight of the soil. The φ'-c' reduction factor was calculated which leads to the failure of the slope due to the self-weight of the soil. With the modification (reduction of φ'-c') of the material parameters the safety factor of the slope can be calculated. Fig. 5.85 shows the calculations with the different reduction factors on φ'-c'. The safety factor of the slope is the reduction factor φ'-c' where the slope fails (collapse). It means that according to the Mohr-Coulomb theory large deformation occurs.

Reduction factor	Max. of total displacement [m]	Computational time [s]	Number of equations [pcs]
1,00	0,100	171	20150
1,40	0,113	201	20150
1,50	0,123	208	20150
1,55	0,145	213	20150
1,56	0,179	213	20150
1,57	0,260	215	20150
1,58	0,552	211	20150
1,60	2,126	240	20150
1,66	229,0	243	20150

Figure 5.85 – The φ'-c' reduction factor and the max. of total displacement due to the self-weight of the soil

Fig. 5.85 also shows the maximum total displacement of the slope with different reduction factors. With this calculation the safety factor is around 1.60 when only the self-weight of the soil was considered. The result is more obvious from Fig. 5.86 where the maximum total displacements (in logarithmic scale) of the slope were plotted in the function of the analyzed reduction factors.

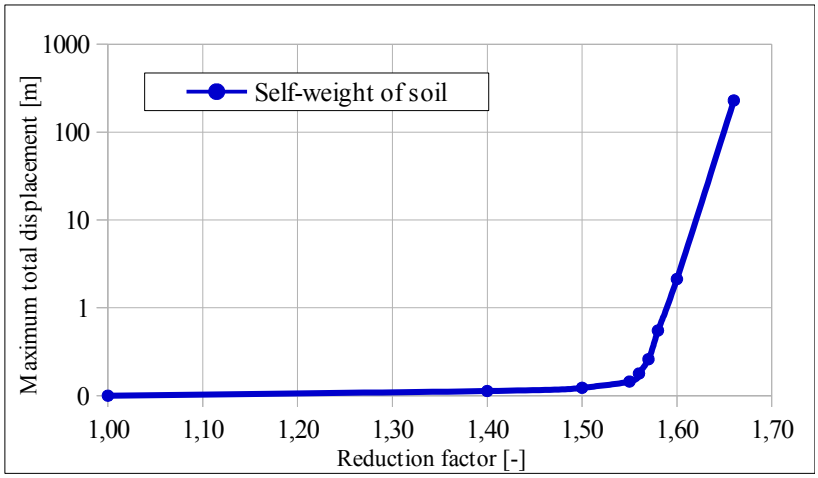

Figure 5.86 – The max. of displacement in terms of φ'-c' reduction factor due to the self-weight of the soil

Fig. 5.87 shows the total displacements of the slope when it fails (reduction factor equals to 1.60). The slip surface due to the self-weight of the soil is noticeable.

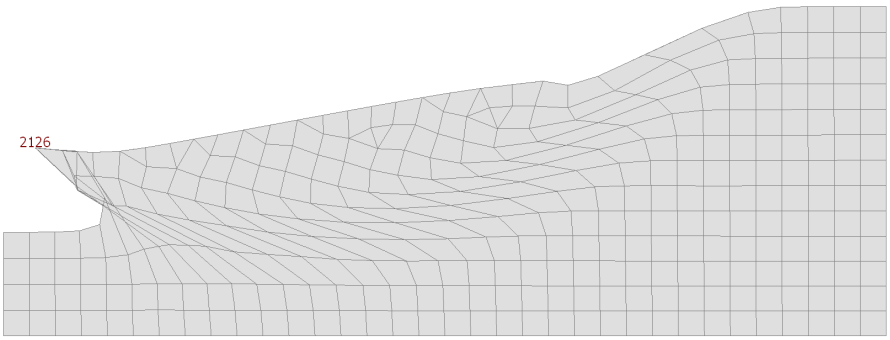

Figure 5.87 – The total displacements [mm] *at failure (φ'-c' reduction factor = 1.60) due to the self-weight of the soil*

5.7.2 Slope stability due to an additional total load

In this chapter the problem was the same as in Chapter 5.7.1 but in addition to the self-weight of the soil an external total vertical distributed load was also considered (see Fig. 5.83). Fig. 5.83 shows that the width of the total external load is 3 m on the top of the slope. According to Chapter 5.7.1 the expected *φ'-c'* reduction factor is smaller than 1.60 due to the additional external load. With the modification (reduction of *φ'-c'*) of the material parameters the safety factor of the slope can be calculated. Fig. 5.88 shows the calculations with the different reduction factors on *φ'-c'*. The safety factor of the slope is the reduction factor *φ'-c'* where the slope fails (collapse). It means that according to the Mohr-Coulomb theory large deformation occurs.

Reduction factor	Max. of total displacement [m]	Computational time [s]	Number of elements [pcs]
1,00	0,052	171	20150
1,10	0,059	201	20150
1,20	0,071	208	20150
1,23	0,100	213	20150
1,25	0,838	213	20150
1,27	1,274	215	20150
1,30	233,3	211	20150
1,35	649,0	240	20150

Figure 5.88 – The φ'-c' reduction factor and the max. of total displacement due to the self-weight of the soil and the additional total external load

Fig. 5.88 also shows the maximum total displacement of the slope with different reduction factors. With this calculation the safety factor is around 1.27 when the additional external total load was also considered. The result is more obvious from Fig. 5.89 where the maximum total displacements (in logarithmic scale) of the slope were plotted in the function of the analyzed reduction factors.

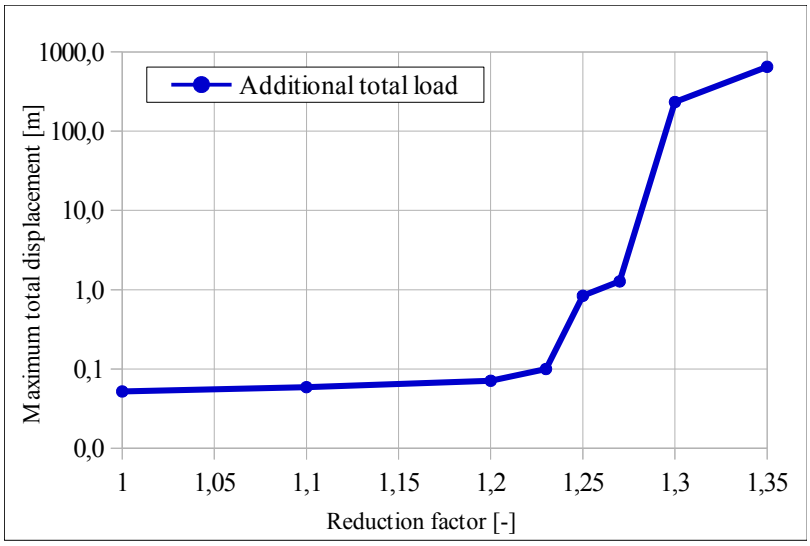

Figure 5.89 – The max. of displacement in terms of φ'-c' reduction factor due to the self-weight of the soil and the additional total external load

Fig. 5.90 shows the total displacements of the slope when it fails (reduction factor equals to 1.27). The slip surface due to the additional external load is noticeable.

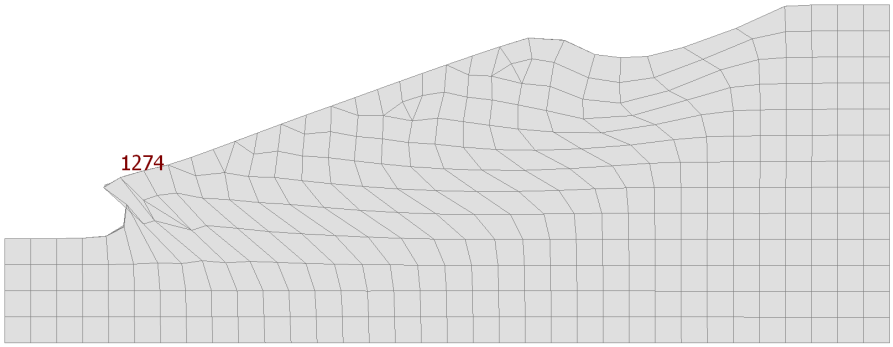

Figure 5.90 – The total displacements [mm] *at failure (φ'-c' reduction factor = 1.27) due to the self-weight of the soil and the additional total external load*

In this chapter we stated that the slope is stable with the mentioned additional total external load (q_z = 30 kN/m^2). If we would like to know the maximum intensity of this external load what the slope can bear with its original material parameters let's increase the intensity of the ditributed load until the slope fails. Fig. 5.91 shows the increasing intensity of the distributed load in the function of the maximum vertical displacement of the slope. According to this diagram based on the finite element calculation the maximum intensity of the load is around $q_{z,max}$ = 65 kN/m^2. Over this amount of distributed load the slope fails because large deformation occurs.

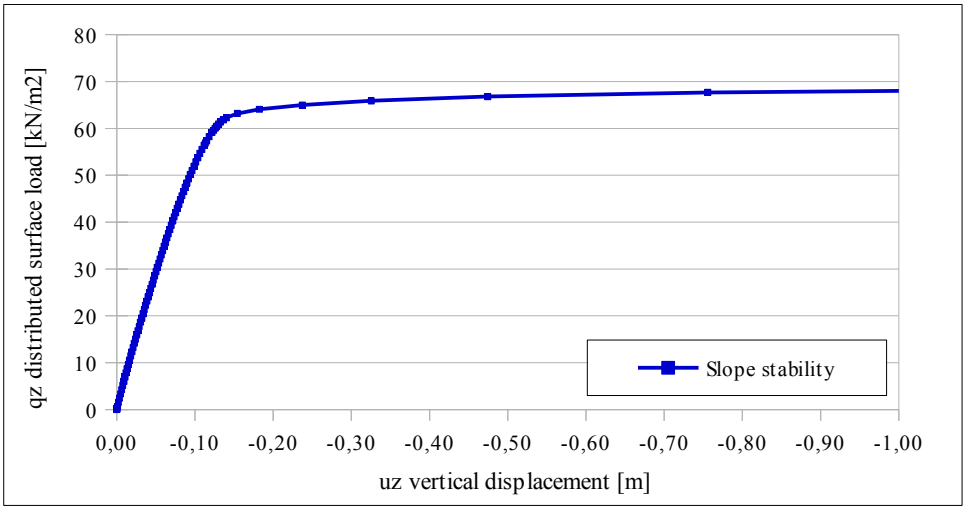

Figure 5.91 – The total external load in the function of vertical displacement

Fig. 5.92 shows the total displacements of the slope when it fails according to $q_{z,max}$ = 65 kN/m^2. The slip surface due to the maximum intensity of total external load is noticeable but in this case it has different shape.

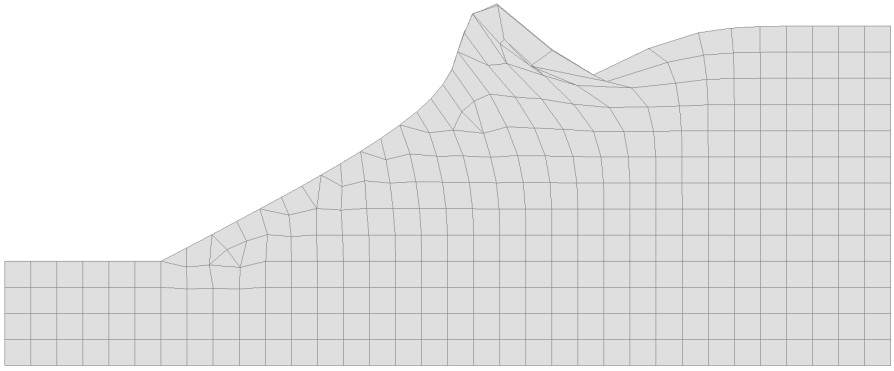

Figure 5.92 – The total displacements at failure due to the maximum allowable external load

5.7.3 Slope stability due to an additional partial load

In this chapter the problem is a bit different than in the former ones. Beyond the self-weight of the soil an external vertical distributed load was also considered but in this case it was only partial (see Fig. 5.93). Fig. 5.94 shows that the area of the partial distributed load was 3x6 m and the width of the model space was 18 m. The default soil supports in FEM-Design around the soil restrict the translation perpendicular to the boundary plain of the soil. Due to the slope stability problem an additional horizontal surface support also needed here at the bottom of the soil strata (see Fig. 5.93). Fig. 5.94 shows the automatically generated 3D finite element mesh with 0.9 m average element size.

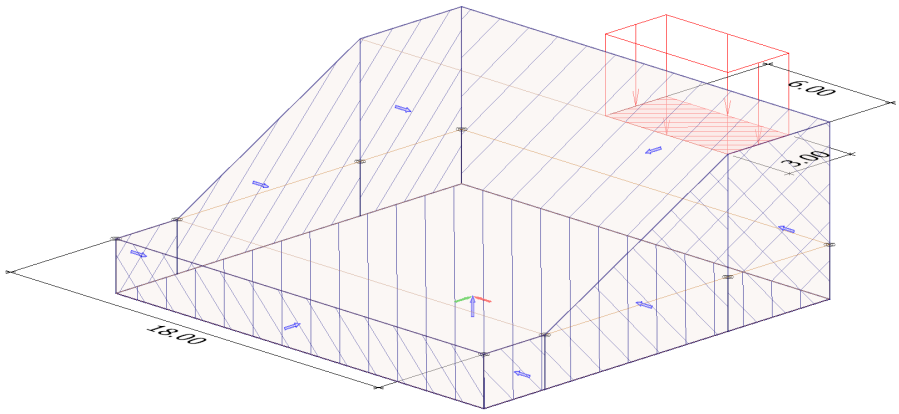

Figure 5.93 – The geomtery of the slope and the physical model with the partial load

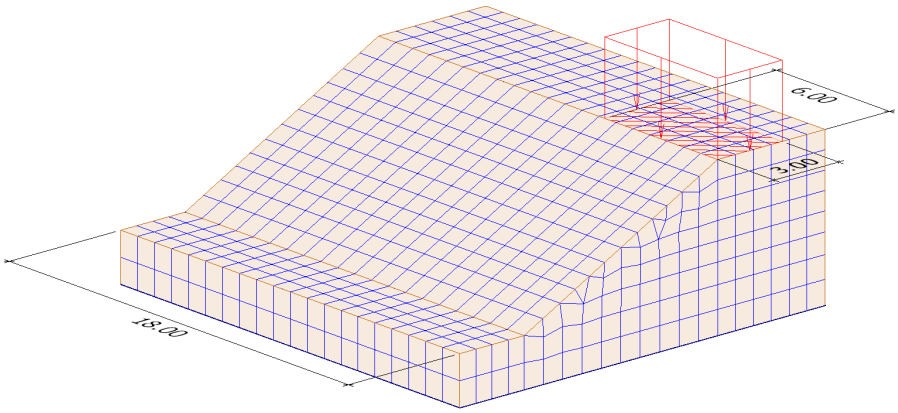

Figure 5.94 – The mesh of the slope and the external vertical partial load q_z = 30 kN/m^2

According to Chapter 5.7.2 the expected φ'-c' reduction factor is larger than 1.27 according to the partial effect of the new additional load. With the modification (reduction of φ'-c') of the material parameters the safety factor of the slope can be calculated. Fig. 5.95 shows the calculations with the different reduction factors on φ'-c'. The safety factor of the slope is the reduction factor φ'-c' where the slope fails (collapse). It means that according to the Mohr-Coulomb theory large deformation occurs.

Reduction factor	Max. of total displacement [m]	Computational time [s]	Number of elements [pcs]
1,00	0,051	1404	60639
1,20	0,064	1521	60639
1,32	0,116	1505	60639
1,35	0,340	1548	60639
1,40	1,133	1510	60639
1,50	1134	1553	60639

Figure 5.95 – The φ'-c' reduction factor and the max. of total displacement due to the self-weight of the soil and the additional partial external load

Fig. 5.95 also shows the maximum total displacement of the slope with different reduction factors. With this calculation the safety factor is around 1.40 when the additional external partial load was considered. The result is more obvious from Fig. 5.96 where the maximum total displacements (in logarithmic scale) of the slope were plotted in the function of the analyzed reduction factors.

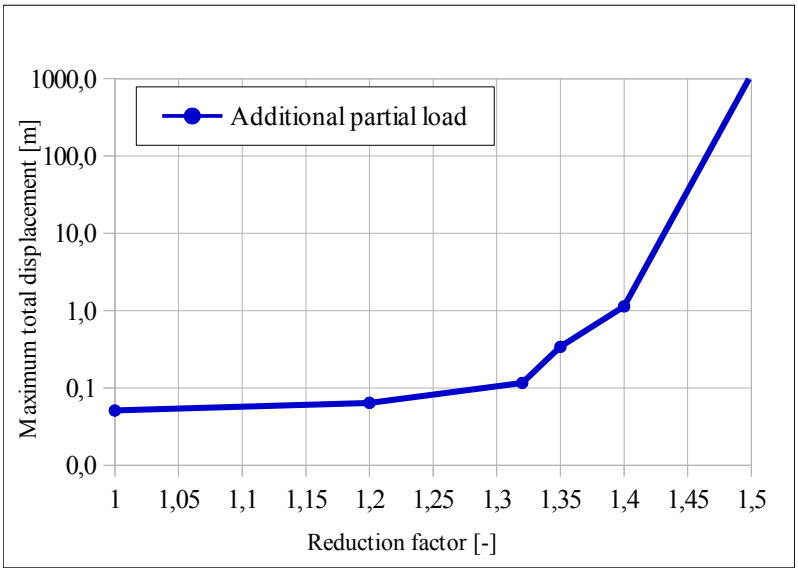

Figure 5.96 – The max. of displacement in terms of φ'-c' reduction factor due to the self-weight of the soil and the additional partial external load

Fig. 5.97 shows the total displacements of the slope when it fails (reduction factor equals to 1.40). The slip surface due to the additional external partial load is noticeable.

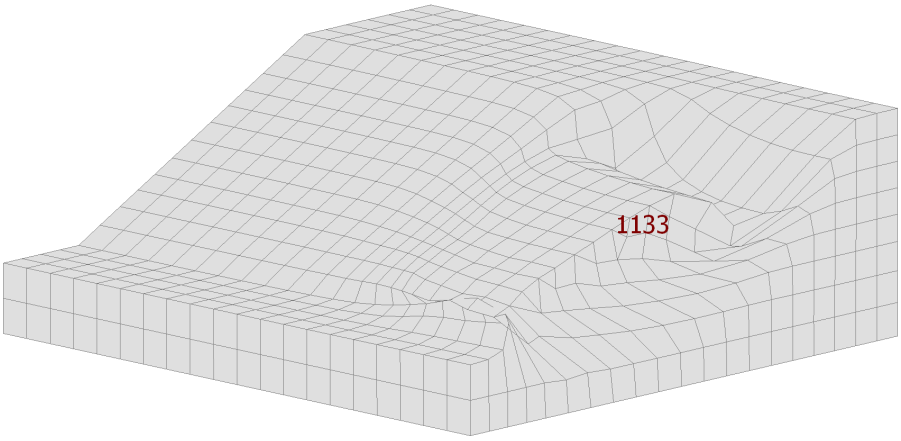

Figure 5.97 – The total displacements [mm] *at failure (φ'-c' reduction factor = 1.40) due to the self-weight of the soil and the additional partial external load*

5.7.4 Additional informations and comparison of slope stability problems

In Chapter 5.7 the parameters of the non-linear calculations were adjusted according to Fig. 5.98 to reach the precise results.

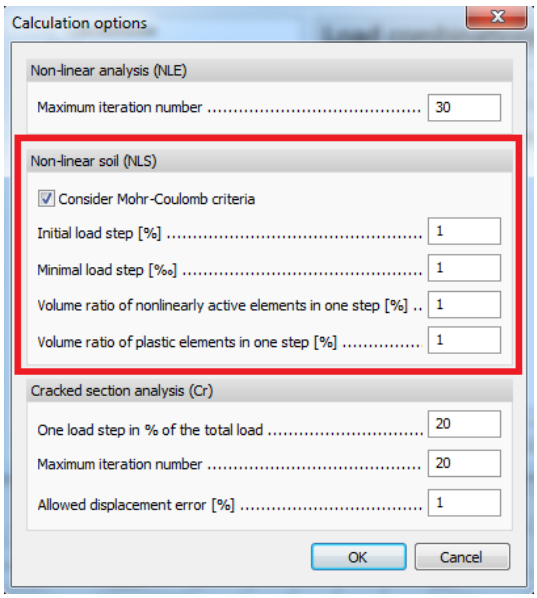

Figure 5.98 – The parameters of the non-linear soil calculation options for this slope stability chapter

Based on [56] according to the *φ'-c'* reduction the safety factor only with the self-weight of the slope is 1.57. With FEM-Design this value was 1.60 (see Fig. 5.85).

Based on [56] according to the *φ'-c'* reduction the safety factor due to the total additional external load is 1.24. With FEM-Design this value was 1.27 (see Fig. 5.88).

Based on [56] the maximum intensity of the total additional load is $q_{z,max}$ = 64 kN/m^2. With FEM-Design this value was $q_{z,max}$ = 65 kN/m^2 (see Fig. 5.91).

Based on [56] according to the φ'-c' reduction the safety factor due to the partial additional external load is 1.34. With FEM-Design this value was 1.40 (see Fig. 5.95).

6. Direct download links for the model files

On the following links you can find the FEM-Design model files which were presented in Chapter 5. For the results after downloading run a load-combination calculation. Before the calculation check the settings.

http://download.strusoft.com/FEM-Design/inst150x/documents//GEOExamples.zip

You can download the latest version of this manual from:

http://download.strusoft.com/FEM-Design/inst150x/documents//3dsoilmanual.pdf

7. Limitations

According to the fact that FEM-Design in the first instance is not only a geotechnical software there are several limitations and restrictions what the users need to keep in mind when using the software for geotechnical purposes. In this Chapter the readers can find severel comments, recommendations and reviews on these limitations.

The dimensions of the modelled half-space of the soil have important effect on the calculated results. These dimensions in vertical (limit depth) and horizontal directions for an adequate FE model depend on the type of the foundation system (isolated, wall, slab or compound foundations) and on the depth of the bedrock. The side of the soil model should be decided in consultation with a geotechnical expert. The users can also find these recommended sizes in several geotechnical handbooks and papers what were mentioned in this manual. First of all the dimensions have effect on the calculated settlements of the structure and secondly the non-linear calculation control parameters (Chapter 4.4.2) also have connection with the applied volume of the soil.

During the modelling of basement walls keep in mind that the friction between the soil layers and basement walls are neglected in FEM-Design. It means that only the perpendicular forces from earth and water pressure have effects on the internal forces of basement walls.

Based on Chapter 4 it is obvious that the computational time is increasing when the users apply smaller and smaller control parameters by non-linear soil calculations (see Chapter 4.4.2). The average mesh size has also a very important effect because the stresses (internal forces) are the secondary (slave) variables of FE calculations. In NLS combination the calculated settlements are very important because the Mohr-Coulomb failure criteria (Chapter 3.2) and the stress dependency of compression modulus (Chapter 3.3) depend on the calculated stresses at the different load levels. According to these information the „fine” calculation gives more accurate results than the „standard” calculation (Chapter 2). In addition, attention should be paid to the local mesh refinement. Summarizing these effects, the users also need to keep in mind that the „fine” (quadratic) non-linear computation time with local mesh refinement is increasing exponentially. Upon these information during the geotechnical use of FEM-Design, the convergence analysis is much more relevant than by a usual FE calculation, thus we reccomend the user to make a convergence analysis with mesh refinements and with the changing of the default values on non-linear soil control parameters to reach an adequate results.

If the users apply the Mohr-Coulomb plasticity theory with medium dense or dense frictional soils (see Table 6) smaller control parameters recommended by the non-linear calculations than the default values („minimal load step” and „volume ratio of plastic elements in one step”, see Chapter 4.4.2) to get the adequate load-bearing capacities.

In FEM-Design after the definition of a soil half-space, the default supports at the

vertical planes of the soil are fixed horizontally and at the bottom of the soil the support is fixed vertically. It means that if the user applied an adequate limit depth these boundary conditions are sufficient but if the limit depth was shallow or the user modelled the end of the half-space at a very stiff soil layer a horizontal surface support also needed manually at the bottom of the soil.

In FEM-Design the users are not able to define an impermeable layer because FEM-Design calculation always consider final state in respect to time thus the time is not a variable (see Chapter 3.3). Based on this fact the shrinkage and the creep effects of the soil are not considered. In FEM-Design the user can adjust different ground water levels by different load-combinations one by one, but only one ground water level is valid for one load-combination. It means that the user is not able to adjust two or more ground water levels for the same load-combination. According to this limitation an overpressured ground water level is not possible in FEM-Design.

8. Suggested material parameters for typical soils

The suggested material parameters below are based on [64].

Material	**Specific weight** [kN/m^3]
Uniform sand	16-21
Well graded sand	17-22
Gravels	17-23
Clays	16-21
Gravelly clays	17-22
Organic clays	14-17
Peat/topsoil	11-14

Table 5 – Typical values of specific weight

Description	**Friction angle** [°]
Very loose	< 28
Loose	28-30
Medium dense	30-40
Dense	40-45
Very dense	45-50
Clayey sand	Reduce 5
Gravely sand	Increase 5

Table 6 – Sand strength

Description	**c_u** [kPa]
Very soft	0-12
Soft	12-25
Firm	25-50
Stiff	50-100
Very stiff	100-200
Hard	> 200

Table 7 – Clay undrained shear strength

Description	**E** [MPa]
Very loose	<10
Loose	10-20
Medium dense	20-30
Dense	30-60
Very dense	>60

Table 8 – Drained sand Young's modulus

Type of clay	E_{oed} [MPa]
Heavily overconsolidated boulder clays	>20
Boulder clays, moderately overconsolidated	10-20
Glacial outwash clays, lake deposits, weathered marl, lightly to normally consolidated clays	3.3-10
Normally consolidated alluvial clays	0.7-3.3
Highly organic alluvial clays and peat	<0.7

Table 9 – Oedometer modulus of clays

Material (plasticity index)	Short term ν [-]	Long term ν [-]
Sands, gravels and other cohesionless soils	≤ 0.30	≤ 0.30
Low PI (<12%)	0.35	0.25
Medium PI (12% < PI < 22%)	0.40	0.30
High PI (22% < PI < 32%)	0.45	0.35
Extremely high PI (PI > 32%)	0.45	0.40

Table 10 – Poisson's ratio for soils

References

[1] Kaliszky S., Kurutzné K.M., Szilágyi Gy., Szilárdságtan (Strength of materials), Nemzeti Tankönyvkiadó, Budapest, 2000.

[2] Beer F.P., Johnston E.R., DeWolf J.T., Mazurek D.F.: Mechanics of materials, McGraw-Hill, 2012.

[3] Budynas R.G., Advanced Strength and Applied Stress Analysis, McGraw-Hill, 1999.

[4] Popov E.P.: Mechanics of materials, Pearson Education, 1978.

[5] Kollár L.P., Springer G.S., Mechanics of composite structures, Cambridge University Press, 2003.

[6] Prager W., Recent developments in mathematical theory of plasticity, Journal of AppliedPhysics, 20, 1949.

[7] Kabai I., Geotechnika I., Műegyetemi kiadó, Budapest, 2005.

[8] Zienkiewicz O.C., Taylor L., The finite element method, ISBN 0 7506 5049 4, 2000.

[9] Bojtár I., Gáspár Z., Végeselemmódszer építőmérnököknek, Budapest, TERC, 2003.

[10] Prathap G., Barlow points and Gauss points and the allasing and best fit paradigms, Computers and Structures, 58, pp. 321-325., 1996.

[11] Sun E.Q., Shear locking and hourglassing in MSC Nastran, ABAQUS and ANSYS, report

[12] Hinton E., Owen D.R.J., Finite element of software for plates and shells, Pineridge Press, Swansea, U.K., 1984.

[13] Ansys, User's manual, 2013.

[14] Burke J.J., A nonlinear finite element analysis of soil deformation, PhD thesis, 1983.

[15] Ho I.H., Hsieh C.C., Numerical modeling for undrained shear strength of clays subjected to different plasticity indexes, Journal of GeoEngineering, 8, pp. 91-100., 2013.

[16] Schanz T., Vermeer P.A., Bonnier P.G., The hardening soil model: Formulation and verification, Beyond 2000 in Computational Geotechnics, Rotterdam, ISBN 90 5809 040 X, 1999.

[17] Mohhamed A.Q., Finite element application for modified cam clay model to analyze silty clay soil under strip footing using matlab, Journal of Engineering and Developmenet, 16, pp. 89-99., 2012.

[18] Wroth P.C., Houlsby G.T., A critical state model for predicting the behaviour of clays, Proceedings of the Workshop on Limit Equilibrium, Plasticity and Generalised Stress-Strain in Geotechnical Engineering, McGill University, Montreal, May 28-30, ISBN 0-87262-282-7, pp. 592-627., 1980.

[19] Lemaitre J., Handbook of materials behavior models I-III, Academic Press, 2001.

[20] Yip S., Handbook of materials modeling I.-II, Springer, 2005.

[21] Borja R.I., Cam-Clay plasticity. Part V: A mathematical framework for three-phase deformation and strain localization analyses of partially saturated porous media, Computational Methods and Applied Mechanical Engineering, 193, pp. 5301-5338., 2004.

[22] Ortiz M., Pandolfi A., A variational Cam-clay theory of plasticity, Computational Methods and Applied Mechanical Engineering, 193, pp. 2645-2666., 2004.

[23] Lade P.V., Duncan J.M., Elastoplastic stress-strain theory for cohesionless soils, Journal of Geotechnical Eng. Div., ASCE, 101, pp. 1037-1318., 1975.

[24] Lade P.V., Kim M.K., Single hardening constitutive model for soil, rock and concrete, Int. Journal of Solids and Structures, 32, pp. 1963-1978., 1995.

[25] Prevost J.H., Mathematical modelling of monotonic and cyclic undrained clay behavior, Int. Journal for Numerical and Analytical methods in Geomechanics, 1, pp. 195-216., 1977.

[26] Prevost J.H., A simple plasticity theory for frictional cohesionless soils, Soil Dynamics and Earthquake Eng., 4, pp. 9-17., 1985.

[27] Andrianopoulos K.I., Papadimitriou A.G., Bouckovalas G.D., Bounding surface models of sands: pitfalls of mapping rules for cyclic loading, Publ. of Geotechnical Dept., School of Civil Engineering, National Technical University of Athens, Greece, 2003.

[28] Hoek E., Brown E.T., Underground excavations in rock, Instn. Min. Metall., London, 1980.

[29] Hoek E., Wood D., Shah S., A modified Hoek-Brown criterion for jointed rock masses, Proc. Rock Characterization, Symp. Int. Soc. Rock Mechanics: Euorock '92 (ed. J. A. Hudson), pp. 209-214., 1992.

[30] Sjöberg J., Estimating rock mass strength using the Hoek-Brown failure criterion and rock mass classification, Internal Report SE-971 87, Division of Rock Mechanics, Lulea University of Technology, 1997.

[31] Hoek E., Carranza-Torres C., Corkum B., Hoek-Brown failure criterion – 2002 edition, Proc. 5th North-American Rock Mech. Symp. and 17th Tunelling Assoc. of Canada Conf. (ed. Hammah R.), pp. 267- 273., 2002.

[32] Zhang L., Zhu H., Three-dimensional Hoek-Brown strength criterion for rocks, J. of Geotechnical and Geoenvir. Eng. ASCE, 133, No. 9, pp. 1128-1135., 2007.

[33] Zhang L., A generalized three-dimensional Hoek-Brown strength criterion, Rock Mechanics and Rock Engineering, 41, pp. 893-915., 2008.

[34] Hoek E., Brown E.T., The Hoek-Brown failure criterion, Proc. 15th Canadian Rock Mech. Symp. (ed. J.H. Curran), pp. 31-38.,1988.

[35] Clausen J., Efficient non-linear finite element implementation of elasto-plasticity for geotechnical problems, Aalborg University, PhD thesis, 2007.

[36] Clausen J., Andersen L., Damkilde L., An efficient formulation of the elasto-plastic constitutive matrix on yield surface corners, Proceedings of the Twenty Second Nordic Seminar on Computational Mechanics, pp. 135-138. Department of Civil Engineering, Aalborg University, 2009.

[37] Roscoe K.H., Schofield M.A., Wroth C.P., On the yielding of soils, Geotechnique, 8, pp. 22-53., 1958.

[38] Kaliszky S., Képlékenységtan, Akadémiai Kiadó, 1975.

[39] Geodzsajev V.O., Some problems of the theory of elastic-plastic deformation of anisotropic materials, Trudi Moszkovszkava Fiziko-Technicseszkava Insztituta, pp. 69-96,1958.

[40] Chen W.F., Plasticity and modeling, Elsevier, 1994.

[41] Budiansky B., A reassesment of deformation theories of plasticity, Journal of Applied Mechanics, 26, 1995.

[42] Chen W. F., Plasticity and modeling, Elsevier, 1994.

[43] https://en.wikipedia.org/wiki/Shear_strength_(soil)

[44] https://en.wikipedia.org/wiki/Lateral_earth_pressure

[45] https://en.wikipedia.org/wiki/Oedometer_test

[46] https://en.wikipedia.org/wiki/Consolidation_(soil)

[47] https://en.wikipedia.org/wiki/Preconsolidation_pressure

[48] Bowles J.E., Foundation analysis and design, McGraw-Hill, 1997.

[49] Vendel J., Determination of consolidation ratio by CPT and its effect on embedded retaining structures Conference: Geotechnika 2011, ISBN: 978-963-89016-2-0, At Hungary, Ráckeve.

[50] http://www.controls-group.com/eng/soil-mechanics-testing-equipment/continuous-consolidation-cell-crs.php

[51] André R., FEM modelling of piled raft foundations in two and three dimensions, Master's Dissertation, ISSN 0281-6679, Malmö, 2011.

[52] Eriksson P., Jendeby L., Rapport 100 – kohesionspalar, palkommisionen, linköping, 2004.

[53] http://www.ngi.no/en/Project-pages/Geofuture2/Implementation-and-validation/, Effective stress soil model for soft scandinavian clays.

[54] Seah T.S., Juinarongrit T., Constant rate of strain consolidation with radial drainage, Geotechnical Testing Journal, 26, pp. 1-12., 2003.

[55] Leroueil S., Samson L.,Bososuk M., Laboratory and field determination of preconsolidation pressures at Gloucester, Canadian Geotechnical Journal, 20, 477-490., 1983.

[56] Plaxis 3D, Verification and validation manual, 2013.

[57] Groud J.P., Tables pour le calcul des foundations, volume 2. Dunod, Paris, 1972.

[58] Gibson R.E., Some results concerning displacements and stresses in a non-homogeneous elastic half-space, Geotechnique, 17, pp. 58-64., 1967.

[59] Lancelotta R., Geotechnical engineering, Balkema, 2008.

[60] Terzaghi K., Theoretical soil mechanics, 1948.

[61] Davis E.H., Booker J.R., The effect of inreasing strength with depth on the bearing capacity of clays, Geotechnique, 23, pp. 551-563., 1973.

[62] Potts D.M., Zdravković L., Finite element analysis in geotechnical engineering application, Thomas Telford, London, 2001.

[63] Cox A.D., Axially-symmetric plastic deformation on soils – II. indentation of ponderable soils, International Journal of Mechanical Science, 4, pp. 371-380., 1962.

[64] Look B.G., Handbook of geotechnical investigation and design tables, Taylor and Francis, London, 2007.

Notes